

**Endolysosomal dysfunction in Parkinson disease:
the role of disease mutations in ATP13A2 and LRRK2**

by

Lauren R. Kett

A dissertation submitted in partial fulfillment
of the requirements for the degree of
Doctor of Philosophy
(Neuroscience)
in the University of Michigan
2014

Doctoral committee:

Associate Professor William T. Dauer, Chair
Associate Professor Andrew P. Lieberman
Professor Miriam H. Meisler
Professor Lois S. Weisman
Associate Professor Haoxing Xu

In loving memory of my grandmother, Barbara Craggs, and the many other patients with Parkinson Disease, with the hope that this research will someday contribute to finding a cure

Acknowledgments

First and foremost, I would like to thank my mentor, Bill Dauer, and the members of the Dauer lab. Bill has been the perfect mentor for me and I am grateful to him for his continued enthusiasm, wisdom, and desire to perform science in the best way possible. Over the past four years, he has taught me to think more clearly and creatively, write more succinctly, not sell myself or my work short, and to use only one space after a period. I will carry with me his overwhelming passion for science and the desire to follow it wherever it leads. I am grateful to him for setting up a laboratory of dedicated and knowledgeable scientists who have enhanced my scientific and personal life during the past four years. In particular, I thank Sam Pappas who has been my closest friend and advisor in the lab. Sam is the most diligent and ethical scientist I have met and inspires me to always take the right, and not the easy, path. Science aside, Sam has been an amazing friend and confidante during times of stress. Thank you for the many cups of tea, hours spent rock climbing, and home made ice cream. I am grateful for the friendship and advice of Corinne Weisheit, Ric Liang, Dan Yellajoshiyula, Jamie Johansen, Aleric Soans, and Hui Lin Lee. They were my first line of help during experiments and commiseration when I grew frustrated. Thank you to the former members of the Dauer lab, especially Cherry Ho, Hardy Rideout, and Yong Peng, for providing the basis for a number of the LRRK2 experiments described in this dissertation. Finally, but not least, thank you to Rebecca Stone for letting me rely on her even when it wasn't her job. She was vital to my success in the lab, from helping me organize committee meetings, to making sure my grant was submitted on time, to providing me with a wonderful work environment.

I am especially appreciative of the two undergraduates I was fortunate enough to work with in the Dauer lab. Megan Bernath is one of the hardest working individuals I have ever met and it was a privilege to work side by side with her on this project and watch her develop her own scientific thinking. I will forever remember the moments spent at the microscope, late at night, when we first realized that we had an interesting result. I thank Aarthi Subramanian for her continued passion and excitement for science, even in the face of many, many failed attempts at cloning. I cannot wait to see what happens to these two amazing scientists as they begin their own careers.

I would like to thank the members of my thesis committee, Andy Lieberman, Miriam Meisler, Lois Weisman, and Haoxing Xu, for their time and scientific acumen. During my dissertation, they have provided me with their time, reagents, advice, and expertise. Each brought a unique perspective to this project and made me think about my work from alternative angles. I am in their debt and will not forget it going forward, when I have the opportunity to mentor others. I am similarly grateful to the larger Michigan neurodegenerative community for providing a wonderful work environment that balances science with camaraderie. I would particularly thank Hank Paulson and Vikram Shakkottai for input on my project and teaching me about larger issues in neurodegeneration. Thank you to Amy Krans for being not only the best cloner that I know, but also a valued friend and constant source of candy.

I would like to thank my many collaborators, both at the University of Michigan and elsewhere. Andrew Goschka and Mohammed Samie from the Xu lab taught me how to isolate lysosomes, while Ted Huston from the Department of Earth and Environmental Sciences performed ion analysis. Brian Gregorka in the Swanson lab provided valuable advice and technical expertise to measure lysosomal pH. Shannon Moore and Geoff Murphy taught me the

Morris Water Maze. I thank Jeongsoon Park of the Lombard lab for an incredible amount of work to measure the oxygen consumption rates of isolated mitochondria. The staff of MIL, especially Chris Edwards, Shelley Almburg, and Dotty Sorensen, were invaluable in teaching me confocal and electron microscopy and the finer points of live cell imaging.

I owe a huge debt of gratitude to the members of the Cuervo lab at the Albert Einstein College of Medicine. Ana Maria Cuervo was a second advisor to me in all matters lysosome, particularly in interpretation of electron microscopy images and any experiments related to the isolation of lysosomes. Barbara Stiller and Inmaculada Tasset provided not only technical help in the isolation of lysosomes and measures of lysosomal activity, but also valuable input into the interpretation of data in the Atp13a2 null project. I am grateful to Robin Chan and Bowen Zhou in Gil di Paolo's laboratory at Columbia laboratory for performing lipidomics analysis and discussions about LBPA. Thank you to Serge Przedborski, Javier Blesa, and Vernice Jackson-Lewis at Columbia University for stereology experiments of dopaminergic neurons. Finally, thank you to Daniela Boassa and Mark Ellisman for a most fruitful collaboration on the LRRK2 project.

I am forever grateful to the University of Michigan MSTP and the Neuroscience Graduate Program. The MSTP has been my home for the past six years and it has been easy to succeed knowing that I have constant support from my colleagues in the program and the administration. Ron Koenig has provided me with advice at every step and I thank him for always having the larger perspective in mind while counseling me. Ellen Elkin has similarly been a valuable resource for me during times of conflict as well as making sure that my academic life was operating smoothly. Thank you to Laurie Koivupalo and Hilikka Ketola (of the MSTP) and Valerie Smith and Rachel Flaten (of the NGP) for always looking out for me and

making sure that I had a paycheck and health insurance. I acknowledge my funding sources during graduate school, which include both the MSTP training grant (T32 GM007863) and NINDS F31 (NS078817).

I would like to thank the people who inspired me to go into science in the first place - Julie Hagelin and Sean Devereaux for my first science project at Swarthmore College, Jeffrey and Mona Morris for telling me about dual degree programs and encouraging me to apply, Byron Caughey and the members of Rocky Mountain Laboratories for exposing me to neuroscience research and prion diseases, Lianna Orlando and Ippolita Cantuti-Castelvetri for facilitating my applications to medical school and making me an expert in Western blotting and qPCR respectively, Zane Hollingsworth for providing a quiet place and supportive ear.

Thank you to my parents, Alan Kett and Ann Hendricks, for their constant support throughout my career. Their love and encouragement has allowed me to find what I am passionate about and pursue it to the best of my abilities. They have provided a haven when I needed it and taught me the value of compassion and a strong work ethic.

Finally, I thank, from the bottom of my heart, the many friends without whom this dissertation would not have happened. Thank you for the countless cups of tea, slices of pie, homemade meals, glasses of beer or wine, soccer games, rock climbs, phone calls, and walks late at night. Thank you for the Skype dates and visits to Canada. Thank you for hours on the microscope in search of the perfect picture. Thank you for talking me down off of cliffs when experiments didn't work and for sharing in my excitement when they did. Thank you for being my cheerleaders and support network.

Table of Contents

Dedication	ii
Acknowledgments	iii
List of Figures	x
Abstract	xiii
Chapter 1. Introduction	1
Genetics	2
Autosomal dominant causes	3
Autosomal recessive causes	10
Genome wide association studies	12
PD Pathogenesis.....	14
α -Synuclein proteostasis	14
α -Synuclein as a prion-like molecule	17
Oxidative stress from defective mitophagy	19
Endolysosomal dysfunction	22
ATP13A2 biology	30
Research objectives	32

Chapter 2. α-Synuclein-Independent Histopathological and Motor Deficits in Mice Lacking the Endolysosomal Parkinsonism Protein <i>Atp13a2</i>	34
Abstract	34
Introduction	35
Results	38
Discussion	57
Materials and Methods	61
Chapter 3. Selective defects in endolysosomal function in <i>Atp13a2</i> null mice	70
Abstract	70
Introduction	71
Results	74
Discussion	87
Materials and Methods	89
Chapter 4. Association between LRRK2 and microtubules enhanced by Parkinson disease mutations and kinase inhibition by LRRK2-IN-1	97
Abstract	97
Introduction	98
Results	100
Discussion	120
Materials and Methods	124

Chapter 5. Conclusions	129
Endolysosomal dysfunction in PD	130
α -Synuclein in PD-related neurodegeneration	133
<i>Atp13a2</i> null mice as a new model of PD-related neurodegeneration	135
LRRK2, microtubules, and the endolysosomal system	136
References	139

List of Figures

Figure

1.1	PD-related genes converge on the endolysosomal and autophagic pathways	15
1.2	Predicted topology of human ATP13A2 structure with location of KRS-linked mutations.....	31
2.1	Generation of <i>Atp13a2</i> null mice	40
2.2	<i>Atp13a2</i> null mice display age-related motor abnormalities	41
2.3	<i>Atp13a2</i> null CNS tissue exhibits widespread age-dependent gliosis	43
2.4	<i>Atp13a2</i> null neurons accumulate lipofuscin and lipid droplets	46
2.5	Age-dependent accumulation of lysosomal proteins and lipids in the <i>Atp13a2</i> null CNS	48
2.6	Abnormal accumulation of ubiquitin-positive aggregates, but absence of α -synuclein-related pathology in <i>Atp13a2</i> null mice	50
2.7	No alteration to tau levels or localization in 18-month-old <i>Atp13a2</i> null mice	51
2.8	Midbrain dopaminergic neurons and Purkinje cells do not degenerate in <i>Atp13a2</i> null mice	53
2.9	Genetic modulation of α -synuclein levels does not affect the onset or extent of histopathology in <i>Atp13a2</i> null mice	55

2.10	Summary of the progression of behavioral and neuropathological changes in <i>Atp13a2</i> null mice	58
3.1	Lysosomal processing of p62 is abnormal in <i>Atp13a2</i> null CNS tissue	75
3.2	Lysosomal processing of cathepsin D is abnormal in <i>Atp13a2</i> null CNS tissue	77
3.3	Isolated lysosomes from <i>Atp13a2</i> null tissue have decreased cathepsin D levels, but normal proteolytic activity	79
3.4	Isolated lysosomes from <i>Atp13a2</i> null tissue have normal proteolysis of α -synuclein	81
3.5	Mitochondria from <i>Atp13a2</i> null CNS tissue have normal oxygen consumption rates.....	84
3.6	Selective increase in late endosome/lysosome lipid BMP in cortical lipid extracts of <i>Atp13a2</i> null tissue.....	86
4.1	Multiple pathogenic mutations enhance LRRK2 oligomerization and filament formation in a kinase-dependent manner	103
4.2	Pattern of expression of LRRK2 using correlated light and EM	106
4.3	Immuno-EM and electron tomography of LRRK2 filaments	107
4.4	LRRK2 filaments associate with microtubules and are modified by microtubule-altering drugs	109
4.5	Kinase dead mutations and loss of the WD40 domain disrupt LRRK2-microtubule association	111

4.6	Inhibition of kinase activity by LRRK2-IN-1 increases LRRK2-microtubule association	114
4.7	Kinetics of LRRK2-IN-1 induced filamentation in LRRK2-G2019S transfected cells	117
4.8	LRRK2 kinase inhibitors show variable effect on LRRK2-microtubule association	119

Abstract

Parkinson disease (PD) is a common, debilitating neurodegenerative disease characterized by profound slowing of movement (bradykinesia), resting tremor, rigidity, and postural instability. Medical therapy of PD is limited to symptom suppression and has not changed substantially in more than forty years, in part because of limited understanding of the mechanisms responsible for PD-related neurodegeneration. Accumulating evidence from genetic and biochemical studies implicate dysfunction of the endolysosomal pathway as a key feature in PD pathogenesis. Most studies have focused on accumulation of neurotoxic alpha-synuclein secondary to defects in autophagy as the cause of neurodegeneration, but abnormalities of the endolysosomal system likely mediate toxicity through multiple mechanisms. To understand how endolysosomal dysfunction causes PD-related neurodegeneration, I conducted *in vivo* and cell biological experiments to examine the effects of PD-associated mutations in the genes *ATP13A2* and *LRRK2* on the endolysosomal system. I generated and characterized a murine model of Kufor-Rakeb syndrome (KRS), a form of early-onset Parkinsonism with additional neurological features caused by recessive loss-of-function mutations in late endosomal/lysosomal protein ATP13A2. I show that *Atp13a2* null mice develop age-related motor abnormalities that are preceded by neuropathological changes including gliosis, accumulation of protein aggregates, lipofuscinosis, and lysosomal abnormalities. Contrary to predictions from *in vitro* data, *in vivo* mouse genetic studies demonstrate that these phenotypes are alpha-synuclein-independent. These

findings indicate that lysosomal dysfunction and abnormalities of alpha-synuclein homeostasis are not synonymous - even in the context of an endolysosomal genetic defect linked to parkinsonism – and highlight the presence of alpha-synuclein-independent neurotoxicity consequent to endolysosomal dysfunction. In addition, I describe a novel interaction between the PD-related protein LRRK2 and microtubules, the main structures responsible for endolysosomal vesicle movement within the cell. Through cell biological studies, I demonstrate that PD-mutant forms of LRRK2 closely associate with microtubules and that loss of LRRK2 kinase activity affects this interaction. As microtubules are necessary for the movement of vesicles within the endolysosomal system, LRRK2 may act as an important signaling molecule on microtubules during vesicular movement. These studies advance our understanding of how PD-related mutations in ATP13A2 and LRRK2 disrupt the endolysosomal system to contribute to PD pathogenesis.

Chapter 1

Introduction

Parkinson disease (PD) is a common, debilitating neurodegenerative disorder, characterized by profound bradykinesia or slowness of movement, resting tremor, muscle rigidity, and postural instability (Dauer and Przedborski, 2003). PD affects 1% of people over 60 years of age (de Rijk et al., 1995), making it the second most common neurodegenerative disease. Patients initially present with motor symptoms such as bradykinesia or tremor, which arise primarily from degeneration of dopaminergic neurons in the substantia nigra pars compacta (SNpC) and can be successfully treated for many years with dopamine replacement strategies (L-3,4-dihydroxyphenylalanine (L-DOPA); Lees et al., 2009). However, PD patients also suffer from non-motor symptoms including dementia and depression, which increase in frequency and severity as degeneration spreads beyond the SNpC. These extra-nigral symptoms are less responsive to dopamine replacement therapy, resulting in profound impairment and morbidity. Medical treatment of PD remains limited to symptom suppression, in part because of a lack of understanding of the mechanisms responsible for PD-related neurodegeneration.

PD is a multifactorial disease, with known genetic factors accounting for approximately 50% of the risk of getting the disease (Hardy, 2010). Over the past 15 years, an increasing number of genes have been found to have a role in familial and sporadic forms of disease. Studies into the function of these implicated genes suggest several hypotheses regarding disease

pathogenesis: 1) altered homeostasis and aggregation of the protein α -synuclein cause selective neurotoxicity; 2) dopaminergic cell death due to increased oxidative stress related to mitochondrial dysfunction. More recent genetic studies identify a third pathway in which endolysosomal dysfunction causes toxicity through an undetermined mechanism. These three pathways are not mutually exclusive and clearly co-occur to varying extents in individual patients. A main site of convergence for the three hypotheses is the autophagic-lysosomal system, which is a major pathway in the cell responsible for clearing both unneeded proteins and damaged mitochondria. Indeed, genetic mutations in lysosomal proteins cause familial forms of PD, highlighting the importance of this pathway in the disease process.

A major, unanswered question is how primary endolysosomal dysfunction results in disease pathogenesis. Specifically, it is unknown 1) how loss of endolysosomal proteins associated with PD cause neuronal toxicity *in vivo* and 2) how α -synuclein and LRRK2, arguably the two most important proteins in PD, contribute to this process. Answering these questions will enhance knowledge of a pathway critical to PD and other neurodegenerative disorders, with the long-term goal of developing novel therapies to limit neuronal injury and disease burden. Therefore, a major goal of my research is to improve our understanding of the connection between primary endolysosomal dysfunction, α -synuclein homeostasis, and neurodegeneration.

Genetics

In 1997, mutations in the gene encoding α -synuclein were linked to a familial form of early-onset PD (Polymeropoulos et al., 1997). Since then, mutations in thirteen additional genes have been linked to familial forms of parkinsonism (Table 1.1) and have implicated new

pathways in disease. Genome-wide association studies have identified additional low-risk genetic variants associated with sporadic disease. While familial forms of the disease constitute less than 5% of PD, known genetic causes account for half of the risk of getting PD (Hardy, 2010), a proportion likely to increase as investigators employ increasingly advanced genetic analyses on large cohorts of PD patients.

Autosomal dominant causes

SNCA

In 1997, the first missense mutation in *SNCA* was identified in the Contursi kindred (Polymeropoulos et al., 1997), with additional *SNCA* missense mutations subsequently identified in other PD kindreds (Kruger et al., 1998; Zarranz et al., 2004). *SNCA* encodes α -synuclein, a synaptic protein consequently found to be highly abundant in Lewy Bodies (LBs), the cytoplasmic, proteinaceous inclusions that are the neuropathological hallmark of idiopathic PD (Spillantini et al., 1997; Spillantini et al., 1998). These studies demonstrated how rare familial forms of PD provide insight into the pathophysiology of more common, sporadic disease. Over the past 15 years, familial early-onset PD has been linked to duplication and triplication events involving the *SNCA* gene (Singleton et al., 2003; Chartier-Harlin et al., 2004; Farrer et al., 2004; Ibanez et al., 2004; Nishioka et al., 2006; Ahn et al., 2008; Ibanez et al., 2009; Sekine et al., 2010), with comparable increases in mRNA and insoluble protein levels (Miller et al., 2004). Copy number of the *SNCA* gene correlates with disease severity, as patients with triplication events develop symptoms earlier than patients with *SNCA* duplication, with more severe dementia, and with more extensive LB pathology in cortical regions (Devine et al., 2011). Together, these genetic linkage studies show that increased levels of the normal α -synuclein

protein are sufficient to cause disease. Clinically, patients with *SNCA* mutations most often present with L-DOPA-responsive, late-onset PD, with an earlier age of symptom onset (Papapetropoulos et al., 2001) and earlier dementia (Muentner et al., 1998; Nishioka et al., 2006). Neuropathologically, *SNCA* mutations are associated with typical PD pathology, including SNpC dopaminergic degeneration and prominent, α -synuclein-positive LBs in the brainstem and neocortical regions (Gwinn-Hardy et al., 2000b).

Table 1.1. Genes linked to familial Parkinson disease (PD) and syndromes with prominent parkinsonism (PD plus).

Locus	Mode of Inheritance	Gene	Protein product	Protein function	Clinical phenotype (age of onset)	Pathology	Citations (first reported)
PARK1/4	AD	<i>SNCA</i>	α -synuclein	Synaptic protein	Early/late onset PD (30s triplication, 40/50s duplication, 30-60s missense)	LB +	Polymeropoulos (1997) Singleton (2003)
PARK8	AD	<i>LRRK2</i>	Leucine-rich repeat kinase 2	GTPase/kinase	Late onset PD (50s)	Pleomorphic, most LB +	Paisan-Ruiz (2004); Zimprich (2004)
PARK17	AD	<i>VPS35</i>	Vacuolar protein sorting 35 homolog	Subunit of retromer complex	Late onset (40-50s)	Unknown	Vilarino-Guell (2011); Zimprich (2011)
	AD	<i>DNAJC13</i>	Receptor mediated endocytosis 8	Regulates clathrin coats on endosomes	Late onset (60s)	Unknown	Vilarino-Guell (2013)
	AD	<i>GBA</i>	Glucocerebrosidase	Lysosomal enzyme	Late onset PD (late 50s), homozygosity associated with Gaucher's	LB +	Goker-Alpan (2004)
PARK2	AR	<i>PARKIN</i>	Parkin	E3 ligase – involved in mitophagy	Early onset PD (20-30s)	Pleomorphic, most LB -	Kitada (1998)
PARK6	AR	<i>PINK-1</i>	Pten-induced kinase 1	Mitochondrial kinase	Early onset PD	1 case - LB +	Valente (2004)
PARK7	AR	<i>DJ-1</i>	DJ-1	Peptidase, oxidative stress sensor	Early onset PD	Unknown	Bonifati (2003)
PARK9	AR	<i>ATP13A2</i>	ATP13A2	Lysosomal ATPase	Juvenile onset PD plus - myoclonus, dementia, psychosis, gaze palsy (teens)	Unknown	Ramirez (2006)
PARK14	AR	<i>PLA2G6</i>	A2 phospho-lipase	Membrane remodeling	Early-onset dystonia-parkinsonism (20s). Commonly associated with NBIA	LB +, tau +, iron deposits	Paisan-Ruiz (2009)
PARK15	AR	<i>FBXO7</i>	F-box protein 7	Ubiquitin protein ligase complex – involved in mitophagy	Juvenile onset PD with pallido-pyramidal symptoms (Late teens)	Unknown	Shojaee (2008)
	AR	<i>DNAJC6</i>	Auxilin	Endocytosis	Juvenile onset PD (7 – 11 years)	Unknown	Edvardson (2013) Koroglu (2013)
	AR	<i>PANK2</i>	Pantothenate kinase 2	Coenzyme A synthesis	Early onset PD (20s), commonly associated with NBIA	LB -, Ub +, iron deposits	Hayflick (2003)
	AR	<i>SYNJ1</i>	Synaptotjanin 1	Endocytosis	Early onset PD plus – seizures, dystonia, cognitive changes (20s)	Unknown	Krebs (2013) Quadri (2013)

AD autosomal dominant, AR autosomal recessive. LB Lewy Body, NBIA neurodegeneration with brain iron accumulation.

LRRK2

First described in 2004, autosomal dominant mutations in *LRRK2*, the gene encoding leucine-rich repeat kinase 2 (LRRK2), are the most common cause of familial PD (Paisan-Ruiz et al., 2004; Zimprich et al., 2004). LRRK2 is a large protein that contains multiple protein-protein interaction domains and GTPase and kinase domains. Five mutations segregate clearly with disease (R1441C, R1441G, Y1699C, G2019S, and I2020T; Cookson, 2010), all of which cluster within the GTPase domain (R1441C/G), the kinase domain (G2019S, I2020T), or the short linker between the two (Y1699C). Additional mutations (N1437H, R1441H) have been suggested as causative in familial PD (Mata et al., 2005; Zabetian et al., 2005; Aasly et al., 2010) and variants (R1628P, G2385R) are risk factors in sporadic disease (Cookson, 2012). The most common mutation, G2019S, is responsible for 2% of sporadic PD and 5% of familial PD in Northern European populations (Houlden and Singleton, 2012). It is especially prominent in select populations, with frequencies of ~20% in Ashkenazi PD patients and ~40% of North African Berber Arab PD patients (Lesage et al., 2006; Ozelius et al., 2006), likely stemming from a common founder effect (Kachergus et al., 2005; Lesage et al., 2005). Clinically, *LRRK2* mutations cause L-DOPA responsive PD, with onset in the 50s to 60s (Houlden and Singleton, 2012). Most *LRRK2* patients show LB-positive pathology in the brainstem. However, case reports from patients with non-G2019S mutations show more variable pathology, including pure nigral degeneration without LBs (Hasegawa et al., 2009), prominent tau-positive aggregates (Zimprich et al., 2004), abundant ubiquitin inclusions (Puschmann et al., 2012), and TDP-43-positive pathology (Wider et al., 2010).

VPS35

In 2011, two separate groups used exome sequencing to link the D620N mutation in *VPS35* to multiple families with typical-appearing PD (Vilarino-Guell et al., 2011; Zimprich et al., 2011). In total, D620N mutations have been identified in 12 familial and 3 sporadic PD cases (Vilarino-Guell et al., 2011; Zimprich et al., 2011; Sharma et al., 2012), making *VPS35* a new cause of monogenic PD, but with no pathological data currently available. The protein VPS35 is a crucial component of the retromer, trafficking vesicles from the endosome back to the *trans*-Golgi network (Hierro et al., 2007). VPS35 has also been implicated in Alzheimer disease (AD), suggesting a broader role for VPS35 and retromer in neurodegenerative processes.

DNAJC13

Whole exome sequencing of a large family with autosomal dominant PD led to the recognition of *DNAJC13* mutations as causative of late-onset, autosomal dominant PD (Vilarino-Guell et al., 2013). *DNAJC13* encodes receptor mediated endocytosis 8 (RME-8), a protein localized to the endosomal membrane and involved in vesicle trafficking (see below). Most patients displayed L-DOPA-responsive, late-onset PD (average age of onset: 69 years) with one patient showing symptoms of progressive supranuclear palsy (PSP), a related neurodegenerative disorder classically associated with tau accumulation, but that may also feature α -synuclein aggregation. Neuropathology of four patients showed LB-positive brainstem pathology in three patients and abundant tau deposition consistent with PSP in the fourth (Vilarino-Guell et al., 2013).

GBA

The identification of mutations in the *glucocerebrosidase (GBA)* gene as a strong risk factor for PD stemmed from the observation that relatives of patients with Gaucher's disease had an increased risk for PD. Since 2004, multiple studies have shown that heterozygous carriers of *GBA* mutations have approximately a five-fold risk of developing PD, making *GBA* mutations the most common genetic risk factor for PD (Lwin et al., 2004; Goker-Alpan et al., 2004; Sidransky and Lopez, 2012). The clinical symptoms associated with *GBA* mutations are similar to typical late-onset PD, with patients developing disease in the late 50s (Nichols et al., 2009). Age of onset is slightly reduced compared to sporadic PD (by 6 years; (Nichols et al., 2009), and patients have an increased risk for dementia and hallucinations relative to non-familial PD (Neumann et al., 2009), consistent with *GBA* mutation carriers also having elevated risk for the related dementia with Lewy Bodies (DLB; Mata et al., 2008). Post-mortem examination of brains from *GBA* mutation carriers shows LB-type neuropathology throughout the brain with increased cortical LBs relative to sporadic PD (Neumann et al., 2009), in keeping with the increased rates of dementia and hallucinations.

Other autosomal dominant disorders that may present with parkinsonism

A number of other autosomal dominant disorders include PD or L-DOPA-responsive parkinsonism in their presentation. Mutations in *MAPT*, encoding the protein tau, cause a series of related disorders collectively referred to as frontotemporal dementia with parkinsonism (FTD-P; Wszolek et al., 1992; Lynch et al., 1994; Wilhelmsen et al., 1994; Hutton et al., 1998). High variability exists in clinical presentation, but some families present with more predominant or early parkinsonism (Wszolek et al., 1992; Wilhelmsen et al., 1994), that is frequently less

responsive to L-DOPA than idiopathic PD (van Swieten and Spillantini, 2007). Pathology shows similar variation, with strong frontotemporal atrophy, tau inclusions, and a marked absence of LBs (Wszolek et al., 1992). Mutations in *progranulin* gene (*PGRN*) also cause FTD, with parkinsonism being a later feature (Rademakers et al., 2007).

Parkinsonism is also a rare presentation in families with CAG expansion mutations in *SCA2* and *SCA3* genes, or CGG expansion in *FMRI*. CAG expansions in *SCA2/3* are more commonly associated with spinocerebellar ataxia, but shorter repeats can present with early PD, especially in certain populations (Gwinn-Hardy et al., 2000a; Gwinn-Hardy et al., 2001; Shan et al., 2001; Subramony et al., 2002; Ragothaman et al., 2004). Similarly, low repeat CGG expansion in the *FMRI* gene, more commonly associated with Fragile X-associated tremor/ataxia syndrome, may also present with parkinsonism early in the disease course (Hagerman et al., 2001; Jacquemont et al., 2004; Hall et al., 2009). While no neuropathology has been reported in PD patients with these mutations, the disease mechanism is presumably related to poly-glutamine aggregation (*SCA2/3*: Costa Mdo and Paulson, 2012) or RNA-mediated toxicity (*FMRI*: Renoux and Todd, 2012) rather than disrupting pathways related to idiopathic or common familial PD.

Finally, several other genes have been linked to syndromes that include parkinsonism, but have yet to be independently confirmed: *GCHI* (Hjermind et al., 2006), *EIF4G1* (Chartier-Harlin et al., 2011), and *UCHL* (Leroy et al., 1998). Case reports of neuropathology show LBs and midbrain degeneration, but the data are preliminary (Chartier-Harlin et al., 2011).

Autosomal recessive causes of early-onset, typical PD

Homozygous and compound heterozygous mutations in three genes cause autosomal recessive, early-onset familial PD: *PARK2* (or *PARKIN* gene; Kitada et al., 1998), *PINK1* (Valente et al., 2004), and *DJ-1* (Bonifati et al., 2003). Mutations in *PARK2* are the most common, responsible for up to half of familial, early-onset PD (Kann et al., 2002), while mutations in *PINK1* and *DJ-1* are less common (1-8% and 1-2% respectively, of early-onset cases; Bonifati, 2014). In one study, the average age of onset for all three was around 25 years (Kilarski et al., 2012), though late-onset cases do rarely occur (Lucking et al., 2000). Symptoms in these patients typically progress more slowly than for sporadic PD, remain confined largely to motor symptoms, with dementia being an unusual feature (Ahlskog, 2009), though rare atypical presentations include increased psychiatric symptoms (Samaranch et al., 2010) or pronounced early dementia (Annesi et al., 2005). Pathology in the majority of cases consists of relatively pure nigral degeneration without LBs (Poulopoulos et al., 2012), but rare α -synuclein-positive LBs have been identified in both *PARK2* (Farrer et al., 2001; Pramstaller et al., 2005) and *PINK1* (Samaranch et al., 2010) patients. Neuropathological findings have not been reported for patients with *DJ-1* mutations. All three proteins are believed to be important in protecting cells from mitochondrial dysfunction and oxidative stress (see below).

Autosomal recessive causes of juvenile, atypical parkinsonism

Rare, autosomal recessive mutations in several genes result in clinical syndromes that include early onset or juvenile parkinsonism, often in association with other neurological signs. Loss-of-function mutations in *ATP13A2* (or *PARK9*), which encodes a late endosomal ATPase of unknown function, cause Kufor-Rakeb Syndrome (KRS), a juvenile, L-DOPA-responsive

parkinsonism with accompanying pyramidal signs, dementia, and supranuclear gaze palsy (Ramirez et al., 2006). Age of onset is between 10 to 20 years of age (Ramirez et al., 2006; Di Fonzo et al., 2007; Ning et al., 2008; Behrens et al., 2010; Paisan-Ruiz et al., 2010; Schneider et al., 2010). Neuropathological findings have not been reported. Neuroimaging shows diffuse cerebral and cerebellar atrophy, including of the nigrostriatal pathway (Di Fonzo et al., 2007; Bruggemann et al., 2010; Schneider et al., 2010; Eiberg et al., 2012), with some reports of basal ganglia iron accumulation (Schneider et al., 2010; Chien et al., 2011). Recessive mutations in *FBXO7* (or *PARK15*) cause a Parkinsonian-pyramidal syndrome whose features include juvenile-onset parkinsonism with variable responsiveness to L-DOPA, as well as additional motor symptoms like muscle weakness and spasticity (Shojaee et al., 2008; Di Fonzo et al., 2009). Neuropathological findings have not been reported.

More recently, mutations in the genes *DNAJC6* and *SYNJ1* were identified by whole exome sequencing as causative of familial forms of juvenile parkinsonism. *DNAJC6* mutations were linked to disease in two families (Edvardson et al., 2012; Koroglu et al., 2013). The six described patients suffered from juvenile-onset parkinsonism (age of onset: 7 to 11 years old) with one family also showing additional neurological features (Koroglu et al., 2013). The same homozygous mutation (R258Q) in *SYNJ1* was found independently in two families (Krebs et al., 2013; Quadri et al., 2013) with early onset parkinsonism (age of onset: early 20s) and generalized seizures (Krebs et al., 2013) or dystonia and cognitive changes (Quadri et al., 2013). All four described patients with *SYNJ1* mutations had to stop L-DOPA therapy due to the rapid development of severe dyskinesias. Neuropathological findings have not been reported, but neuroimaging of *SYNJ1* patients showed diffuse cerebral atrophy (Quadri et al., 2013). *DNAJC6*

and *SYNJ1* encode for auxilin and synaptojanin 1, respectively, proteins involved in clathrin-mediated endocytosis (see below).

Other syndromes have atypical presentations that can include parkinsonism. Recessive mutations in the *phospholipase A2, group VI (PLA2G6 or PARK14)* gene or the *pantothenate kinase (PANK2)* gene cause juvenile-onset infantile neuroaxonal dystrophy and neurodegeneration associated with brain iron accumulation (Hayflick et al., 2003; Morgan et al., 2006). The classic presentation of these disorders occurs before 5 years of age and features prominent dystonia, spasticity, and ataxia. Patients with variants of the disease can present with later onset (age: 20s to 30s), L-DOPA-responsive dystonia-parkinsonism with psychiatric symptoms, dementia, and pyramidal signs (Zhou et al., 2001; Paisan-Ruiz et al., 2009; Paisan-Ruiz et al., 2010). Neuropathologically, both *PLA2G6* and *PANK2* patients show iron accumulation in the basal ganglia. Post-mortem studies show that *PLA2G6* mutation carriers develop widespread LB and tau pathology, especially prominent in the neocortex (Paisan-Ruiz et al., 2012). *PANK2* mutation carriers show more prominent changes in the globus pallidus, with a lack of LB pathology and prominent ubiquitin and tau aggregates (Kruer et al., 2011; Li et al., 2012a).

Genome-wide association studies

Recent work has utilized genome-wide association studies (GWAS) as a complementary approach to identify common genetic variants associated with risk of sporadic disease. Two initial studies found four genes strongly predictive of PD risk in the general population (Satake et al., 2009; Simon-Sanchez et al., 2009). Unsurprisingly, *SNCA* was the first locus identified, confirming the importance of α -synuclein in disease pathogenesis. These studies suggest that

even a 10% increase in *SNCA* levels can result in a 40% increase in disease risk in the general population (Fuchs et al., 2008; Simon-Sanchez et al., 2009). Variation in the *LRRK2* locus also associated with disease risk in both studies, though it is unclear if this reflects the high prevalence of previously identified *LRRK2* mutations in the general population (described above) or a new mechanism by which variation in *LRRK2* expression influences disease. More interestingly, *MAPT*, the gene encoding tau, was strongly associated with disease risk. Familial mutations in *MAPT* cause FTD-P (Hutton et al., 1998) and tau pathology is frequently seen in, though not pathognomonic for, PD. The identification of *MAPT* as a modifier of risk in sporadic PD therefore implicates tau aggregation in PD pathogenesis and links PD to other tauopathies like FTD-P and AD. Satake et al. (2009) identified a novel locus, *PARK16*, which further study has refined to the *RAB7LI* gene, as a modifier of disease risk (Gan-Or et al., 2012; MacLeod et al., 2013). Follow-up studies with more power identified a strong association between variation at the major histocompatibility complex (*HLA*) locus and PD risk (Hamza et al., 2010; Saiki et al., 2010). The identification of *HLA* as a PD-related gene likely reflects how variability in immune response to damage can contribute to disease. GWAS studies of other neurodegenerative diseases have similarly found that changes to the innate response impacts disease risk (Klein et al., 2005; Harold et al., 2009; Lambert et al., 2009). Together, the GWA studies reinforce the importance of *SNCA* and *LRRK2* in both familial and sporadic disease, highlight a potentially more prominent role for tau, and uncover a new gene (*RAB7LI*) in the endolysosomal pathway implicated in PD pathogenesis.

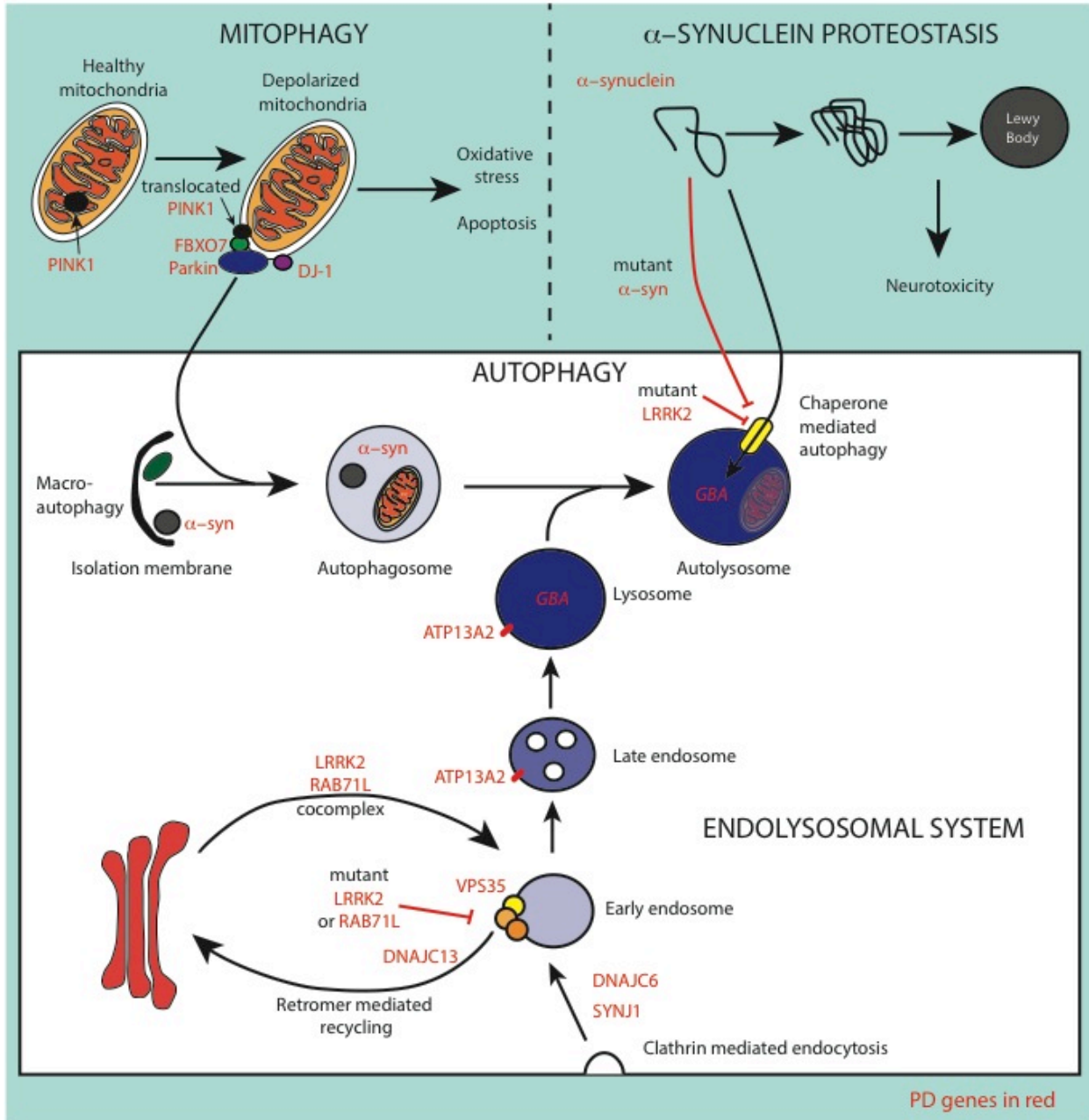
PD pathogenesis

α-Synuclein proteostasis

α -Synuclein's prominent role in PD pathogenesis has been extensively studied (for review, see Cookson, 2005; Lee and Trojanowski, 2006; Gupta et al., 2008; Kalia et al., 2013). Genetically, mutations in *SNCA* cause familial PD, while GWAS show that common variations in the *SNCA* locus associate with elevated risk for sporadic disease (Satake et al., 2009; Simon-Sanchez et al., 2009). Furthermore, the number of genetic copies of *SNCA* correlates positively with disease severity and inversely with age of onset in familial PD (Devine et al., 2011). Post-mortem tissue from both sporadic and familial PD patients shows that α -synuclein aggregates into intraneuronal LBs (Spillantini et al., 1997) and LB spread correlates with extra-nigral symptoms like dementia and hallucinations (Irwin et al., 2013). These studies from human patients suggest that increased levels of α -synuclein cause PD-related neurodegeneration (Figure 1.1).

α -Synuclein is a small, membrane-associated protein whose normal function important to synaptic vesicle release (reviewed in Bendor et al., 2013). Its natively unfolded structure makes it particularly aggregation prone and PD-related mutant forms of the protein are more likely to self-associate (Bertoncini et al., 2005). This aggregation appears key to its neurotoxicity, similar to proteins like amyloid- β and tau that also aggregate to cause toxicity in AD and FTD. Overexpression of α -synuclein in midbrain neuronal cultures results in selective dopaminergic toxicity (Zhou et al., 2000; Petrucelli et al., 2002; Xu et al., 2002). Multiple transgenic mice overexpressing wild type or A53T mutant α -synuclein develop protein aggregates and subsequent neurotoxicity, though the SNpc appears remarkably resistant to cell death (Masliah et al., 2000; Giasson et al., 2002; Lee et al., 2002). More recent work suggests that oligomeric

Figure 1.1. PD-related genes converge on the endolysosomal and autophagic pathways. Genes important in familial and sporadic PD (shown in red) encode many proteins involved in the degradation of damaged mitochondria (or mitophagy), α -synuclein proteostasis, or the endolysosomal system.



and/or fibrillar α -synuclein are the principle toxic species. Addition of preformed α -synuclein fibrils to primary neurons can induce α -synuclein aggregation and cell death (Luk et al., 2009; Volpicelli-Daley et al., 2011), while injection of oligomeric or fibrillar α -synuclein into mouse brains can cause *in vivo* neurotoxicity and LB-like protein aggregates (Winner et al., 2011; Luk et al., 2012a; Luk et al., 2012b). The precise mechanism of α -synuclein-mediated toxicity remains obscure, though its aggregation causes widespread dysfunction including of protein degradation pathways, mitochondria function, membrane dynamics and programmed cell death (Cookson and van der Brug, 2008).

α -Synuclein is in part degraded by autophagy, both by macroautophagy (Webb et al., 2003) and chaperone-mediated autophagy (CMA; Cuervo et al., 2004), particularly during times of cell stress (Ebrahimi-Fakhari et al., 2011). Disruption of autophagy results in increases in α -synuclein, either by pharmacologic inhibition in cell culture models (Webb et al., 2003; Cuervo et al., 2004) or through genetic decrease of key autophagic proteins *in vivo* (Ebrahimi-Fakhari et al., 2011; Ahmed et al., 2012; Friedman et al., 2012). Mutant forms of α -synuclein block CMA (Martinez-Vicente et al., 2008) while aggregates impair macroautophagy (Tanik et al., 2013). This inhibition creates a positive feedback loop whereby mutant or aggregated α -synuclein prevents its own degradation, leading to further aggregation and greater autophagy inhibition. The lysosomal protease cathepsin D is a likely candidate for a cellular synucleinase (Sevlever et al., 2008; Crabtree et al., 2013) and cathepsin D knockout mice show increased α -synuclein insolubility and aggregates (Qiao et al., 2008; Cullen et al., 2009). Furthermore, a functional interaction between α -synuclein and LRRK2 occurs at the lysosome (Orenstein et al., 2013). *GBA* mutations appear to increase levels of α -synuclein by disrupting lysosomal function (Mazzulli et al., 2011). These findings suggest that PD-related mutations in other proteins disrupt

α -synuclein homeostasis by impairing its autophagic clearance, potentially providing a unifying mechanism for several genetic causes of the disease. Indeed, increasing autophagic flux either chemically or genetically protects against α -synuclein-mediated toxicity *in vivo* (Decressac et al., 2013; Xilouri et al., 2013). Autophagy is therefore an attractive therapeutic target to reduce the impact of α -synuclein-mediated neurodegeneration in PD patients. The details of autophagic dysfunction in PD remain unclear, including whether it is a cause or consequence of α -synuclein aggregation.

α -Synuclein as a prion-like molecule

Emerging work suggests that α -synuclein may transit between cells in a prion-like fashion, providing a plausible mechanism for the hypothesis of spreading pathology in PD posited by Braak et al. (Braak et al., 2003), though much work remains to test this hypothesis more rigorously (Burke et al., 2008). Interest in this mechanism was ignited by two reports of LBs in fetal neurons grafted into the striata of PD patients (Kordower et al., 2008a; Kordower et al., 2008b; Li et al., 2008). The presence of α -synuclein aggregates in grafted neurons suggested either that the toxic environment in late stages of disease promoted intracellular α -synuclein aggregation in healthy donor cells or that misfolded α -synuclein spread from neighboring cells to seed aggregation. *In vitro* studies are consistent with the possibility that cells can release (Lee et al., 2005) and take up α -synuclein (Lee et al., 2008; Luk et al., 2009; Nonaka et al., 2010; Waxman and Giasson, 2010; Volpicelli-Daley et al., 2011), together promoting the cell-to-cell spread of toxic species. *In vivo* work from Virginia Lee and colleagues demonstrated that injected α -synuclein fibrils can be taken up by cells and template endogenous α -synuclein into misfolded, toxic protein aggregates (Luk et al., 2012a; Luk et al., 2012b). This prion-like

hypothesis has important implications for both pathogenesis and therapeutics. It implies that not just intracellular protein levels but also the release and uptake of α -synuclein between neurons are important aspects of disease pathogenesis. Therapeutically, this pool of extracellular α -synuclein would present a seemingly tractable target, being more accessible than intracellular protein and, if removed, could halt the intercellular spread of disease processes.

Prion-like propagation requires both the release and uptake of α -synuclein by cells. Under basal conditions, a small amount of α -synuclein is released into the extracellular space (Lee et al., 2005; Hansen et al., 2011), an amount that increases under conditions of misfolded proteins (Jang et al., 2010). α -Synuclein is present in both cerebrospinal fluid and plasma of patients (El-Agnaf et al., 2003; Emmanouilidou et al., 2010) and oligomeric α -synuclein is elevated in the plasma of PD patients (El-Agnaf et al., 2006). Cell culture experiments suggest that α -synuclein is secreted through non-classical exocytosis (Lee et al., 2005; Emmanouilidou et al., 2010; Alvarez-Erviti et al., 2011), likely because of its ability to associate with and translocate into multiple components of the endolysosomal pathway, including recycling endosomes (Hansen et al., 2011), exosomes (Emmanouilidou et al., 2010), and secretory vesicles (Lee et al., 2005). Chemical or genetic modulation of autophagy, in either direction, causes a corresponding change in α -synuclein release (Ejlerskov et al., 2013; Lee et al., 2013). Similarly, preventing lysosome fusion or autophagosome movement along microtubules leads to increased secretion of α -synuclein (Ejlerskov et al., 2013). As less α -synuclein is degraded by autophagy, flux through the endolysosomal pathway seems to shunt more of it into exocytosis. PD patients, who have both increased α -synuclein burden and defects in autophagy, may therefore have increased release of α -synuclein into the extracellular space. Independent of controlled α -synuclein release by cells, processes during cell injury and death may also cause dying cells to

spill intracellular α -synuclein into the extracellular space, further increasing extracellular α -synuclein burden.

Uptake of α -synuclein similarly relies upon vesicular transport through the endolysosomal pathway. Addition of recombinant α -synuclein to cultured cells is taken up via endocytosis (Danzer et al., 2007; Danzer et al., 2009; Luk et al., 2009; Nonaka et al., 2010; Waxman and Giasson, 2010), but requires high concentrations of recombinant protein, raising questions of physiological relevance. Higher order oligomers enter the cell more readily than lower order species (Danzer et al., 2007) as does α -synuclein associated with exosomes rather than free protein (Danzer et al., 2012). Volpicelli-Daley et al. recently approached more physiological conditions in which they incubated primary neurons with preformed α -synuclein fibrils (Volpicelli-Daley et al., 2011). The fibrils were successfully endocytosed by the cells and templated cytosolic, endogenous α -synuclein into insoluble aggregates that eventually induced neuronal dysfunction and cell death. Increased concentration of fibrils resulted in greater endocytosis and intracellular aggregation seeding, highlighting the importance of both α -synuclein levels and oligomer state. However, the cell culture and *in vivo* experiments described have had to utilize extremely high concentrations of α -synuclein over a short time frame that causes an overload of normal cellular degradation pathways. These conditions are unlikely to reflect human pathogenesis, making it too soon to know the relevance of these findings to human disease.

Oxidative stress from defective mitophagy

A second major pathway implicated in PD is the defective clearance of damaged mitochondria through autophagy, or mitophagy (Figure 1.1), reviewed extensively elsewhere

(Dauer and Przedborski, 2003; Banerjee et al., 2009). Both sporadic and familial PD patients have increased oxidative damage and mitochondrial dysfunction relative to controls (Hauser and Hastings, 2013). Poisons such as MPTP cause rare cases of human disease by inhibiting respiratory chain activity, increasing reactive oxygen species and selectively killing dopaminergic cells (Langston et al., 1983). As pacemaker cells, dopaminergic SNpC neurons have especially high metabolic activity (Surmeier et al., 2012), a greater number of mitochondria, and a smaller threshold for oxidative damage (Dauer and Przedborski, 2003). Furthermore, the metabolism of dopamine itself generates both reactive oxygen species and the toxic compound dopamine-quinone (Graham et al., 1978). Thus, any disease process leading to reactive oxygen species may preferentially damage dopaminergic cells. Most human studies, however, are by necessity correlative between mitochondrial damage and end-stage human disease and provide little evidence of primary mitochondrial dysfunction causing PD. The strongest support for the causative role of mitochondrial dysfunction, at least in familial PD, came with examination of the cellular pathways disturbed with mutations in parkin, PINK1, DJ-1, and FBXO7.

Genetic studies using *Drosophila* knockout models first demonstrated that PINK1 functions upstream of parkin in the maintenance of mitochondrial health (Clark et al., 2006; Park et al., 2006). *In vitro* experiments have delineated more of the details. PINK1 normally resides within healthy mitochondria where it is rapidly cleaved by proteases and degraded. Following membrane depolarization, PINK1 accumulates in the outer mitochondrial membrane (OMM; Geisler et al., 2010; Matsuda et al., 2010; Narendra et al., 2010; Vives-Bauza et al., 2010), where it recruits parkin to depolarized mitochondria (Jin et al., 2010; Lazarou et al., 2012). Parkin ubiquitinates mitochondrial surface proteins like mitofusin 1 and 2. Tagged mitochondria are

subsequently engulfed by autophagosomes in a p62-dependent manner and degraded by mitophagy (Gegg et al., 2010; Ziviani et al., 2010). More recently, FBXO7, another familial PD protein, was shown to function in this same pathway, upstream of parkin recruitment and downstream of PINK1 translocation to the OMM (Burchell et al., 2013). DJ-1 likely does not operate in the same pathway as PINK1 and parkin (Thomas et al., 2011; though see also Hao et al., 2010), but does act as a sensor of mitochondrial oxidative stress (Canet-Aviles et al., 2004). Inactivation of DJ-1 causes impairment in mitochondrial complex I activity, production of reactive oxygen species, and injury to mitochondria (Ariga et al., 2013). Thus, these genes all seem to function in common pathways that sense and mitigate mitochondrial damage and oxidative stress.

Other PD-related proteins, including α -synuclein, glucocerebrosidase, and ATP13A2, also affect mitochondria health and function. α -Synuclein interacts with mitochondrial membranes in overexpression cell models and *in vivo* resulting in decreased ATP production, increased free radical production, and increased mitochondrial fragmentation (Devi et al., 2008; Chinta et al., 2010; Nakamura et al., 2011). Transgenic mice overexpressing α -synuclein develop greater mitochondrial defects compared to controls when treated with the complex I inhibitor MPTP (Song et al., 2004). Mitochondria from glucocerebrosidase mutant mice similarly show reduced membrane potential and increased fragmentation of mitochondria, presumably because of decreased mitophagy (Osellame et al., 2013). Cell culture experiments suggest that a similar process may occur with loss of ATP13A2. Knockdown of *Atp13a2* in primary neurons causes an increase in mitochondrial mass and fragmentation, along with increased oxygen consumption and reactive oxygen species production (Gusdon et al., 2012). These mitochondrial changes appear due to poor mitophagy, rather than a primary mitochondrial defect, as they mimic defects

seen with autophagy inhibitors (Gusdon et al., 2012). Mutations in α -synuclein and glucocerebrosidase cause broad cellular dysfunction. Mitochondrial dysfunction, therefore, is likely not a selective deficit, but may reflect the overall deteriorating health of dying cells. It is unknown if *ATP13A2* mutations cause widespread dysfunction or are selective to defects in mitophagy.

As more genes and pathways are identified in PD, it seems likely that mitophagy dysfunction does not play a causative role in sporadic disease, even if it does contribute to the later stages of cell death. Clinically, the disease linked with *PARKIN*, *PINK1*, and *DJ-1* mutations is distinct from the classic, idiopathic disease course (Puschmann et al., 2012). In addition to presenting decades earlier than sporadic PD, these mutations cause disease with a predominance of motor symptoms and a distinct lack of non-motor symptoms like cognitive changes. Symptoms progress more slowly than in idiopathic disease and remain L-DOPA responsive for longer. Most importantly, post-mortem tissue shows degeneration confined principally to the brainstem and SNpC and an absence of α -synuclein-positive LBs in all but a few cases. The absence of α -synuclein aggregation, more than anything else, suggests a fundamental difference in pathogenesis with parkin, PINK1, and DJ-1 mutants that may not apply to idiopathic disease.

Endolysosomal dysfunction

More recent PD genetic studies have linked mutations in endolysosomal proteins to familial forms of PD and parkinsonism. These include the lysosomal enzyme glucocerebrosidase (*GBA*), late endosomal/lysosomal ATP13A2 (*ATP13A2*), and many proteins involved in endocytosis and retromer mediated recycling: VPS35 (*VPS35*), synaptojanin 1 (*SYNJI*), RME-8

(*DNAJC13*), auxilin (*DNAJC6*), and RAB7L1 (*RAB7L1/PARK16*). Glucocerebrosidase mutations directly impair lysosomal function, in keeping with the theory that defective α -synuclein or mitochondrial degradation drives disease. ATP13A2, initially thought to be a lysosomal ATPase, may localize instead to the late endosomal compartment (Kong et al., 2014), where mutant forms may either cause autophagy defects (Dehay et al., 2012; Usenovic et al., 2012) or otherwise impair late endosome function. How dysfunction of late endosomes, endocytosis or vesicle recycling contributes to PD pathogenesis needs to be further investigated in the context of both familial and sporadic disease.

The endolysosomal pathway is a complex intracellular membrane system that sorts and transports proteins to allotted destinations. Two of its main functions are: 1) the movement of cargo to/from extracellular space and 2) the degradation of organelles and proteins via autophagy. Several features of neurons and neuronal function may convey particular susceptibility to endolysosomal dysfunction. Effective inter-cellular communication in the nervous system relies on precise control of the levels of membrane-embedded neurotransmitter receptors and transporters. In addition, the unique biophysical properties of neurons, which may bear axons stretching the length of a human leg, require effective intracellular transport great distances from the neuronal cell body. Especially for post-mitotic cells, autophagy is crucial for the degradation of toxic proteins that accumulate with senescence, and as a source of amino acid and lipid building blocks needed to counteract cellular stress.

Movement of vesicles within the endolysosomal system requires accurate fusion and fission of membranes with one another, a process tightly controlled by signaling pathways of which Rab GTPases are key regulators (for review see Ng and Tang, 2008; Stenmark, 2009). Within the endolysosome system, different Rab proteins label distinct membranous

compartments and facilitate cargo movement by recruiting relevant signaling molecules. Evidence implicating Rab proteins in PD came initially from yeast screens designed to identify modifiers of toxicity induced by α -synuclein overexpression. α -Synuclein overexpression can cause dysfunction in ER to Golgi trafficking (Willingham et al., 2003; Cooper et al., 2006) and in retrograde transport from endosomes to Golgi (Soper et al., 2011), presumably by binding to vesicular membranes and preventing correct protein recruitment or vesicular movement. Overexpressing endolysosomal proteins Rab1, Rab3, and Rab8 rescue α -synuclein-mediated toxicity in neurons by offsetting impairments in ER to Golgi trafficking (Cooper et al., 2006; Gitler et al., 2009). Work in cell culture and post-mortem tissue has since demonstrated a physical interaction between α -synuclein and other Rab proteins, including Rab3 (Dalfo et al., 2004), Rab5 (Sung et al., 2001), and Rab11 (Liu et al., 2009). At least for Rab3, the association is stronger between higher molecular weight α -synuclein species and the Rab protein, suggesting a gain of function in disease state (Dalfo et al., 2004). These studies generally employed marked overexpression of α -synuclein, which may lead to association with membranes and related proteins that do not occur *in vivo*. Future experiments that more closely reflect *in vivo* conditions will be needed to determine the endolysosomal compartments affected by α -synuclein function in normal and disease states. Other familial PD genes suggest three aspects of the endolysosomal system potentially important in PD pathogenesis: clathrin-mediated endocytosis, retromer mediated recycling, and the autophagic-lysosomal pathway.

Clathrin-mediated endocytosis

In addition to physically interacting with the synaptic vesicle-associated Rab3 (Dalfo et al., 2004) and endosomal Rab5 (Sung et al., 2001), α -synuclein overexpression also causes a

reduction in the recycling pool of synaptic vesicles (Nemani et al., 2010; Scott and Roy, 2012) causing a decrease in presynaptic dopamine release (Nemani et al., 2010). LRRK2 physically interacts with Rab5 to mediate synaptic vesicle endocytosis in primary neurons (Shin et al., 2008; Heo et al., 2010), suggesting that vesicle recycling might be a common location for LRRK2 and α -synuclein function.

The recent identification of mutations in synaptojanin 1 (*SYNJI*) and auxilin (*DNAJC6*) in families with early onset parkinsonism further implicates alterations in clathrin-mediated endocytosis in PD. Both proteins are necessary for effective endocytosis of clathrin-coated vesicles (McMahon and Boucrot, 2011). Auxilin is recruited to vesicles by phosphatidylinositol (4,5)-bisphosphate (PIP₂) and works in concert with Hsc70 to uncoat vesicles (Ungewickell et al., 1995). Synaptojanin 1 is the main neuronal PIP₂ phosphatase, is enriched at synapses, and is similarly necessary in both the endocytosis and uncoating of vesicles (Mani et al., 2007). Individuals with Down Syndrome (DS), who carry an extra chromosomal copy of *SYNJI*, as well as DS mouse models, show enlarged endosomes, which are normalized following *SYNJI* silencing (Cossec et al., 2012). Furthermore, synaptojanin 1 has been implicated in AD (Berman et al., 2008). Hemizygoty of *Synj1* in mice rescues AD behavioral and synaptic phenotypes (McIntire et al., 2012), likely by altering the flux of amyloid precursor protein (APP) away from the endosome and towards lysosomal degradation (Zhu et al., 2013). It is unknown how mutations in *SYNJI* and *DNAJC6* cause parkinsonism, but recessive inheritance and loss of phosphatase activity with the R58Q synaptojanin 1 mutation (Krebs et al., 2013) suggest a loss of function mechanism.

Alterations in synaptic clathrin-mediated endocytosis may lead to decreased availability of vesicles for dopamine with corresponding increases in extra-vesicular dopamine at the

synapse. Increased dopamine within the synapse could react with reactive oxygen species to form toxic species. Endocytosis changes could also affect the membrane localization of other pre- or post-synaptic proteins at the nigrostriatal synapse (Cheng et al., 2011; Kisos et al., 2014) or affect the uptake of α -synuclein during prion-like transmission. Finally, disruption of clathrin-mediated endocytosis may have still to be determined effects on vesicle trafficking that may affect intracellular α -synuclein levels, signaling cascades, or synaptic function.

Retromer mediated recycling

Recently, two independent studies showed an interaction between several PD-related proteins in vesicle trafficking between the *trans*-Golgi network (TGN) and endosomes. Both studies began by looking for genes and proteins that interact with LRRK2, either genetically or physically and both identified the Rab GTPase, Rab7L1, whose gene is one of five within the *PARK16* locus, as functioning in a common pathway with LRRK2. MacLeod et al. found that variation in the *RAB7L1* gene interacts with *LRRK2* to influence risk of sporadic PD (MacLeod et al., 2013). Rab7L1 overexpression rescues mutant LRRK2 neurodegenerative phenotypes in both primary neurons and *Drosophila*. To understand the cellular function of these two proteins, MacLeod et al. showed that LRRK2 and Rab7L1 function in a common pathway where loss of either protein causes lysosomal swelling and decreased recycling of the cation-independent mannose-6-phosphate receptor (CI-MPR) to the TGN. Loss of LRRK2 or Rab7L1 caused decreased levels of the retromer proteins VPS35 and VPS26, likely accounting for the decreased recycling of CI-MPR. The PD-related proteins VPS35 and RME-8 both function in retromer-mediated recycling, further implicating this pathway in PD pathogenesis.

In a complementary study, Beilana et al. used unbiased protein-protein interaction arrays to show that LRRK2 forms a co-complex with Rab7L1, Cyclin-G-associated kinase (GAK), and Bcl2-associated athanogene (BAG5) (Beilana et al., 2014). In overexpression studies *in vitro*, this co-complex mediates the clearance of the *trans*-Golgi network via autophagy, which initially seems the inverse of the results from MacLeod et al. However, experimental differences make direct comparisons difficult between the two. Importantly, two independent screens looking for genetic or physical interactors of LRRK2 both identified Rab7L1 as a LRRK2-interacting protein. Most likely, the two proteins function (perhaps in conjunction with GAK, BAG5, and/or retromer) to coordinate the movement of vesicles between endosomes and TGN. Disruption of this complex results in a relative increase in flux from TGN to lysosomes, but whether this increase occurs from enhancement of forward trafficking or inhibition of retrograde trafficking is unclear. How this retromer-mediated recycling contributes to PD pathogenesis requires more cell biological and *in vivo* studies. Retromer proteins are decreased in post-mortem tissue from AD patients (Small et al., 2005), causing increased retention and cleavage of APP into toxic amyloid β in the endosomal compartment (Small and Gandy, 2006). A comparable process is unlikely to happen with α -synuclein in PD, but perhaps a relative increase in flux to the lysosome affects α -synuclein degradation or aggregation through another mechanism.

Autophagic-lysosomal pathway

Autophagy is one of two major degradation pathways in the cell. It allows the delivery of cytosolic components to the lysosome for degradation and recycling. Macroautophagy (Figure 1.1) occurs when a double membrane vesicle sequesters a large portion of the cytosol and then fuses with a lysosome or late endosome to mediate the degradation of its contents (Yang and

Klionsky, 2010). Microautophagy involves a small invagination of the cytosol directly into the lysosome (Uttenweiler and Mayer, 2008). Finally, CMA is a process whereby proteins with KFERQ motifs are bound to Hsc70 and translocated across the lysosomal membrane by the lysosomal membrane protein LAMP2A (Kaushik and Cuervo, 2012).

Autophagy was first implicated in PD pathogenesis in studies of α -synuclein proteostasis. α -Synuclein degradation is incompletely understood. The ubiquitin-proteasome system, macroautophagy, and CMA all can degrade α -synuclein, but the relative proportion of α -synuclein degraded by these pathways is unclear, and changes depending on folding state, cellular localization, or oligomeric state of α -synuclein, and the presence of cellular stressors (Webb et al., 2003; Cuervo et al., 2004; Ebrahimi-Fakhari et al., 2011). α -Synuclein itself can inhibit macroautophagy (Winslow et al., 2010) and CMA (Cuervo et al., 2004) blocking the degradation of itself and other proteins. Inhibition of autophagy upregulates the ubiquitin-proteasome and vice versa, providing crosstalk between the various intracellular pathways (Ebrahimi-Fakhari et al., 2011). One unifying theory, widely embraced, is that an upstream event either promotes α -synuclein aggregation or inhibits autophagy, creating a positive feedback loop between autophagic deficits and α -synuclein aggregation ultimately leading to cell death.

One prediction from this theory is that other PD-related proteins could initiate this feedback loop by disrupting autophagic function. *In vitro*, LRRK2 has been found on the membranes of multivesicular bodies and autophagic vacuoles, with a PD-mutant LRRK2 causing incomplete autophagic degradation (Alegre-Abarategui et al., 2009). The *Drosophila* LRRK2 homolog physically interacts with Rab7 to position lysosomes (Dodson et al., 2012). LRRK2 null mice develop age-related impairment of autophagy in the kidney, resulting in α -synuclein aggregation (Tong et al., 2010). Yet, further study showed that autophagy is initially increased in

younger LRRK2 null animals (Tong et al., 2012), making it unclear if LRRK2 serves a primary function in autophagy or if the autophagic changes observed were secondary to other cellular defects.

Mazzulli et al. (2011) provide the most compelling evidence for a positive feedback loop between autophagy disruption and α -synuclein aggregation using PD-related mutations in glucocerebrosidase. Loss of glucocerebrosidase function caused a disruption of lysosomal degradation both *in vitro* and *in vivo*, causing the accumulation of α -synuclein, and corresponding neurotoxicity. Aggregating α -synuclein caused further impairment of lysosomal function, completing the loop (Mazzulli et al., 2011). *In vitro* work suggests a similar mechanism for mutations in *ATP13A2* (Dehay et al., 2012; Usenovic et al., 2012). Whether other endolysosomal proteins implicated in PD have similar effects on autophagic function and α -synuclein aggregation is unknown and will be important to elucidate pathogenesis.

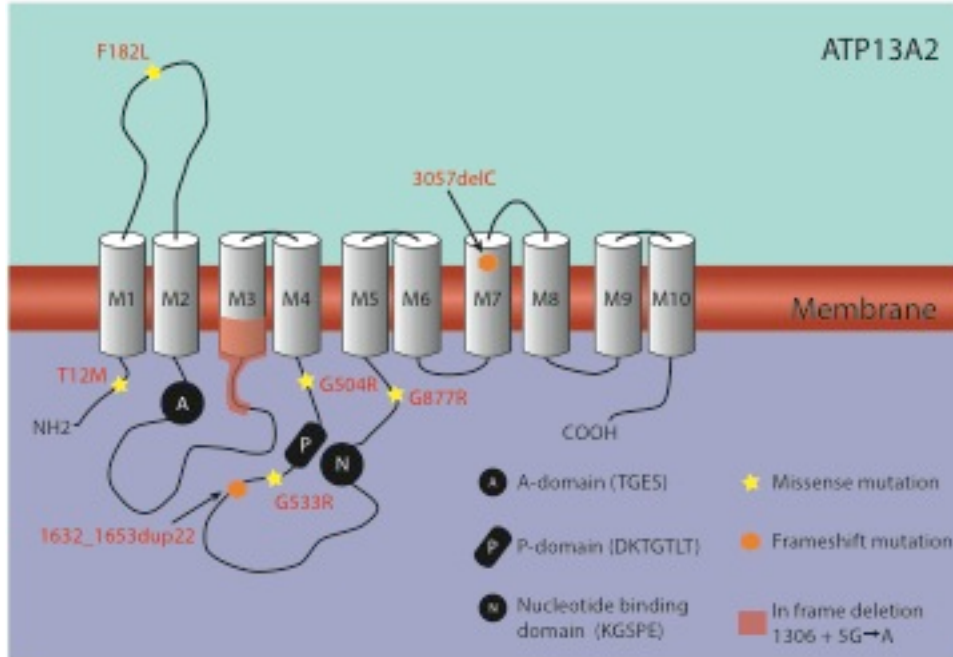
The discovery of PD-related mutations in multiple endolysosomal proteins suggests several lines of inquiry important for future study. First, it will be important to understand the specific steps in the endolysosomal pathway that are affected by mutations in these proteins and delineate the subsequent sequence of pathogenic events. Vesicle trafficking has predominantly been examined in the context of α -synuclein accumulation and transmission. Cell biological and *in vivo* studies are needed to clarify if, and how, primary dysfunction of the lysosome, late endosome, retromer, or endocytic pathway causes neurodegeneration. Perhaps most pressing is to what extent and how these various pathways interact. Some preliminary studies, primarily in cell culture, suggest overlap between α -synuclein homeostasis, mitochondrial dysfunction, and/or vesicle trafficking, but no work has demonstrated *in vivo* if these pathways converge on a

common endpoint or operate in parallel to one another. Depending on the degree of interaction, it will be important to identify early sites of dysfunction as points of maximal therapeutic intervention. For example, if lysosomal dysfunction is ‘upstream’ of both α -synuclein aggregation and oxidative stress, then normalizing lysosomal function early in the disease course may limit later sequelae like spreading α -synuclein pathology or non-motor symptoms.

ATP13A2 biology

ATP13A2 is a P-type ATPase of unknown function that localizes to the lysosome (Ramirez et al., 2006) and/or late endosome (Podhajska et al., 2012), though recent work with antibody against the endogenous protein raises questions as to precisely which of the two compartments it localizes to (Kong et al., 2014). In addition to the established association with juvenile-onset KRS (described above), mutations have been linked to a family with early-onset neuronal ceroid lipofuscinosis (NCL; Bras et al., 2012) and a form of NCL in Tibetan terriers (Farias et al., 2011; Wohlke et al., 2011). Mutations likely cause loss of function of the ATP13A2 protein as they have recessive inheritance patterns (Ramirez et al., 2006; Di Fonzo et al., 2007; Bras et al., 2012; Eiberg et al., 2012), include early frame-shift mutations or large, in frame deletions (Ramirez et al., 2006).

Figure 1.2. Predicted topology of human ATP13A2 structure with location of KRS-linked mutations. As a P-type ATPase, ATP13A2 has 10 transmembrane domains with an actuator domain (A-domain), catalytic phosphorylation site domain (P-domain), and nucleotide binding domain. Disease-linked mutations include frameshift mutations (orange hexagon), missense mutations (yellow stars), or an in-frame exon skipping (pink shading).



Phylogenetically, ATP13A2 is related to ion transporters and lipid flippases (Schultheis et al., 2004). It likely functions in the endolysosomal membrane compartments to transport heavy metals or alter lipid composition of membrane, though its exact function and substrate remain unclear. *In vitro* studies have tenuously linked it to the transport of multiple heavy metals (Gitler et al., 2009; Tan et al., 2011; Covy et al., 2012; Podhajska et al., 2012; Tsunemi and Krainc, 2013). ATP13A2 knockdown in cell culture causes increased lysosome size and number, autophagic deficits, modestly elevated levels of α -synuclein, and neurotoxicity (Dehay et al., 2012; Usenovic et al., 2012). In a recent report, *Atp13a2* null mice show mild behavioral abnormalities, increased autofluorescence indicative of lipofuscinosis, and modest increases in insoluble α -synuclein (Schultheis et al., 2013).

Several features make *ATP13A2* an excellent candidate gene for probing the link between endolysosomal dysfunction and PD pathogenesis. Human patients with KRS present with prominent early parkinsonism (age of onset: 10-20 years old), and with additional neurological features suggestive of widespread neurodegeneration. The presence of behavioral abnormalities in both a dog (Farias et al., 2011; Wohlke et al., 2011) and mouse model of the disease (Schultheis et al., 2013) suggests that the neurodegenerative processes occur within the lifespan of a mouse, making it easier to model than other PD-related genes, which have been largely unrevealing (Dawson et al., 2010). The changes to autophagy and α -synuclein proteostasis *in vitro* (Dehay et al., 2012; Usenovic et al., 2012) coincide with pathogenesis occurring in a time frame amenable to study. Establishment of a *Atp13a2* null mouse model will allow the careful dissection of the behavioral, pathological, and endolysosome biological changes that result in PD-related neurodegeneration.

Research objectives

Despite recent genetic and biochemical understanding of the link between endolysosomal biology and PD, it remains unclear how primary endolysosomal dysfunction results in disease pathogenesis. A better knowledge of the mechanisms underlying neurotoxicity is necessary to pursue more directed therapeutic strategies that halt or reverse PD progression. My research seeks to address this gap in knowledge by concentrating on two major questions. The first objective is to establish a novel mouse model in which primary endolysosomal dysfunction results in clear behavioral and neuropathological phenotypes consistent with PD-related neurodegeneration. In Chapter 2, I present a new mouse model in which the PD-related gene *Atp13a2* has been knocked out, resulting in age-related motor abnormalities and progressive

neuropathology including gliosis, lipofuscinosis, and protein accumulation. I then demonstrate via biochemical and genetic studies that these pathological changes are independent of α -synuclein proteostasis. Chapter 3 then addresses the mechanisms by which loss of *Atp13a2* results in these behavioral and pathological phenotypes and shows the accumulation of autophagic substrates and selective changes to cathepsin D maturation. As a secondary objective, Chapter 4 explores a novel interaction between the PD-related protein LRRK2 and microtubules, the main structures responsible for endolysosomal vesicle movement within the cell. Taken together, these results provide new understanding into the mechanisms by which mutations in *ATP13A2* and *LRRK2* result in neurodegeneration and PD.

Chapter 2

α -Synuclein-Independent Histopathological and Motor Deficits in Mice Lacking the Endolysosomal Parkinsonism Protein *Atp13a2*¹

Abstract

Accumulating evidence from genetic and biochemical studies implicate dysfunction of the autophagic-lysosomal pathway as a key feature in the pathogenesis of Parkinson disease (PD). Most studies have focused on accumulation of neurotoxic α -synuclein secondary to defects in autophagy as the cause of neurodegeneration, but abnormalities of the autophagic-lysosomal system likely mediate toxicity through multiple mechanisms. To further explore how endolysosomal dysfunction causes PD-related neurodegeneration, I generated a murine model of Kufor-Rakeb syndrome (KRS), characterized by early-onset Parkinsonism with additional neurological features. KRS is caused by recessive loss-of-function mutations in the *ATP13A2* gene encoding the late endosomal/lysosomal ATPase ATP13A2. I show that *Atp13a2* null mice develop age-related motor abnormalities that are preceded by neuropathological changes including gliosis, accumulation of ubiquitinated protein aggregates, lipofuscinosis, and lysosomal abnormalities. Contrary to predictions from *in vitro* data, *in vivo* mouse genetic

¹ This chapter was submitted for publication, in combination with part of Chapter 3, as Kett LR, Bernath M, Stiller B, Tasset I, Blesa J, Jackson-Lewis V, Chan RB, Di Paolo G, Przedborski S, Cuervo AM, Dauer WT. α -Synuclein-Independent Histopathological and Motor Deficits in Mice Lacking the Lysosomal Parkinsonism Protein *Atp13a2*.

studies demonstrate that these phenotypes are α -synuclein-independent. Our findings indicate that lysosomal dysfunction and abnormalities of α -synuclein homeostasis are not synonymous - even in the context of a lysosomal genetic defect linked to parkinsonism – and highlight the presence of α -synuclein-independent neurotoxicity consequent to endolysosomal dysfunction.

Introduction

Parkinson disease (PD) is a common, debilitating neurodegenerative disease characterized by profound slowing of movement (bradykinesia), resting tremor, rigidity, and postural instability. Symptoms are linked to degeneration of dopaminergic neurons in the substantia nigra pars compacta (SNpC; Dauer and Przedborski, 2003). Patients also suffer from gait abnormalities and non-motor symptoms such as depression and dementia, which relate to extranigral degeneration; these symptoms are unresponsive to dopamine replacement and cause significant morbidity. Medical therapy of PD is limited to symptom suppression and has not changed substantially in more than forty years, in part because of limited understanding of the mechanisms responsible for PD-related neurodegeneration.

Autophagic-lysosomal pathway (ALP) dysfunction is increasingly recognized as a key element of disease pathogenesis. α -Synuclein, which forms characteristic protein aggregates (Lewy Bodies) in PD and other neurodegenerative diseases, is degraded in part by the ALP (Webb et al., 2003; Cuervo et al., 2004). Familial PD has been linked to genetic mutations in α -synuclein and several endolysosomal proteins, including glucocerebrosidase (Aharon-Peretz et al., 2004; Sidransky et al., 2009), VPS35 (Vilarino-Guell et al., 2011; Zimprich et al., 2011), Rab7L1 (Satake et al., 2009; Simon-Sanchez et al., 2009; MacLeod et al., 2013), synaptojanin 1 (Krebs et al., 2013; Quadri et al., 2013), and ATP13A2 (Ramirez et al., 2006). Disruption of

lysosomal glucocerebrosidase, encoded by *GBA*, causes ALP dysfunction, α -synuclein accumulation, and neurotoxicity (Mazzulli et al., 2011). These studies suggest a common mechanism by which ALP dysfunction may cause PD: autophagic dysfunction leading to α -synuclein accumulation and neurotoxicity. Yet, few studies of lysosomal proteins have directly tested this hypothesis and loss of most lysosomal proteins causes accumulation of substrates other than α -synuclein suggesting additional mechanisms through which ALP dysfunction can cause neurodegeneration.

Recessive mutations in *ATP13A2*, the gene encoding late endosomal/lysosomal ATP13A2, cause Kufor-Rakeb Syndrome (KRS; Ramirez et al., 2006), an autosomal-recessive form of L-DOPA-responsive juvenile parkinsonism with additional neurological features, including pyramidal signs, dementia, psychosis, supranuclear gaze palsy, and myoclonus (Najim al-Din et al., 1994; Williams et al., 2005; Ramirez et al., 2006; Di Fonzo et al., 2007; Behrens et al., 2010; Bruggemann et al., 2010; Fong et al., 2011; Santoro et al., 2011). No neuropathological data exists from human patients, though a recent study of *Atp13a2* null mice showed increased autofluorescence in multiple brain regions (Schultheis et al., 2013), indicative of increases in the storage material lipofuscin. Neuroimaging of KRS subjects demonstrates diffuse cerebral and cerebellar atrophy (Behrens et al., 2010; Bruggemann et al., 2010). A recessive mutation in canine *ATP13A2* causes adult-onset neuronal ceroid lipofuscinosis (NCL) in Tibetan terriers (Farias et al., 2011; Wohlke et al., 2011). Affected terriers display brain atrophy and behavioral changes with diffuse lipofuscinosis (Farias et al., 2011), but SNpC histopathology was not commented upon specifically.

ATP13A2 is a Type 5 P-type ATPase of unknown function. A loss-of-function mechanism of disease pathogenesis is suggested by the recessive inheritance pattern and *in vitro*

studies showing that mutant proteins do not traffic correctly to the lysosome (Park et al., 2011; Podhajska et al., 2012). ATP13A2 knockdown in cell culture causes increased lysosome size and number, reduced protein degradation through the ALP, modestly elevated levels of α -synuclein, and neurotoxicity (Dehay et al., 2012; Usenovic et al., 2012).

To dissect the relationship between endolysosomal dysfunction, α -synuclein accumulation, and neurodegeneration in the context of parkinsonism, I generated and characterized *Atp13a2* null mice. I hypothesized that *Atp13a2* null mice would recapitulate key features of KRS and the molecular abnormalities identified *in vitro*, including endolysosomal dysfunction, α -synuclein accumulation, neurotoxicity, and consequent behavioral abnormalities. Consistent with this hypothesis, *Atp13a2* null mice exhibit age-related motor deficits accompanied by widespread gliosis, endolysosomal abnormalities, increased lipofuscin deposits and ubiquitinated protein aggregates. Strikingly, loss of *Atp13a2* caused no α -synuclein-related abnormalities in mice up to 18 months old, including absence of α -synuclein aggregates, no increase in high molecular weight species or change in steady state α -synuclein levels. Moreover, modulating α -synuclein levels by intercrossing *Atp13a2* null mice with α -synuclein null or overexpressing transgenic lines did not change the onset or extent of pathological changes observed in *Atp13a2* null mice. These findings highlight that α -synuclein homeostasis may remain normal in the presence of significant disruption of the endolysosomal system, and emphasize that ALP dysfunction, even when provoked by Parkinson-related triggers, can cause neurotoxicity through α -synuclein-independent mechanisms.

Results

*Generation of *Atp13a2* null mice.*

To investigate the relationship between endolysosomal dysfunction and PD-related neurodegeneration, I generated *Atp13a2* null mice and examined these animals for relevant behavior and histopathological abnormalities. Insertion of LoxP sites around exons 2 and 3 generated *Atp13a2*-flx mice. Crossing *Atp13a2*-flx mice to a Rosa-Cre mouse that expresses Cre in the germline resulted in *Atp13a2* null mice (Figure 2.1A). RT-PCR analysis and cDNA sequencing of RNA derived from these animals confirmed the expected recombination, and deletion of *Atp13a2* mRNA (Figure 2.1B). *Atp13a2* protein levels were not examined due to lack of specific *Atp13a2* antibodies.

**Atp13a2* null mice have decreased spontaneous movement and develop abnormal movements*

All *Atp13a2* genotypes were obtained in Mendelian ratios (84 wild type, 150 heterozygous, 87 *Atp13a2* null mice, total 321; $\chi^2 = 1.43$, d.f. = 2, $p = 0.49$). Initially indistinguishable from littermate controls, 18-month-old *Atp13a2* null mice adopted abnormal clasping positions during tail suspension (Figure 2.2A). While wild type mice reflexively kicked their limbs and rarely exhibited any form of limb clasping, a significant proportion of *Atp13a2* null mice clasped their rear limbs, a behavior unseen in any mice at 12 months of age. To further characterize the temporal profile of motor abnormalities in these mice, I tested a cohort of 13 null and 16 wild type littermate male mice every three months from 9 to 18 months of age in tests of motor behavior, including open field, balance beam and accelerating rotarod. Three null mice died during the study at 6, 12, and 13 months of age. The 12-month old mouse died of an eye infection; the other two died of unknown causes. In the open field, *Atp13a2* null mice displayed

decreased spontaneous horizontal movement relative to wild type littermates (2-way repeated measures ANOVA: $F_{\text{genotype}}(1, 21) = 7.09$; $p = 0.015$; $F_{\text{time}}(3, 63) = 1.31$; $p = 0.28$; $F_{\text{interaction}}(3, 63) = 0.16$; $p = 0.92$; Figure 2.2B). No significant difference was observed in the number of rears (2-way repeated measures ANOVA: $F_{\text{genotype}}(1, 21) = 3.69$; $p = 0.069$; $F_{\text{time}}(3, 63) = 1.83$ $p = 0.15$; $F_{\text{interaction}}(3, 63) = 0.054$; $p = 0.98$; Figure 2.2C). No significant differences between *Atp13a2* null and littermate control mice were observed in balance beam or Rotarod testing up to 18 months of age (Figure 2.2D). To determine the selectivity of the motor abnormalities, I assessed the mice in the Morris water maze, a test of learning and memory. At 9 months of age, *Atp13a2* null mice had no deficits locating the hidden platform both during the learning (Figure 2.2E top) and memory (Figure 2.2E bottom) components of the Morris water maze. *Atp13a2* null mice located a visible platform in the same time as wild type mice, indicating no alteration in motor ability at this age (data not shown).

Figure 2.1. Generation of *Atp13a2* null mice. **A**, Targeting strategy to generate *Atp13a2* null mice. Diagram shows the *Atp13a2* locus and insertion of LoxP sites around exons 2 and 3. Crossing to a mouse that expresses Cre recombinase in the germline resulted in deletion of exons 2 and 3 and the insertion of a premature stop codon in exon 4. **B**, Levels of *Atp13a2* cDNA generated from RNA isolated from 6-month old wild type, heterozygous, or *Atp13a2* null mouse brain (left). cDNA sequencing of *Atp13a2* locus shows successful recombination resulting in a premature stop codon (right).

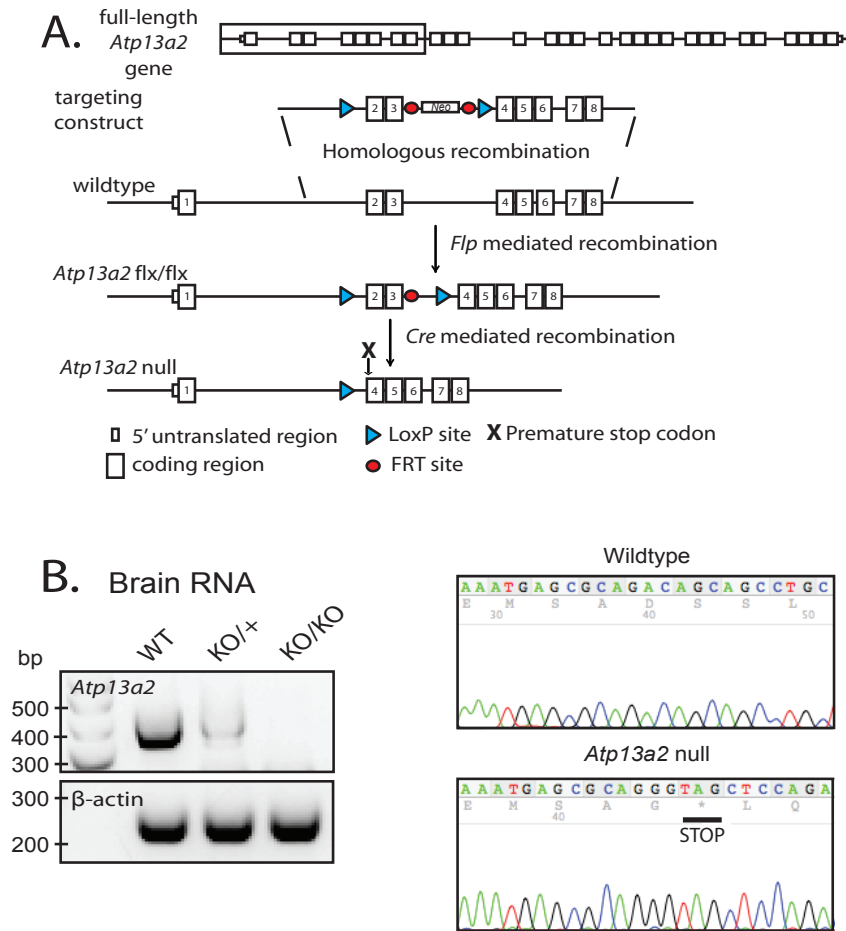
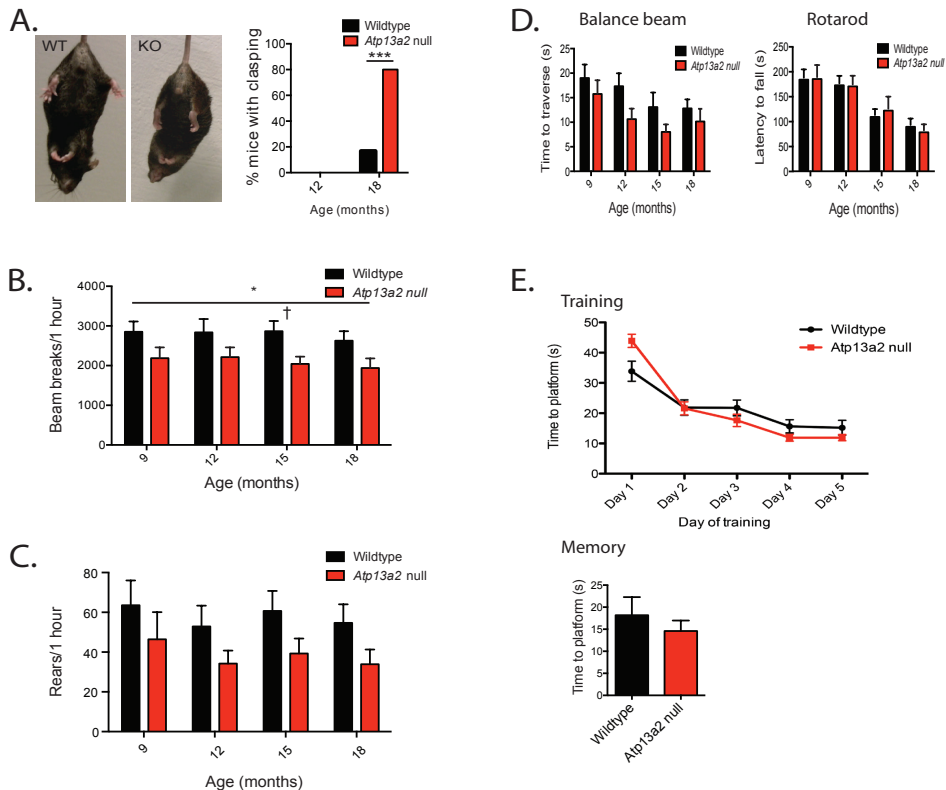


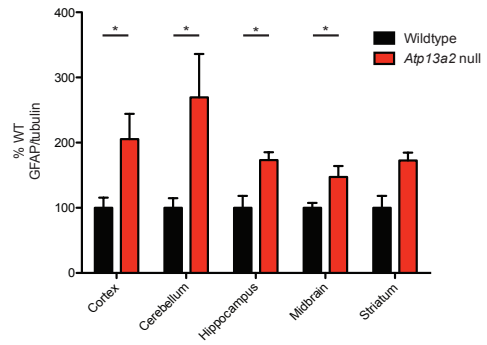
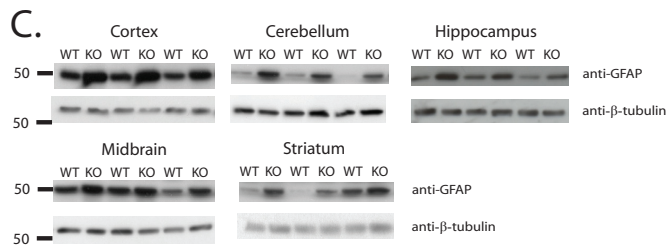
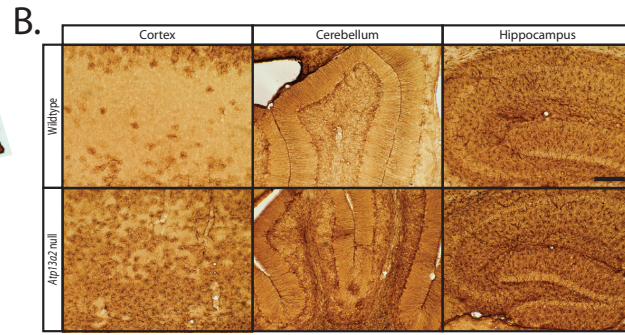
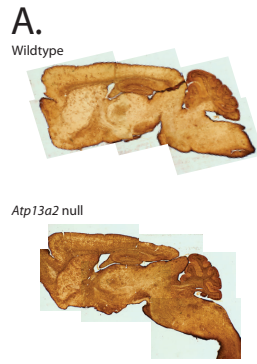
Figure 2.2. *Atp13a2* null mice display age-related motor abnormalities. **A**, 18-month-old wild type (left) or *Atp13a2* null mouse (right) during tail suspension. *Atp13a2* null mice adopted abnormal claspings position, which was quantified as the percentage of mice displaying claspings at 12 months and 18 months ($\chi^2 = 7.27$, $N = 18$ wild type, 15 *Atp13a2* null, $p < 0.05$). **B**, Spontaneous beam breaks during 1 hour in the open field apparatus. Wild type and *Atp13a2* null mice were tested every 3 months from 9 months to 18 months of age, with beam breaks measured in five-minute bins for 1 hour. There was an effect of genotype but not of time (Repeated measures ANOVA: $F_{\text{genotype}}(1, 21) = 7.09$; $p = 0.015$; $F_{\text{time}}(3, 63) = 1.31$; $p = 0.28$; $F_{\text{interaction}}(3, 63) = 0.16$; $p = 0.92$). A Bonferroni's post-hoc test showed decreased movements at 15 months (\dagger ; $t = 2.42$, $p = 0.024$). **C**, Spontaneous rears during 1 hour in the open field apparatus. Wild type and *Atp13a2* null mice were tested every three months from 9- to 18-months-old, with rears measured in five-minutes bins for 1 hour. **D**, Wild type and *Atp13a2* null mice were tested for time to traverse a 5 mm balance beam (left) and latency to fall from an accelerating rotarod (right) every three months from 9- to 18-months old. **E**, Wild type and *Atp13a2* null mice were trained over five days to find a hidden platform in the Morris water maze at 9 months of age (top). Six days after training concluded, mice were probed for ability to recall platform location (bottom). $N = 13$ wild type and 17 *Atp13a2* null male mice. Error bars represent SEM; statistically significant differences are indicated (* $p < 0.05$, *** $p < 0.001$).



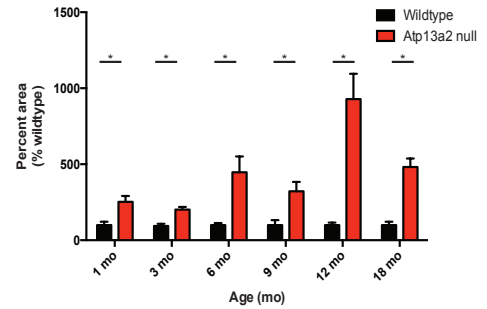
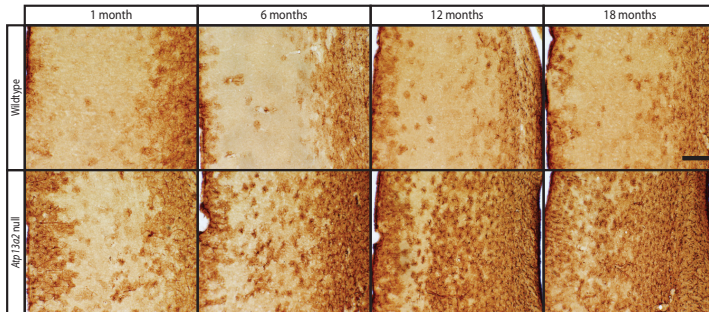
Atp13a2 null mice develop widespread gliosis

The decreased horizontal movements observed in open field testing, in combination with age-related abnormal movements during tail suspension, suggested that *Atp13a2* null mice would exhibit neuropathological changes consistent with PD and KRS, including neuroinflammation, lipofuscinosis, protein aggregation, and accumulation of α -synuclein. I first examined brains from 18-month-old *Atp13a2* null mice and littermate controls, the age of onset of the motor phenotype. I assessed markers of neurodegeneration, lipofuscinosis, and protein aggregation. Aged *Atp13a2* null brains exhibited a pronounced increase in gliosis throughout many brain regions, including, but not limited to, cortex, striatum, hippocampus, cerebellum, thalamus, and midbrain (Figure 2.3A, B). Gliosis was confirmed by Western blot analysis of microdissected brain tissue, with elevated levels of GFAP protein observed in the cortex, cerebellum, hippocampus, and midbrain of *Atp13a2* null brain lysates relative to wild type controls (Figure 2.3C). In contrast to the delayed onset of claspings, gliosis was present in the cortex as early as 1 month of age, though showed the most dramatic increase by 12 months (Figure 2.3D). The GFAP-positive percentage of cortex was increased in *Atp13a2* null mice at all ages relative to their wild type littermates, with a five-fold increase in glial immunostaining at 6 months of age, and a 10-fold increase in glial reactivity by 12 months of age, consistent with an age-related worsening of gliosis. The neuroinflammation was selective for activation of astrocytes as no increase in microglia numbers (as assessed by Iba1) or activation (F4/80) was observed (Figure 2.3E).

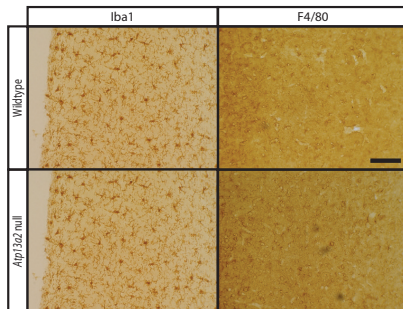
Figure 2.3. *Atp13a2* null CNS tissue exhibits widespread age-dependent gliosis. **A, B,** 40 μ m sagittal sections from 18-month-old wild type (A, above) or *Atp13a2* null (A, below) mouse brains show diffuse GFAP immunoreactivity throughout the brain, including the cortex, cerebellum, and hippocampus. **C,** Quantitative Western blot analysis of GFAP expression in the cortex, cerebellum, hippocampus, midbrain, and striatum of 18-month-old mice; 5 μ g protein loaded/lane; n = 11 wild type and 10 *Atp13a2* null mice. **D,** Immunohistochemistry for GFAP in the cortex of wild type and *Atp13a2* null mice at the indicated ages. Quantification (right) shows percent area of the cortex that is GFAP-positive normalized to wild type tissue of the same age; n = 4 to 8 animals/genotype at each time point. **E,** Immunostaining for microglia number (Iba1) and activation (F4/80) in cortex of 18-month-old wild type or *Atp13a2* null mice. Statistically significant differences are indicated (* p < 0.05). Error bars indicate SEM. Scale bars: **B, D, E,** 200 μ m.



D. Cortex



E. Cortex

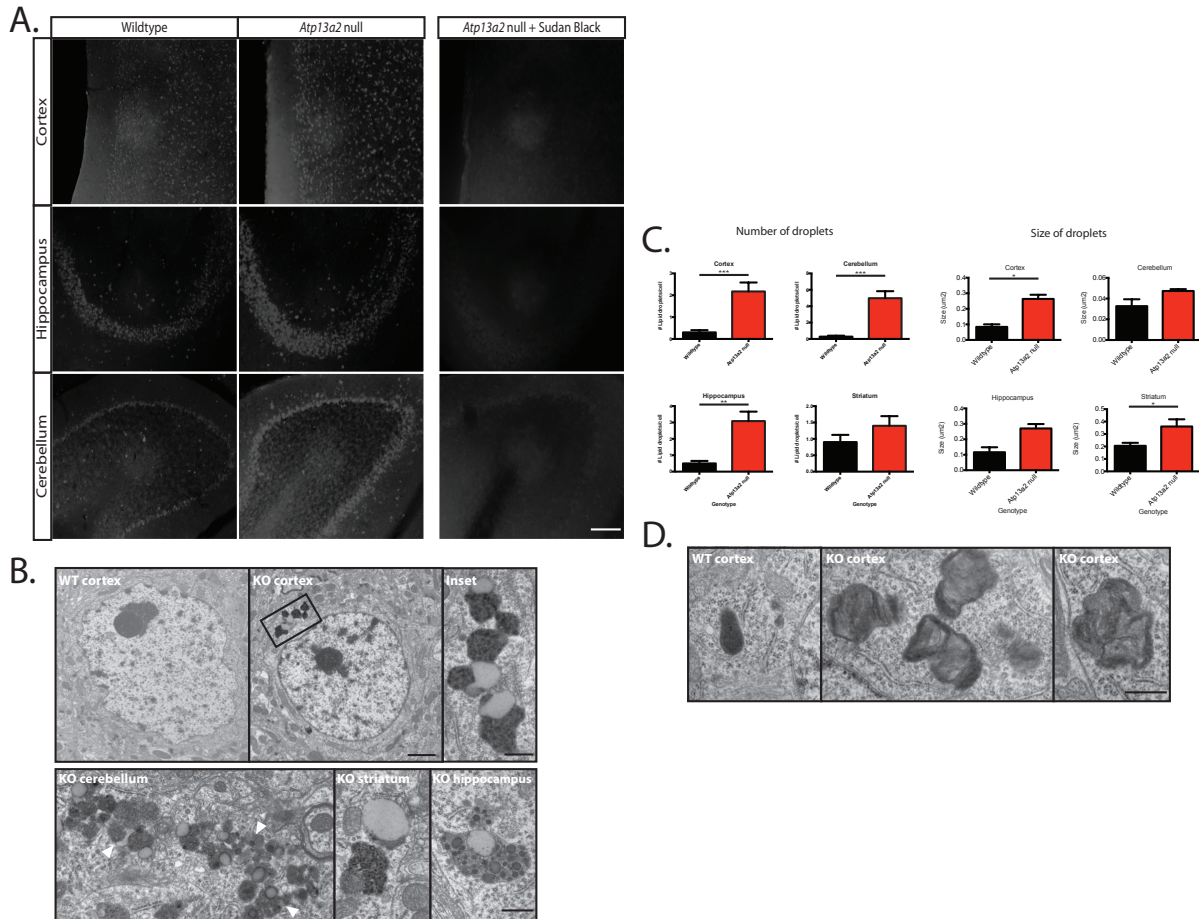


Increased lipofuscinosis and lysosomal markers in Atp13a2 null mice.

Previous studies have suggested increased autofluorescence and lipofuscin deposits with loss of *Atp13a2 in vivo* (Farias et al., 2011; Schultheis et al., 2013). Similar to these previous reports, I observed increased autofluorescence (Figure 2.4A) and lipofuscinosis (Figure 2.4B) in multiple brain regions in *Atp13a2* null mice relative to age-matched wild type controls. The autofluorescence was successfully quenched by treatment with 0.3% Sudan Black in 70% ethanol (Figure 2.4A, right panel), allowing us to perform immunofluorescence in tissue from *Atp13a2* null brains. Animal models of NCL with increased autofluorescence and gliosis, including the Tibetan Terrier model, exhibit lipofuscinosis by electron microscopy (Koike et al., 2000; Gupta et al., 2001; Katz et al., 2005; Katz et al., 2007; Weimer et al., 2009; Farias et al., 2011). To determine whether similar abnormalities occurred in aged *Atp13a2* null mice, I performed electron microscopy on multiple brain regions displaying gliosis and autofluorescence, including cortex, cerebellum, hippocampus, and striatum. Similar to other animal models of NCL, I observed prominent lipofuscin deposits in neurons from all regions displaying autofluorescence and gliosis (Figure 2.4B). The lipofuscin deposits consisted of large, electron dense material, frequently containing membranous structures, in close association with large lipid droplets. Lipid droplets typically contain neutral lipids such as triglycerides and cholesterol esters and are ALP substrates (Singh et al., 2009). Lipid droplets were larger and more numerous in *Atp13a2* null compared to wild type littermate tissue (Figure 2.4C). To clarify the temporal relationship between lipofuscin and gliosis, I performed an EM analysis of cortex from one-month-old tissue, when there is gliosis but no autofluorescence. One-month-old *Atp13a2* null tissue exhibited increases in the number of lipofuscin deposits, but no difference in

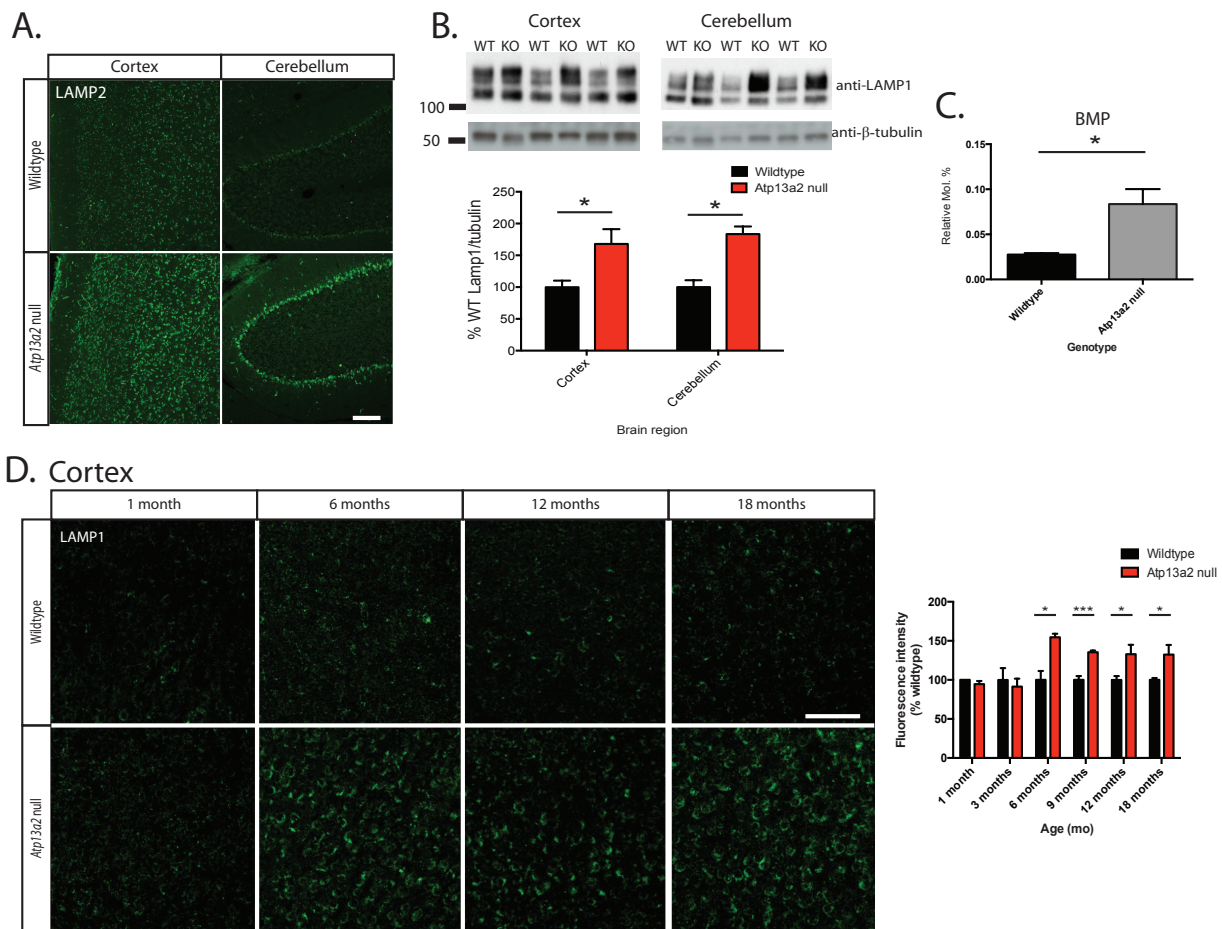
lipid droplets (Figure 2.4D). This analysis suggests a close association between lipofuscin deposition and gliosis, and indicates that abnormalities of lipid homeostasis occur later in the pathogenic cascade.

Figure 2.4. *Atp13a2* null neurons accumulate lipofuscin and lipid droplets. A, Autofluorescence in 40 μm sagittal sections from wild type or *Atp13a2* null mice (18-months-old). Ten-minute incubation with 0.3% Sudan Black in 70% ethanol (right panel) quenched autofluorescence. **B,** Ultrastructural analyses of 12-month-old wild type (top left) or *Atp13a2* null mouse cortex (top middle, right), Purkinje cell of the cerebellum (bottom left), striatum (bottom middle) or hippocampus (bottom right); $n = 40$ neurons/genotype. **C,** Quantification of the number and size of lipid droplets associated with lipofuscin in neurons from 12-month-old wild type and *Atp13a2* null mice; $n = 40$ neurons/genotype. **D,** Ultrastructural analyses of cortex from 1-month-old wild type (left) and *Atp13a2* null mice (middle, right); $n = 40$ neurons/genotype. Scale bars: **A,** 200 μm , **B left, middle,** 2 μm , **B inset, bottom panels, D,** 500 nm.



In vitro studies suggest that loss of ATP13A2 function causes increases in the number and size of lysosomes (Dehay et al., 2012; Usenovic et al., 2012), potentially as compensation for poor lysosomal function. Similar to these reports, I found increases in immunofluorescent staining (Figure 2.5A) and protein levels (Figure 2.5B) of the lysosomal markers LAMP1 and LAMP2. Bis(monoacyl-glyceryl)phosphate (BMP) is a lipid species found exclusively within late endosomes and lysosomes (Kobayashi et al., 1998; Gallala and Sandhoff, 2011) and has been found to accumulate in the lysosomal storage disorder Niemann-Pick type C disease (Chevallier et al., 2008) and AD (Chan et al., 2012). Lipidomic analysis demonstrated increased levels of BMP in 18-month *Atp13a2* null cortical lipid extracts (Figure 2.5C), but no changes in a range of other lipid species (see Chapter 3 for discussion of lipidomic analysis), consistent with a rather selective perturbation of these organelles. These findings are consistent with the previous *in vitro* studies and may reflect compensatory changes in the ALP following improper clearance of lysosomal substrates. Increased LAMP1 immunofluorescence was not observed until six months of age (Figure 2.5D), demonstrating that lysosomal accumulation follows abnormal lipofuscin deposition and gliosis. Although I observed an increase in cortical lipid droplets by ultrastructural analysis, there were no changes to triglycerides and/or cholesterol esters by lipidomic analysis (Triglycerides: wild type mol. % = 0.049 ± 0.002 %, *Atp13a2* null mol. % = 0.053 ± 0.003 %, $t = 1.085$, d.f. = 4, $p = 0.34$; cholesterol esters: wild type mol. % = 1.635 ± 0.577 %, *Atp13a2* null mol. % = 1.694 ± 0.272 %, $t = 0.092$, d.f. = 4, $p = 0.93$).

Figure 2.5. Age-dependent accumulation of lysosomal proteins and lipids in the *Atp13a2* null CNS. **A**, 40 μm sections from 18-month-old *Atp13a2* null or littermate wild type mouse brain sections stained for LAMP2 immunofluorescence in cortex and cerebellum. **B**, Quantitative Western blot analysis of LAMP1 expression in the cortex and cerebellum of 18-month-old mice; 20 μg protein loaded/lane; $n = 7$ wild type and 6 *Atp13a2* null mice. **C**, Levels of the lysosomal lipid bis(monoacylglyceryl)phosphate (BMP) isolated from 18-month-old cortical lipid extracts from wild type and *Atp13a2* null animals; $n = 3$ per genotype. Data are shown as the mean mol %, which was calculated by summing up the total moles of all lipid species and then normalizing the total to mol %. **D**, LAMP1 immunofluorescence of cortex from wild type and *Atp13a2* null mice at the indicated ages. Immunofluorescence was quantified as mean fluorescence intensity for images taken from 5 cortical fields per animal and normalized to wild type tissue of the same age; $n = 4$ animals/genotype at each time point. Statistically significant differences are indicated (* $p < 0.05$, *** $p < 0.001$). Error bars indicate SEM. Scale bars: **A**, **D**, 100 μm .



*Protein aggregation but no α -synuclein abnormalities in *Atp13a2* null mice*

The observed lysosomal abnormalities and *in vitro* studies of ATP13A2 function (Dehay et al., 2012; Usenovic et al., 2012) suggested that proteolysis was disrupted in *Atp13a2* null mice, a situation commonly associated with abnormal deposition of aggregated protein. Consistent with this notion, *Atp13a2* null tissue exhibited large ubiquitin-positive aggregates (Figure 2.6A) most prominently in the cortex and hippocampus, and sparingly in other regions such as the SNpC; such deposits were never observed in wild type tissue. These ubiquitin-positive inclusions co-localized with immunofluorescence for NeuN, but not GFAP or Iba1, indicating a selective localization within neurons (Figure 2.6B). Given the central role of α -synuclein in PD pathogenesis and *in vitro* data linking ATP13A2 function to α -synuclein homeostasis (Dehay et al., 2012; Usenovic et al., 2012), I next assessed aged *Atp13a2* null tissue for changes in α -synuclein levels or aggregation. In contrast to predictions from *in vitro* studies, no α -synuclein-positive aggregates or changes in α -synuclein levels were observed in *Atp13a2* null tissue (Figure 2.6C, D). Furthermore, α -synuclein antibodies did not co-label the ubiquitin-positive inclusions found in 18-month-old *Atp13a2* null mice (data not shown). No difference in α -synuclein solubility was observed in lysates from 18-month-old *Atp13a2* null cortex sequentially extracted in buffers of increasing detergent (Figure 2.6E; high salt, 1% Triton-X, and 1% SDS), consistent with the immunohistochemical and Western blot analyses. The neurodegenerative protein tau also accumulates in both human patients with PD and in mouse models of the disease (Li et al., 2009), especially as pathology spreads to non-nigral regions (Irwin et al., 2013). However, loss of *Atp13a2* did not increase tau levels or localization in 18-month-old mice in any of the brain regions examined (Figure 2.7).

Figure 2.6. Abnormal accumulation of ubiquitin-positive aggregates, but absence of α -synuclein-related pathology in *Atp13a2* null mice. **A**, 40 μ m sections of cortex and hippocampus from *Atp13a2* null or littermate control mouse brains stained for ubiquitin. **B**, Ubiquitin inclusions (shown in red) from *Atp13a2* null mice colocalize with the neuronal marker NeuN, but not GFAP (shown in green). **C**, 40 μ m sections from 18-month-old wild type or *Atp13a2* null mouse brains stained for α -synuclein with tissue from α -synuclein null brain shown as a control. **D**, Quantitative Western blotting of α -synuclein protein levels from multiple brain regions; 5 μ g protein loaded/lane; n = 12 wild type and 10 *Atp13a2* null mice. Error bars indicate SEM. **E**, Sequential extraction of cortical lysates from 18-month-old wild type or *Atp13a2* null mice in either high salt (HS), high salt plus 1% Triton-X100 (HS + Tx), or 1% SDS lysis buffer; n = 3 per genotype. Scale bars: **A**, 200 μ m, **B**, 50 μ m, **C**, 400 μ m.

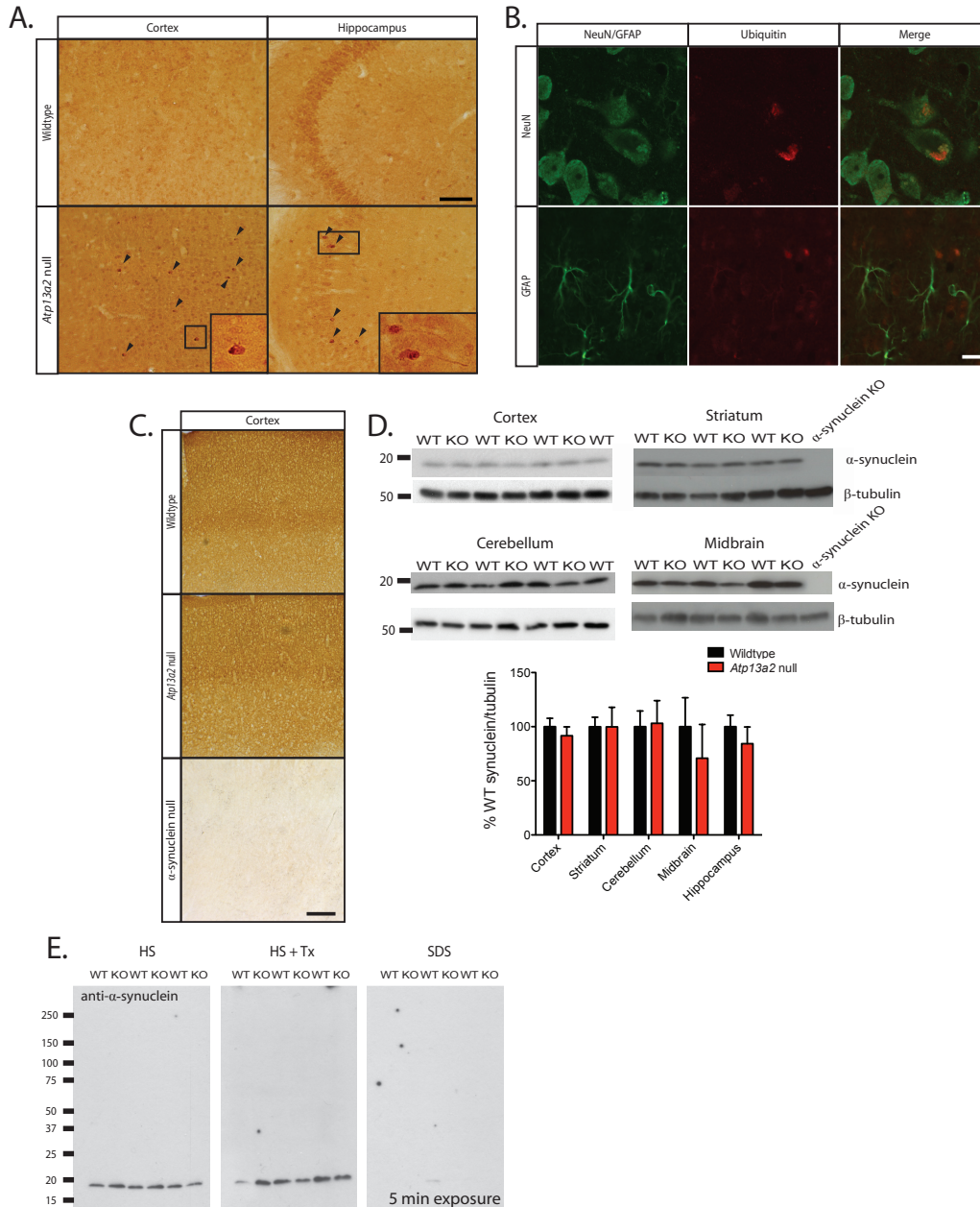
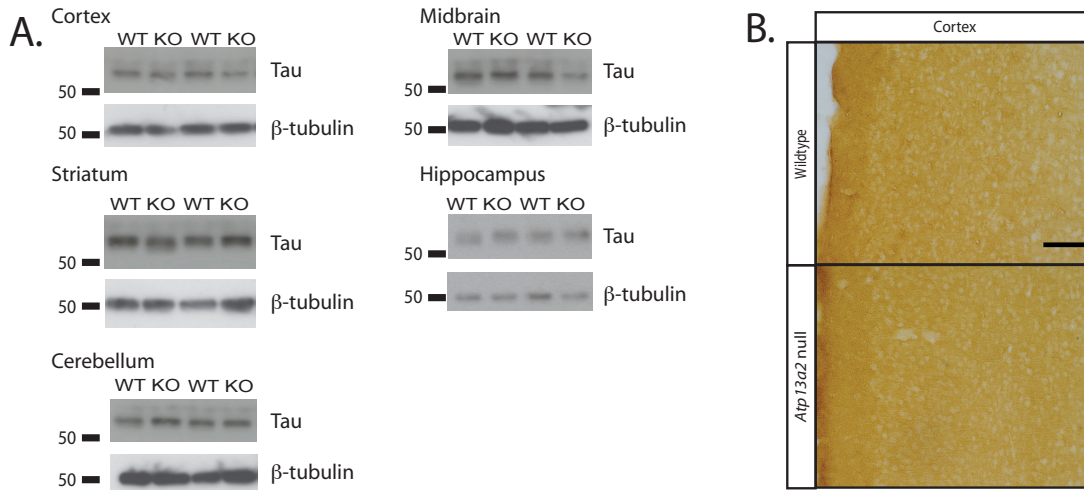


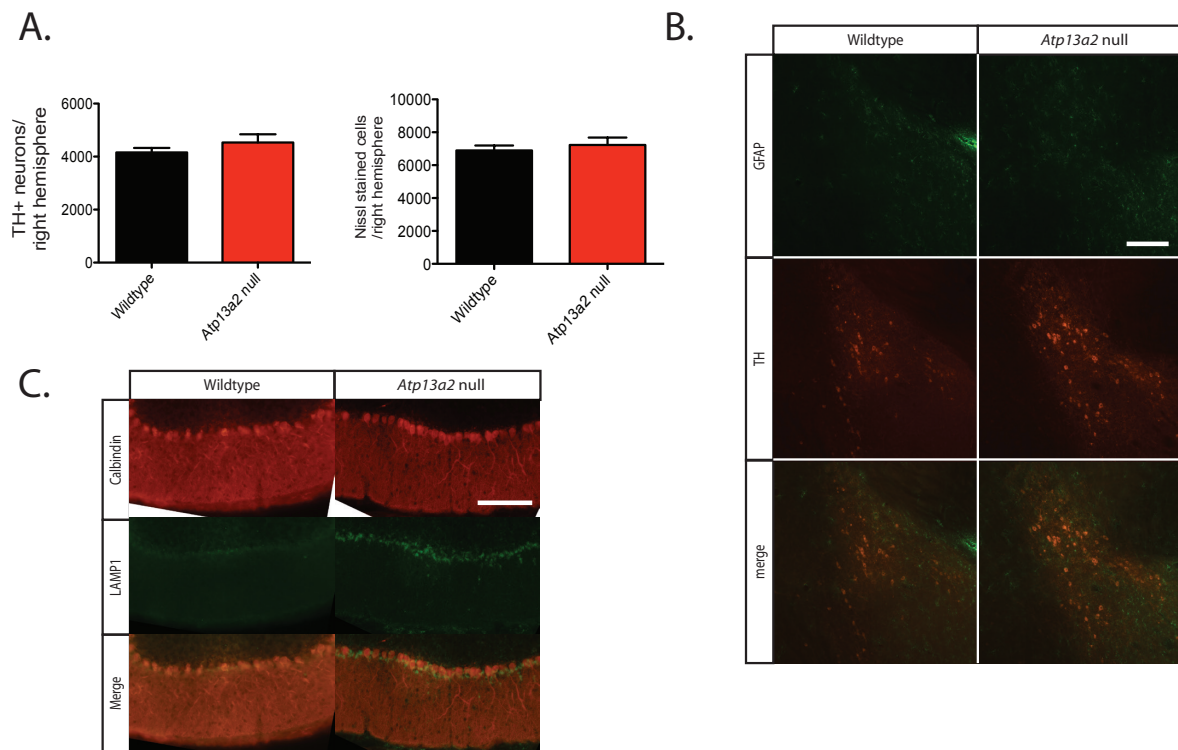
Figure 2.7. No alteration to tau levels or localization in 18-month-old *Atp13a2* null mice. **A**, Western blotting of total tau protein levels from multiple brain regions of wild type or *Atp13a2* null mice; 5 μ g protein loaded/lane. **B**, 40 μ m sections from 18-month-old wild type or *Atp13a2* null cortex stained for tau. Scale bar: 200 μ m.



KRS subjects have levodopa-responsive parkinsonism, so we performed a detailed assessment of the SNpc of aged *Atp13a2* null mice for protein aggregation and neurodegeneration. No ubiquitin- or α -synuclein-positive aggregates were observed in dopaminergic cell bodies (data not shown). We conducted unbiased stereology (Tieu et al., 2003) to compare the numbers of SNpc dopaminergic cell bodies between wild type and *Atp13a2* null tissue. We observed no changes in the number of SNpc dopaminergic neurons in the midbrains of aged *Atp13a2* null mice (Figure 2.8A). Although increased GFAP levels were present in microdissected midbrain lysates (Figure 2.3C), immunohistochemical analysis did not demonstrate enhanced co-localization of GFAP and tyrosine hydroxylase (TH) in the SNpc (Figure 2.8B). These studies suggest that despite widespread neuropathological changes in other regions, loss of *Atp13a2* function seems to largely spare the SNpc dopaminergic system, similar to other genetic models of PD (Dawson et al., 2010).

While KRS subjects do not develop ataxia or other signs of cerebellar dysfunction, they have prominent cerebellar atrophy on neuroimaging (Behrens et al., 2010; Bruggemann et al., 2010), suggesting degeneration. In addition, Purkinje cells are a population of neurons prone to degenerate in other neurodegenerative disorders, including the spinocerebellar ataxias (Costa Mdo and Paulson, 2012) and lysosomal storage disorders (Walkley and Suzuki, 2004). I therefore examined Purkinje cells for toxicity, protein aggregation, and lysosomal abnormalities. *Atp13a2* null mice had no overt loss of calbindin-positive Purkinje cells (Figure 2.8C), nor ubiquitin aggregates in the cerebellum at 18-months age (data not shown). Increased LAMP1 and LAMP2 staining occurred in calbindin-positive neurons (Figure 2.8C). Purkinje neurons therefore develop some of the observed pathological abnormalities, but are no more susceptible to protein aggregation or neurotoxicity than other neuronal populations in *Atp13a2* null mice.

Figure 2.8. Midbrain dopaminergic neurons and Purkinje cells do not degenerate in *Atp13a2* null mice. **A**, Stereological analysis of SNpC neurons with tyrosine hydroxylase (TH) immunostaining or Nissl staining. The number of dopaminergic neurons in the SNpC was identified by TH immunoreactivity at 18 months of age; n = 10 wild type and 7 *Atp13a2* null mice. **B**, Immunofluorescence of midbrain structures for GFAP (green) or tyrosine hydroxylase (TH; red) of 18-month-old wild type or *Atp13a2* null mice. **C**, Immunofluorescence for calbindin (red) or LAMP1 (green) in cerebellum of 18-month-old wild type or *Atp13a2* null mice. Scale bars: 100 μ m.

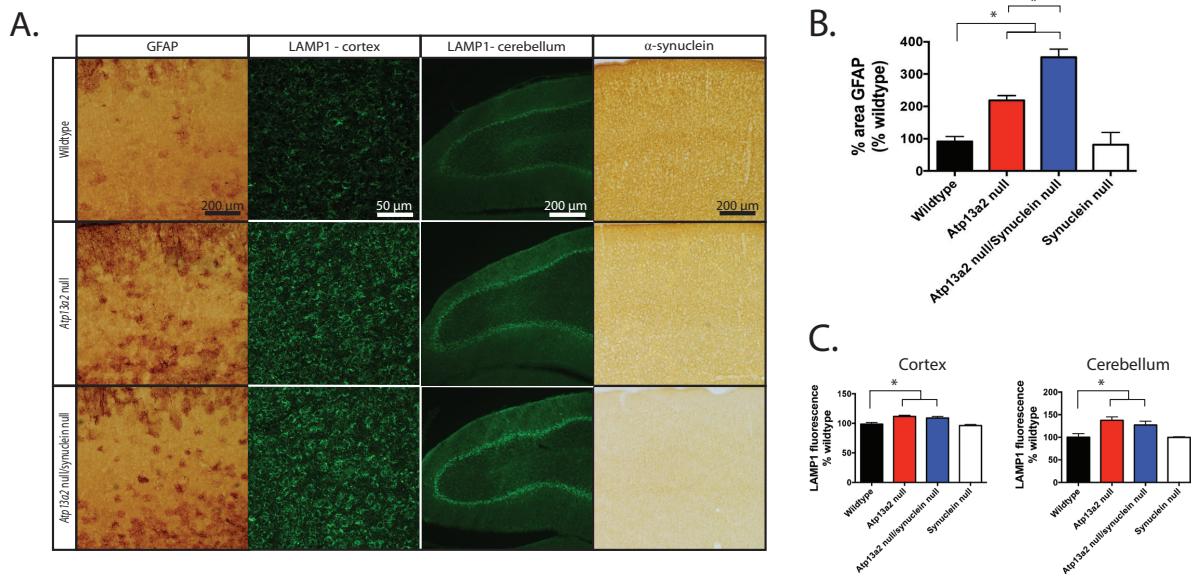


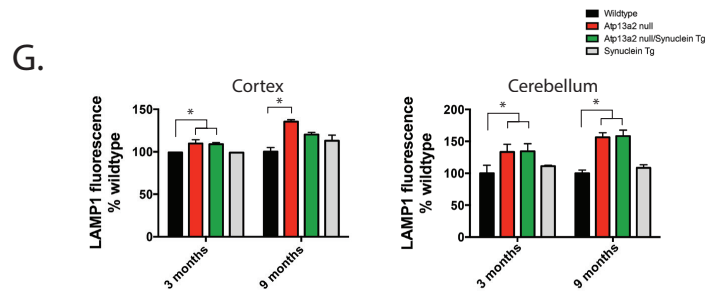
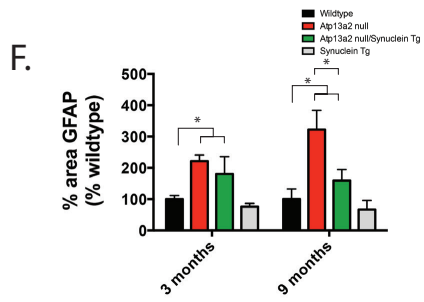
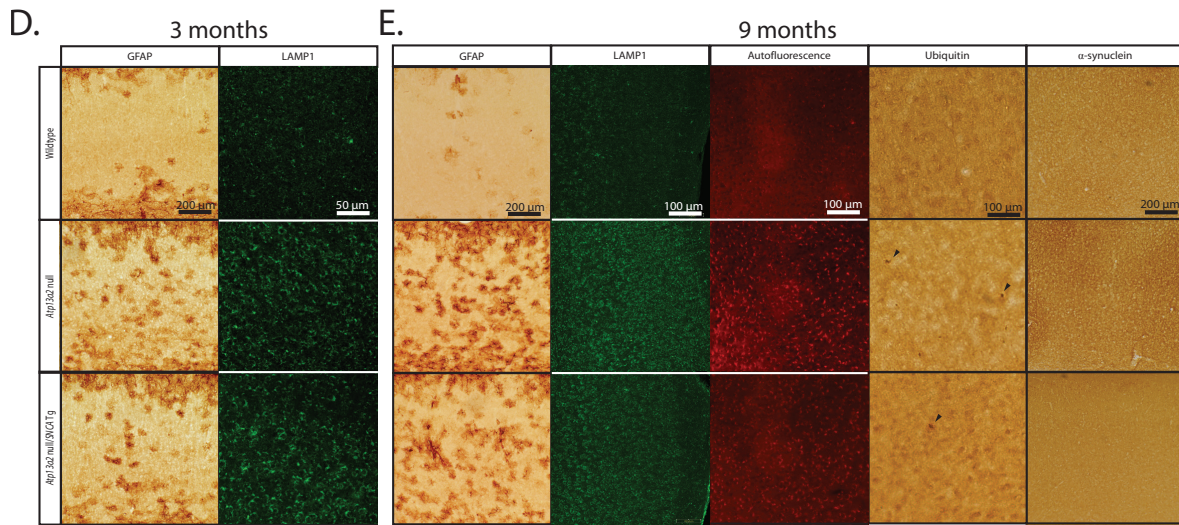
*Modulation of α -synuclein levels does not affect the onset or extent of histopathology in *Atp13a2* null mice*

The lack of α -synuclein abnormalities in *Atp13a2* null tissue (Figure 2.6) suggests that the histopathologic consequences of *Atp13a2* loss-of-function are α -synuclein-independent. I tested this possibility by genetically manipulating the levels of α -synuclein in *Atp13a2* null mice. I eliminated α -synuclein by generating α -synuclein/*Atp13a2* double knockouts using an established knockout line (Dauer et al., 2002). Loss of α -synuclein did not affect the extent of

gliosis or accumulation of lysosomes as assessed at 3 months of age, shortly following the onset of these pathologies (Figure 2.9A; quantification in Figure 2.9B and C). Conversely, I increased α -synuclein levels by at least four-fold in the cortex (Giasson et al., 2002) by ingressing a α -synuclein-overexpressing transgene (Giasson et al., 2002) onto the *Atp13a2* null background and examined onset and severity of pathology at 1-month (prior to the onset of pathology), 3-months (earliest observed pathology) and 9-months (onset of protein inclusions). This substantial increase in α -synuclein levels did not accelerate the time of onset of gliosis or lysosomal accumulation, as no pathology was observed at 1-month (data not shown), and a similar extent of pathology was observed at 3-months (Figure 2.9D). Similarly, severity of histopathology at 9-months did not differ in double mutant compared to the *Atp13a2* null animals (Figure 2.9E; quantified in 2.9F, G). These *in vivo* genetic studies are in accordance with biochemical studies and suggest that the neuropathological changes in *Atp13a2* null mice are independent of disruption in α -synuclein homeostasis.

Figure 2.9. Genetic modulation of α -synuclein levels does not affect the onset or extent of histopathology in *Atp13a2* null mice. **A**, 40 μ m sections from cortex or cerebellum of 3-month-old wild type, *Atp13a2* null, or *Atp13a2* null/*SNCA* null stained for GFAP, LAMP1, or α -synuclein. **B**, Quantification of percent area of the cortex positive for GFAP immunoreactivity, as in Figure 2.3D (One-way ANOVA: $F = 33.99$, $p < 0.0001$; $n = 6$ animals/genotype). Tukey's multiple comparisons tests were performed to detect differences between individual genotypes. Statistically significant differences are indicated (* $p < 0.05$). **C**, Quantification of average fluorescence intensity of the cortex (left) or Purkinje cell layer of the cerebellum (right), as in Figure 2.5D (One-way ANOVA: $F_{\text{cortex}} = 8.24$, $p = 0.001$; $F_{\text{cerebellum}} = 5.50$, $p = 0.008$; $n = 6$ animals/genotype). Tukey's multiple comparisons tests were used to detect differences between individual genotypes. Statistically significant differences are indicated (* $p < 0.05$). **D, E**, 40 μ m sections from cortex of 3- (**D**) or 9-month-old (**E**) wild type, *Atp13a2* null, or *Atp13a2* null/*SNCA* transgenic (Tg) either unstained or stained for GFAP, LAMP1, ubiquitin, or α -synuclein. **F**, Quantification of percent area of the cortex positive for GFAP immunoreactivity, as in Figure 2.3D (One-way ANOVA: $F = 4.71$, $p = 0.01$; $n = 9$ animals/genotype). Tukey's multiple comparisons tests were used to detect differences between individual genotypes. Statistically significant differences are indicated (* $p < 0.05$). **G**, Quantification of fluorescence intensity of the cortex (left) or Purkinje cell layer of the cerebellum (right) as in Figure 2.5D (One-way ANOVA: $F_{\text{cortex}} = 23.20$, $p < 0.0001$; $F_{\text{cerebellum}} = 18.03$, $p = 0.0001$; $n = 9$ animals/genotype). Tukey's multiple comparisons tests were used to detect differences between individual genotypes. Statistically significant differences are indicated (* $p < 0.05$). Scale bars as indicated in panels **A**, **D**, and **E**.





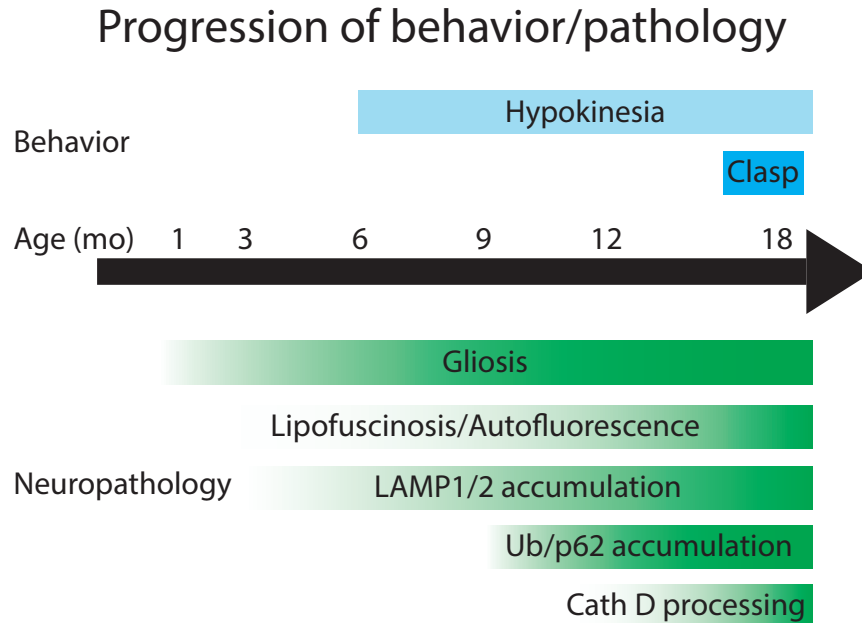
Discussion

Considerable attention has focused on the hypothesis that in PD, endolysosomal dysfunction causes neurodegeneration by increasing α -synuclein levels. Our findings dissociate alterations in α -synuclein homeostasis from neuropathological and behavioral abnormalities in a model of endolysosomal dysfunction similar to that causing L-DOPA-responsive parkinsonism in humans. Even in the absence of α -synuclein, the neuropathological consequences of *Atp13a2* loss-of-function emerge with the same time course and progress to the same extent as in its presence, emphasizing the α -synuclein independence of these abnormalities. Our findings emphasize that, even in the context of a PD-related insult, endolysosomal dysfunction and abnormalities of α -synuclein are not synonymous. These findings highlight the importance of broadly considering the consequences of endolysosomal dysfunction that may contribute to neurodegeneration in PD.

I describe novel molecular, neuropathological and behavioral features of *Atp13a2* loss-of-function, and outline the temporal sequence of these events *in vivo* - information critical for unraveling the pathogenic cascade leading to neurodegeneration. *Atp13a2* null mice develop age-related neuropathological changes, including reactive astrocytosis, lipofuscinosis, protein aggregation, and lysosomal abnormalities in multiple brain regions, including the cortex, cerebellum, hippocampus, and striatum (see Figure 2.10 for summary of progression). The widespread distribution of these changes, with particularly prominent abnormalities in cortex and cerebellum, are consistent with the clinical features of KRS. Similar to lipid changes seen in Niemann-Pick type C (Chevallier et al., 2008), AD (Chan et al., 2012), and in cathepsin D deficient mice (Jabs et al., 2008), I describe a rather selective increase in the lipid BMP,

suggesting changes to both late endosomal/lysosomal proteins and lipids following *Atp13a2* deficiency.

Figure 2.10. Summary of the progression of behavioral and neuropathological changes in *Atp13a2* null mice. Behavioral changes are indicated in blue, pathological changes are indicated in green, and progression of changes is shown by the color gradient.



Several of our findings are consistent with previous work, including the identification of abnormalities of lysosomal size and number, alterations in protein homeostasis and autophagy, and impaired neuronal viability (Dehay et al., 2012; Usenovic et al., 2012). My work is the first, however, to demonstrate several additional features of *Atp13a2* deletion, including astrocytosis, protein aggregation, and ultrastructural evidence of lipofuscin and lipid accumulation. Together, these results suggest a model by which loss of *Atp13a2* results in lysosomal dysfunction, an increase in lysosomal proteins and lipids, and decreased clearance of autophagic substrates including lipid droplets and ubiquitin. The temporal sequence of abnormalities in this KRS

model is particularly informative. I find that lipofuscin accumulation and glial activation occur early in the course of these pathological changes, months prior to observable abnormalities in lysosomes and protein aggregation. This early accumulation of lipofuscin and inflammation, in combination with alterations to protein homeostasis, likely disrupts neuronal health and function prior to the accumulation of protein aggregates. The identification of the temporal sequence of these events will enable future work aimed at blocking early abnormalities, which will be required to determine causal relationships.

In contrast to previous work *in vivo* (Schultheis et al., 2013), I find that *Atp13a2* null mice do not develop changes in α -synuclein solubility, despite exhibiting abnormal accumulation of ubiquitinated protein aggregates. This absence of α -synuclein pathology differs from *in vitro* studies which report a modest increase in α -synuclein levels in cells following *ATP13A2* knockdown or mutation (Dehay et al., 2012; Usenovic et al., 2012) and is in clear contrast with other cell and mouse models of PD where autophagic-lysosomal dysfunction seems to cause neurotoxicity and elevated α -synuclein levels (Mazzulli et al., 2011; Ahmed et al., 2012; Friedman et al., 2012). These findings could not exclude the possibility that soluble toxic forms of α -synuclein not detected by our methods might contribute to the abnormalities in *Atp13a2* null mice. To rigorously explore this possibility, I genetically altered α -synuclein levels by crossing *Atp13a2* null mice to either mice lacking or overexpressing α -synuclein. In these double mutants, I observed no change in the neuropathology seen in *Atp13a2* null mice, even up to 9 months of age. These results suggest that abnormalities of α -synuclein homeostasis or folding are not required for the development of gliosis, lipofuscinosis, or neuronal injury resulting from *Atp13a2* loss of function.

α -Synuclein aggregation is a frequent byproduct following complete loss of specific lysosomal enzymes such as glucocerebrosidase (Mazzulli et al., 2011) or cathepsin D (Cullen et al., 2009) or direct alterations in the delivery of α -synuclein to lysosomes by autophagic pathways (Webb et al., 2003; Cuervo et al., 2004; Orenstein et al., 2013). In contrast, our results suggest that loss of *Atp13a2* does not prevent lysosomal targeting or degradation of α -synuclein. In KRS patients, then, the principle insult may result not from α -synuclein, but from either neuroinflammation caused by early astrocytic activation, or from increased burden within neurons from lipofuscinosis and aggregation of proteins other than α -synuclein. My results do not preclude the possibility that α -synuclein aggregation occurs later in the course of the disease, beyond the 18-month age time point that I examined.

Many aspects of our KRS model more closely resemble the lysosomal storage disorders of NCL than PD. Most strikingly, *Atp13a2* null mice develop extensive autofluorescence and lipofuscinosis in the cortex, hippocampus, and cerebellum. This accumulation of granular osmophilic deposits is similar in appearance and regional selectivity to that seen in both Tibetan terriers with NCL (Riis et al., 1992; Katz et al., 2005; Katz et al., 2007; Farias et al., 2011) and mouse models of NCLs (Koike et al., 2000; Gupta et al., 2001; Weimer et al., 2009). Similar to our findings, NCL mouse models display motor dysfunction, including abnormal clasping (Sleat et al., 2004; Macauley et al., 2009; Weimer et al., 2009). The enhanced vulnerability of cortical, cerebellar, and hippocampal neurons replicates findings in NCL models lacking *Ppt1* (Gupta et al., 2001; Bible et al., 2004; Macauley et al., 2009), *Tpp1* (Chang et al., 2008), and *Cln3* (Weimer et al., 2009). Early gliosis precedes neuronal loss in NCL models (Kopra et al., 2004; Chang et al., 2008), similar to my observations of prominent gliosis in *Atp13a2* null mice as young as one-month-old. Finally, similar to the subcellular localization of ATP13A2, most

proteins linked to human NCL reside in the lysosome.

Increasingly, genetic, biochemical, and mouse studies emphasize the importance of lysosomal dysfunction in many neurodegenerative diseases, including PD. Mutations in multiple proteins related to the endolysosomal system, including the Gaucher's protein glucocerebrosidase, VSP35, Rab7L1, synaptotagmin 1, and ATP13A2, lead to increased risk for familial forms of parkinsonism. While loss of endogenous Atp13a2 in the mouse more closely resembles neuronal ceroid lipofuscinoses, this does not preclude dopaminergic degeneration in human patients with KRS. Many genetic models of Parkinson disease do not display overt loss of neurons in the SNpC (Dawson et al., 2010), suggesting fundamental differences between neuronal susceptibility in humans and mice. Our findings highlight the importance of defining more clearly how particular alterations to the autophagic-lysosomal system results in neurodegeneration, in the context of NCL, PD, and other neurological disease.

Materials and Methods

Antibodies and materials. The following antibodies were used: calbindin (1:500; Sigma Aldrich #C9848), cathepsin B (1:500; Santa Cruz Biotechnology Inc. #sc-6493), cathepsin D (1:300; Santa Cruz Biotechnology Inc. #sc-6486), cathepsin L (1:200; Santa Cruz Biotechnology Inc. #sc-10778), EEA1 (1:5000; BD Biosciences #610456), glial fibrillary acidic protein (GFAP; IHC: 1:2000; WB: 1:50,000; Dako Cytomation #Z0334), GAPDH (1:3000; Abcam #AB8245), hsc-70 (1:5000; Novus Biologicals #NB120-2788), ionized calcium-binding adaptor molecule-1 (Iba1; 1:500; Wako Chemicals #019-19741), LAMP1 (1:1000; Developmental Studies Hybridoma Bank #1D4B-C), LAMP2 (1:1000; Developmental Studies Hybridoma Bank #ABL-93-C), LAMP2A (1:1000; Invitrogen #51-2200), LC3 (1:5000; Novus Biologicals #NB100-

2220), NeuN (1:1000; Millipore #MAB377), p62/SQSTM1 (WB: 1:10,000; AbNova #H00008878-01; IF: 1:1000; American Research Products #03-GP62-C), Rab9 (1:3000; Santa Cruz Biotechnology Inc. #sc-28573), α -synuclein (1:10,000; Santa Cruz Biotechnology Inc. #sc-5587 or 1:500; BD Biosciences #610786), human α -synuclein (LB509; 1:10,000; Santa Cruz Biotechnology Inc. #sc-58480), tau (IHC: 1:200; WB: 1:5000; Santa Cruz Biotechnology Inc. #sc-5587), tyrosine hydroxylase (TH; IHC: 1:2000; Chemicon #AB152; IF: 1:2000; Millipore #AB1542), ubiquitin (1:500; Dako Cytomation #Z0458) and Vps4 (1:2000; Sigma-Aldrich, #SAB4200025).

Mouse lines. *Atp13a2* null mice were generated by inserting LoxP sites around Exons 2 and 3 (Figure 2.1A) to create an *Atp13a2*-flx line on a mixed C57Bl6/129 background. Floxed *Atp13a2* mice were intercrossed with a germline-expressing “Cre-deletor” mouse to create *Atp13a2*-KO/+ heterozygous mice. Intercrossing KO/+ heterozygotes produced *Atp13a2* null mice and wild type littermates. The α -synuclein null and transgenic mouse lines have been characterized previously (Dauer et al., 2002; Giasson et al., 2002). Double mutants were generated by crossing *Atp13a2* null mice to α -synuclein null mice to generate double heterozygotes. Double heterozygotes were then intercrossed to generate double null mice and the appropriate control mice. *Atp13a2* null/*SNCA* transgenics were generated in a similar manner.

Motor Behavior. Mice were housed 4 per cage and maintained on a 12-hour light/dark schedule (lights on at 6:00am). Food and water were provided *ad libitum*. Behavioral testing was conducted in accordance with the National Institutes of Health laboratory animal care guidelines and with the University Committee of Use and Care of Animals at the University of Michigan

approval. Male littermates (n = 16 wild type and 13 *Atp13a2* null) were tested for motor behavior every three months from 9 months to 18 months of age in the open field, rotarod, balance beam, and tail suspension tests.

Open field. Mice at the indicated ages were tested for spontaneous activity during a 60-min period using the Open Field 16 x 16 Photobeam Activation System and Flex-Field software (San Diego Instruments, San Diego, CA). Data were analyzed as number of beam breaks and number of rears over time.

Rotarod. Mice were placed in one of five slots on an accelerating rotarod apparatus (Ugo Basile, Comerio, Italy) and latency to fall was recorded using an accelerating rotarod protocol from 3 rpm to 30 rpm over 5 min. Mice were trained on 2 consecutive days with each trial ending with the mouse's fall or when 300 seconds elapsed. On the third day, mice were tested with an accelerating rotarod from 3 rpm to 30 rpm over 5 min, for 3 trials, with the endpoint being latency to fall in each trial up to 300 seconds.

Balance beam. Mice were trained to cross a square, 5 mm wide, 41-cm-long Plexiglass beam. The beam was placed horizontally 50 cm above a table, with a bright light illuminating the start platform and a darkened enclosed 8000 cm³ escape box (20 x 20 x 20 cm; PlasticTech, Ann Arbor, MI) at the end of the beam. Mice were trained for 3 consecutive days with 4 trials per day. The fourth day, mice were tested with 3 consecutive trials. The time to traverse was recorded for each trial with a 30 s maximum cutoff and falls scored as 30 s. The number of footslips was also recorded.

Tail suspension test. At 12 months and 18 months of age, mice were suspended by the tail and videotaped for 30 seconds. An observer blinded to genotype scored the videos for presence of clasping behavior of at least 2 seconds duration.

Morris water maze. The Morris water maze was performed as previously described (McKinney and Murphy, 2006). A 1.2 m diameter pool was filled with opaque water with a 10-cm² escape platform submerged 0.5 cm below the surface of the water in the center of one of the quadrants. Distinctive, high-contrast posters on the walls provided distal cues. For 2 weeks prior to training, 9-month-old male mice were handled daily to acclimatize them (13 wild type, 17 *Atp13a2* null mice). During training, each mouse was placed into the water facing the wall of the pool and allowed to search for the platform. The trial ended when the mouse successfully located the platform or 60 s elapsed. At the end of each trial, the mouse was allowed to rest on the platform for 15 s before return to its home cage. Training consisted of six trials per day (in blocks of two trials, 1-min intertrial intervals and 1-h interblock intervals) for 5 days, with the starting position chosen pseudorandomly among six start positions. 24 hours after the last training day, mice were tested for time to locate the hidden platform. Subsequent to the test day, mice were run through the Morris water maze with a visible platform to control for motor performance. The visible platform version consisted of a single day of training with six trials during which the platform was moved to a new location and marked with a distinct local cue. Data were acquired with a digital video camera 1.5 m from the water surface. Images from the digital camera were processed with Actimetrics WATERMAZE version 2.6 software (Actimetrics, Wilmette, IL, USA).

cDNA synthesis and sequencing. Total RNA was extracted from whole brains of 6-month old wild type, *Atp13a2* heterozygous, or *Atp13a2* null mice using TRIzol Reagent (Invitrogen, Carlsbad, CA) according to manufacturer instructions. Complementary DNA (cDNA) was synthesized from 5 µg of purified total RNA using SuperScript III One-Step RT-PCR System (Invitrogen). cDNA was amplified with primers specific for *Atp13a2* RNA (forward: 5'-GCGAGGAGCCGAAATGAG-3'; reverse: 5'-CGTAAATGGTCTTCCTCGTAGC-3'). The resulting PCR product was sequenced at the University of Michigan Sequencing Core.

Immunocytochemistry. Wild type and *Atp13a2* null male mice at the indicated ages were anesthetized with a lethal dose of xylazine and ketamine HCl and transcardially perfused with a 0.9% saline solution followed by 4% paraformaldehyde in phosphate buffer. Whole brains were post-fixed overnight, equilibrated in 30% sucrose, and embedded in O.C.T. (Tissue-Tek, Sakura Finetek Europe, The Netherlands). 40 µm frozen sagittal sections were collected on a Leica CM1850 cryostat (Leica Biosystems, Buffalo Grove, IL). For immunofluorescence, sections were blocked in 5% Normal Donkey Serum (NDS) in PBS-Tx (PBS plus 0.01% TritonX-100). Following overnight incubation at 4°C in primary antibodies in 1.5% NDS/PBS-Tx, sections were incubated in an AlexaFluor 488- or 555-conjugated secondary (Invitrogen), incubated with 0.3% Sudan Black in 70% ethanol to quench autofluorescence, and mounted using ProLong Gold. For DAB immunohistochemistry, the following modifications were made to the above protocol. Prior to block, sections were first subjected to 30 min in 0.3% H₂O₂ in PBS to quench endogenous peroxidase activity. After a 1-hour incubation in a biotinylated secondary antibody (Jackson ImmunoResearch, West Grove, PA), sections were incubated in ABC for 1 hour

(Vector Laboratories, Burlingame, CA) followed by DAB reaction (Sigma-Aldrich). Images were acquired with a Zeiss Axioskop microscope (Carl Zeiss Group, Jena, Germany). Confocal images were acquired on an Olympus FluoView 500 (Olympus America, Centerville, PA) in the University of Michigan Microscopy and Image Analysis Laboratory. For each experiment, a representative image was selected after examination of four to ten animals.

Stereology. Dopamine cell number in the SNpC of 18-month-old *Atp13a2* null or wild type mice was assessed by unbiased stereology using TH immunocytochemistry and Nissl stain as previously described (Tieu et al., 2003).

Tissue homogenization and Western blot. To prepare brain lysates, microdissected frozen brains were homogenized with a Dounce homogenizer in an appropriate volume of ice-cold RIPA buffer (50mM Tris-HCl, pH 7.4, 150 mM NaCl, 0.1% SDS, 0.5% SDOC, and 1% NP-40) containing protease inhibitors (Roche Molecular Biochemicals, Indianapolis, IN). The samples were then sonicated to solubilize all proteins. Protein concentrations were determined using the BCA assay (Pierce Biotechnology, Rockford, IL). Proteins were separated by SDS-PAGE using Tris-HCl 4-20% gradient gels (BioRad, Hercules, CA) and transferred onto PVDF membranes (BioRad). Membranes were blocked in 5% non-fat milk in TBS-T (TBS plus 0.1% (v/v) Tween 20) for 1 hour, followed by overnight incubation at 4°C in primary antibodies in 5% non-fat milk in TBS-T. After a 1-hour incubation in an HRP-conjugated secondary antibody, immunoreactive bands were visualized on film by enhanced chemiluminescence (SuperSignal West Pico, Pierce Biotechnology).

Cortical homogenates were sequentially extracted in increasing detergents using a protocol previously described (Luk et al., 2012b). Briefly, cortices from 18-month-old mice were microdissected and sequentially extracted in buffers containing high salt (HS; 50 mM Tris, pH 7.5, 750 mM NaCl, and 5 mM EDTA), HS buffer containing 1% Triton-X100, and 1% SDS buffer (50 mM Tris, pH 7.5, and 1% SDS). Protease and phosphatase inhibitors (Roche) were added to buffers before use. Following extraction, samples were sonicated and subjected to ultracentrifugation at 100,000 x g for 30 min in a 70.1 Ti rotor (Beckman Coulter Inc., Brea, CA). At each step, the supernatant was removed and the pellet extracted in 3 mL buffer per gram of tissue. Proteins were then subjected to SDS-PAGE analysis as described above.

Transmission electron microscopy. 1- or 12-month-old *Atp13a2* null or wild type mice were prepared for ultrastructural analysis as previously described (Goodchild et al., 2005). Briefly, mice were transcardially perfused with 4% paraformaldehyde/ 2.5% glutaraldehyde in 100 mM sodium phosphate buffer (pH 7.4), followed by overnight postfixation in the same solution. Samples were postfixated with 1% osmium tetroxide in 0.1 M cacodylate buffer (pH 7.4) for 1 hour, followed by treatment with 3% uranyl acetate, dehydration with alcohol, propylene oxide treatment, and embedding in Embed 812 (Electron Microscopy Sciences, Fort Washington, PA). The resin was polymerized in a 60°C oven for 2 days and sections were cut with a Dupont diamond knife on a Reichart Ultracut-E microtome (Leica), collected on copper grids, and double stained with saturated aqueous uranyl acetate and lead citrate. Images were taken using a Philips CM-100 transmission electron microscope (Philips Research, Eindhoven, The Netherlands) and AMTV540 image capture software (Advanced Microscopy Techniques, Woburn, MA) in the University of Michigan Microscopy and Image Analysis Laboratory.

Lipid analysis using high performance liquid chromatography-mass spectrometry. Lipid extracts were prepared from 18-month-old cortical lysates using a modified Bligh/Dyer extraction procedure as previously described (Chan et al., 2012). Samples were analyzed using an Agilent Technologies 6490 Ion Funnel LC/MS Triple Quadrupole system with front end 1260 Infinity HPLC. Phospholipids and sphingolipids were separated by normal phase HPLC while neutral lipids were separated using reverse phase HPLC. For normal phase analysis, lipids were separated on an Agilent Rx-Sil column (i.d. 2.1 x 100 mm) using a gradient consisting of A: chloroform/methanol/ammonium hydroxide (89.9:10:0.1) and B: chloroform/methanol/water/ammonium hydroxide (55:39:5.9:0.1), starting at 5% B and ramping to 70% B over a 20 min period before returning back to 5% B. Neutral lipids were separated on an Agilent Zorbax XDB-C18 column (i.d. 4.6 x 100 mm) using an isocratic mobile phase chloroform:methanol:0.1M ammonium acetate (100:100:4) at a flow rate of 300 μ L/min. Multiple reaction monitoring transitions were set up for quantitative analysis of different lipid species and their corresponding internal standards as described previously (Chan et al., 2012). Lipid levels for each sample were calculated relative to the spiked internal standards and then normalized to the total amount of all lipid species measured and presented as relative mol %. Data are presented as mean mol % for 3 samples of each genotype.

Statistics. Results were analyzed using GraphPad Prism 5.0. A χ^2 test was used to determine Mendelian ratios and analyze tail suspension behavioral test. Behavioral studies were performed blind. Data were first examined for equal variance and then subjected to two-way Repeated Measures ANOVA with time and genotype as variables, with Bonferroni's post-hoc tests at

specific ages. Student's *t*-tests were used for Western blotting analyses. In all studies, *n* indicates the number of samples per group and a critical value of $p \leq 0.05$ was used. Data are plotted as means \pm SEM.

Chapter 3

Selective defects in endolysosomal function in *Atp13a2* null mice

Abstract

Genetic mutations in *ATP13A2* cause Kufor-Rakeb Syndrome (KRS), a neurological disorder whose features include juvenile-onset parkinsonism. ATP13A2 is a late endosomal/lysosomal ATPase of unknown function whose loss *in vitro* causes lysosomal abnormalities, proteolysis defects, increased oxygen consumption, and signs of mitochondrial injury. I showed in Chapter 2 that loss of *Atp13a2* *in vivo* causes age-related behavioral and neuropathological abnormalities including protein aggregation and lysosomal accumulation. Both autophagy and mitophagy have been implicated in PD pathogenesis, so I therefore undertook detailed analyses of autophagic-lysosomal function as well as mitochondrial health from aged *Atp13a2* null mice. Despite widespread changes to CNS pathology, I observed selective alterations to autophagic function in 18-month-old *Atp13a2* null mice including altered processing of cathepsin D and the accumulation of ubiquitin and p62-positive aggregates. In contrast to previous *in vitro* reports, these results suggest a selective role for *Atp13a2* in lysosomes that result in neuronal injury and motor deficits.

Introduction

ATP13A2 is a P-type ATPase of unknown function that localizes to the lysosome (Ramirez et al., 2006) and late endosome (Podhajska et al., 2012). Phylogenetically, ATP13A2 is related to ion transporters and lipid flippases (Schultheis et al., 2004). It therefore likely functions in the late endosomal/lysosomal membrane to move heavy metals or lipids across the lysosomal membrane. Its exact function and substrate remain unclear, though *in vitro* studies have tenuously linked it to the transport of multiple heavy metals (Gitler et al., 2009; Tan et al., 2011; Covy et al., 2012; Podhajska et al., 2012; Tsunemi and Krainc, 2013). ATP13A2 knockdown in cell culture causes increased lysosome size and number and autophagic deficits (Dehay et al., 2012; Usenovic et al., 2012), increased mitochondrial oxygen consumption (Gusdon et al., 2012), and zinc dyshomeostasis (Tsunemi and Krainc, 2013; Park et al., 2014). Based on these *in vitro* studies and prevailing theories, loss of Atp13a2 in our novel mouse model could be causing neuronal injury in a PD-related mechanism through autophagic deficits, changes in lipid signaling, dysfunctional mitophagy, or ion imbalances.

Autophagy dysfunction is increasingly recognized as a key element of PD pathogenesis. α -Synuclein is degraded in part by autophagy (Webb et al., 2003; Cuervo et al., 2004), by both macroautophagy and chaperone-mediated autophagy (CMA). Mutations in the glucocerebrosidase gene are the most common risk factor for PD (Sidransky et al., 2009) and disruption of glucocerebrosidase causes autophagy dysfunction, α -synuclein accumulation, and neurotoxicity (Mazzulli et al., 2011). α -Synuclein accumulation in turn feeds back to further inhibit glucocerebrosidase function. These studies suggest a common mechanism by which loss of lysosomal proteins may cause PD: autophagic dysfunction leading to α -synuclein accumulation and neurotoxicity. Yet, few studies of lysosomal proteins have directly tested this

hypothesis and loss of most lysosomal proteins causes accumulation of substrates other than α -synuclein suggesting additional mechanisms through which autophagic deficits can cause neurodegeneration.

Another likely mechanism by which loss of Atp13a2 may cause neuronal injury is by altering mitophagy. The PD-related proteins PINK1, parkin, and FBXO7 function in a common pathway to mediate the clearance of damaged or depolarized mitochondria (Jin et al., 2010; Lazarou et al., 2012; Burchell et al., 2013). Loss-of-function mutations in these genes cause a build-up of abnormal mitochondria, reactive oxygen species, and alterations to oxygen consumption (Exner et al., 2007; Dagda et al., 2009; Lutz et al., 2009; Amo et al., 2011). Similarly, PD-related mutations in mouse glucocerebrosidase cause mitochondria to become fragmented and dysfunctional, with impaired mitochondrial respiration and decreased potential (Osellame et al., 2013). Cell culture experiments suggest that a similar process may occur with loss of ATP13A2. Knockdown of Atp13a2 in primary neurons caused an increase in mitochondrial mass and fragmentation, along with increased oxygen consumption and reactive oxygen species production (Gusdon et al., 2012). These mitochondrial changes appear due to poor mitophagy, rather than a primary mitochondrial defect, as they mimic defects seen with autophagy inhibitors (Gusdon et al., 2012) and have concomitant build up of other autophagy substrates like p62 and ubiquitinated proteins (Osellame et al., 2013).

Finally, as a putative lipid flippase, loss of Atp13a2 may cause neuronal injury through changes to lipid profiles and signaling at the lysosomal membrane. Lipid alterations are increasingly recognized as an important component of neurodegenerative disease. Some diseases, such as the neuronal ceroid lipofuscinoses, Niemann Pick type C, and Gaucher's disease, have selective lipid accumulation and neurodegeneration due to improper lysosomal

degradation. In other multifactorial diseases, such as Alzheimer disease (AD), lipid regulation is a major contributing factor (Di Paolo and Kim, 2011). The cholesterol regulator APOE4 is the single biggest risk factor for sporadic AD and alters the endosomal compartment and consequent processing of key AD proteins like amyloid precursor protein and β -secretase (Cataldo et al., 1997; Li et al., 2012b; Zhao et al., 2014). In PD, lipid changes are similarly a contributing factor to disease. α -Synuclein binds to lipids (Sharon et al., 2001) and α -synuclein null or transgenic mice have CNS lipid alterations (Barcelo-Coblijn et al., 2007; Rappley et al., 2009). Lipids promote the formation of Lewy Bodies (LBs), and lipid profiles changes occur in post-mortem tissue from PD patients (Sharon et al., 2003; Assayag et al., 2007). Increased risk of parkinsonism with mutations in glucocerebrosidase, PLA2G6, and synaptotagmin 1, all of which are enzymes involved in lipid metabolism, further suggests that altered lipid metabolism may be causative for increased risk of familial PD.

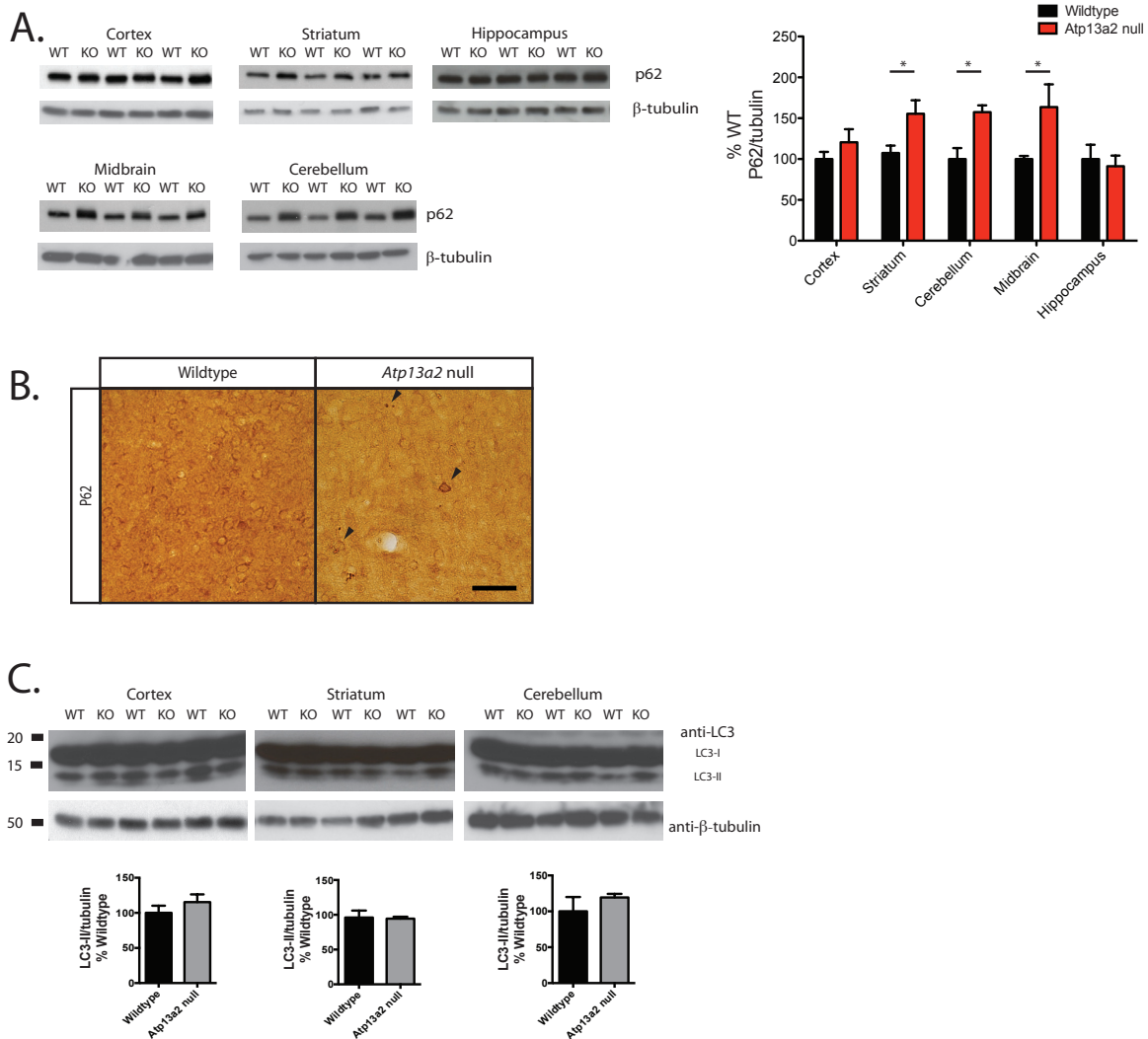
To investigate the mechanism by which loss of ATP13A2 causes parkinsonism, I utilized our novel mouse model to probe autophagy function, mitochondrial health, and lipid profiles in the context of *Atp13a2* loss. *Atp13a2* null mice show alterations to autophagy, including p62 accumulation and altered cathepsin D processing, that likely contribute to the neuropathology and behavioral abnormalities observed in these mice. These changes to p62 and cathepsin D occur in the absence of more widespread lysosomal dysfunction, with no change to proteolysis, lysosome acidification, or chaperone-mediated autophagy. Similarly, despite subtle alterations to mitochondrial morphology, mitochondria isolated from *Atp13a2* null mice had normal oxygen consumption rates, suggesting that mitophagy was not dramatically impaired. These results, together with the neuropathology studies, suggest that even minor alterations to lysosomal function can result in widespread CNS abnormalities.

Results

Selective defects in autophagy function in Atp13a2 null mice

Based on its localization to the lysosome, the presence of ubiquitin aggregates in aged mice (Figure 2.6A), and *in vitro* evidence (Dehay et al., 2012; Usenovic et al., 2012), I hypothesized that loss of Atp13a2 would result in autophagic defects in *Atp13a2* null mice. P62 is an autophagy substrate commonly used as a marker of autophagy function. I observed increased p62 levels in the striatum, cerebellum, and midbrain of *Atp13a2* null tissue compared to littermate controls (Figure 3.1A). Despite comparable p62 protein levels, the presence of p62-positive protein aggregates in the cortex of *Atp13a2* null tissue (Figure 3.1B) provided further evidence of defective proteostasis in these mutants. To assess autophagy induction, I examined LC3 levels. Steady-state levels of LC3-II did not differ between *Atp13a2* null and wild type tissue (Figure 3.1C), consistent with an absence of marked change in the abundance of autophagic vacuoles by ultrastructural analysis (data not shown).

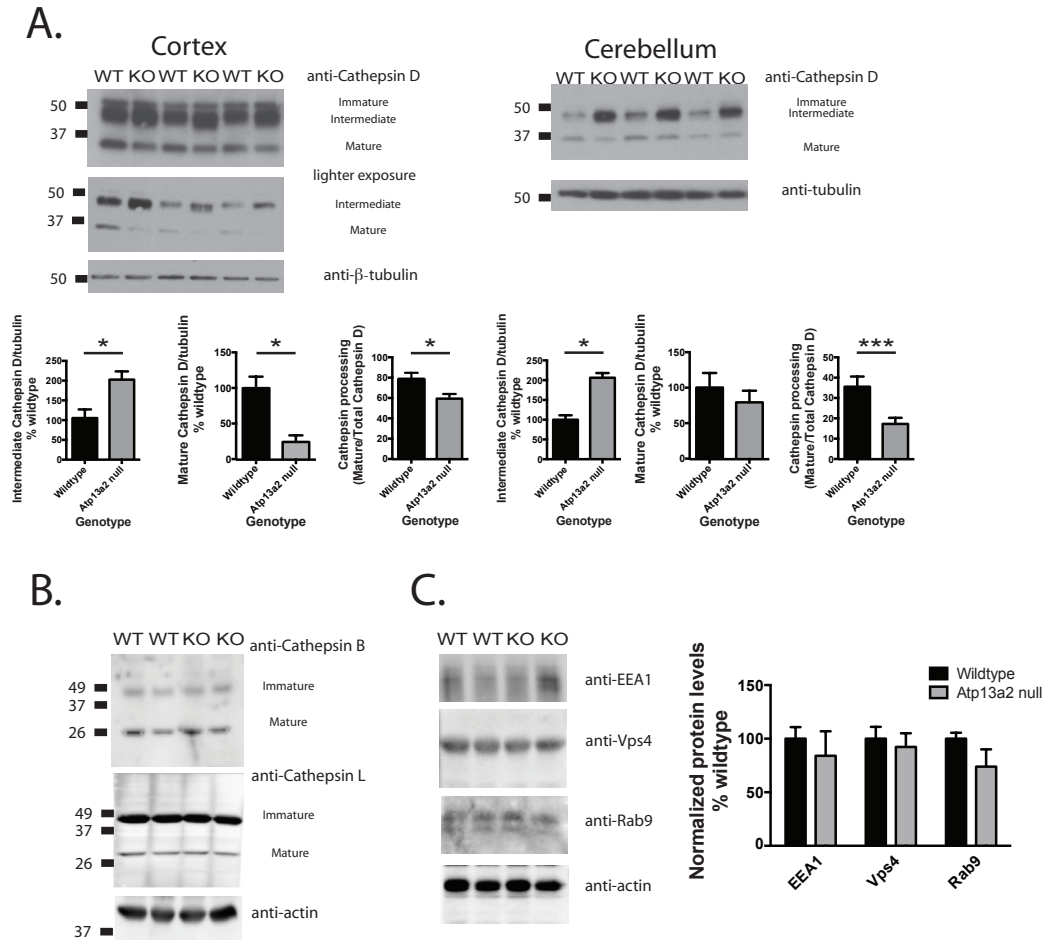
Figure 3.1. Lysosomal processing of p62 is abnormal in *Atp13a2* null CNS tissue. A, Quantitative Western blotting of p62 levels from 18-month-old mice; 5 μ g protein loaded/lane; n = 12 wild type and 10 *Atp13a2* null mice. **B,** P62 immunohistochemistry of 18-month-old wild type or *Atp13a2* null cortex. Scale bar: 100 μ m. **C,** Western blotting of LC3-II from 18-month-old mice; quantitation shown on right. 30 μ g protein loaded/lane; n = 7 wild type and 6 *Atp13a2* null mice. Statistically significant differences are indicated (* $p < 0.05$, ** $p < 0.01$). Error bars indicate SEM.



Further biochemical analysis confirmed that the most pronounced changes were observed in lysosomal compartments. Maturation of cathepsin D occurs as it traffics to more acidic compartments (Zaidi et al., 2008), and was impaired in 18-month-old *Atp13a2* null cortical and

cerebellar lysates, which exhibited higher levels of the immature and intermediate forms and a corresponding decrease in the cleaved, mature form (Figure 3.2A). These abnormalities in cathepsin D processing (defined as mature/total cathepsin D) were not observed in 9-month-old *Atp13a2* null tissue, demonstrating that this defect occurs relatively late in the pathogenic cascade, long after the onset of reactive astrocytosis and lysosome accumulation (see Figure 2.10 for summary timeline of phenotypes). In contrast to the defects identified for cathepsin D, levels and maturation of cathepsin B and cathepsin L did not differ from wild type controls (Figure 3.2B). The selective abnormality in cathepsin D processing and the lack of differences between wild type and *Atp13a2* null mice in the analyzed markers of different endocytic compartments (early endosomes, multivesicular bodies and late endosomes markers shown in Figure 3.2C) raised the possibility that loss of *Atp13a2* function may disrupt only a subset of ALP components and suggested that the compartment most severely affected were secondary lysosomes (also termed autolysosomes).

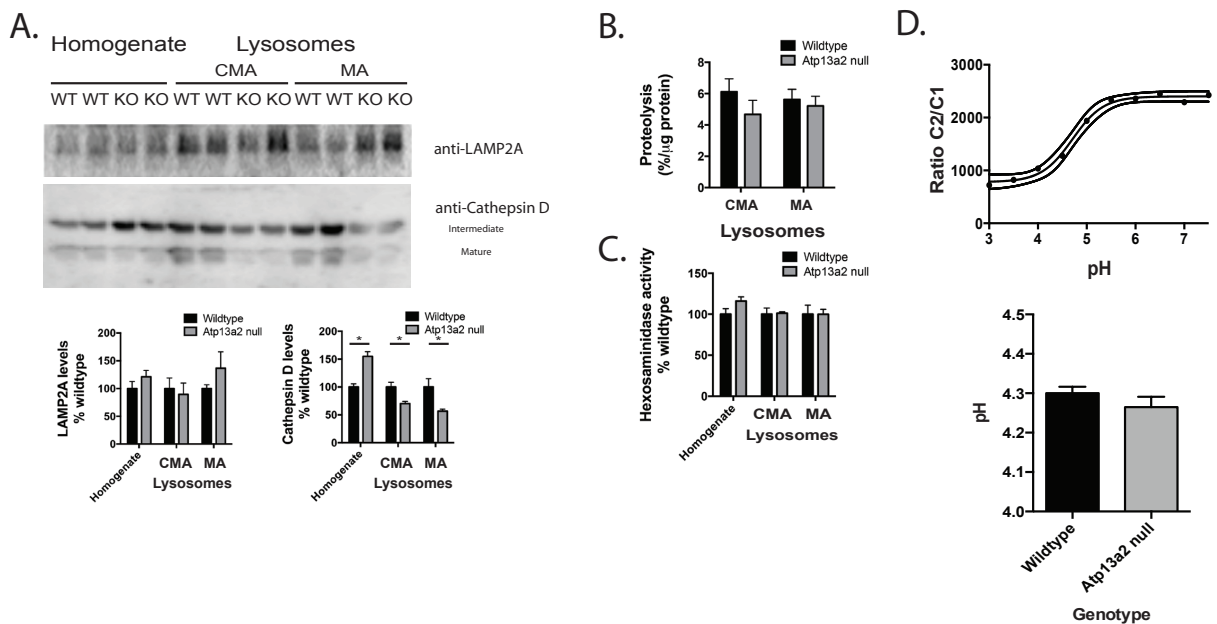
Figure 3.2. Lysosomal processing of cathepsin D is abnormal in *Atp13a2* null CNS tissue. A, Quantitative Western blot of cathepsin D levels in the cortex and cerebellum of 18-month-old mice; 30 μ g protein loaded/lane; n = 7 wild type and 6 *Atp13a2* null mice. Cathepsin D processing was defined as the ratio of mature cathepsin D to total cathepsin D (mature + intermediate). **B, C,** Western blotting of cathepsin B and cathepsin L (**B**) and of markers of early, late and multivesicular endocytic compartments (**C**) from whole brain homogenates from 18-month-old mice; n = 4 samples of 2 pooled brains from wild type and *Atp13a2* null mice. Statistically significant differences are indicated (* p < 0.05, ** p < 0.01). Error bars indicate SEM. Panels **B, C** in collaboration with B. Stiller and I. Tasset, Cuervo laboratory.



To examine the lysosomal compartment directly, we isolated two subpopulations of lysosomes from whole brains of 18-month-old wild type and *Atp13a2* null mice: those preferentially involved in macroautophagy (MA) or chaperone-mediated autophagy (CMA) (Cuervo et al., 1997; Koga et al., 2010). There were no differences in the membrane integrity of

lysosomes from wild type or *Atp13a2* null mice, as measured by the amount of hexosaminidase in the extralysosomal media during isolation (Figure 3.3C), indicating that the loss of *Atp13a2* does not render lysosomal membranes more fragile. Consistent with the decrease in cathepsin D processing observed in cortical and cerebellar tissue lysates (Figure 3.2A), levels of mature cathepsin D were decreased in both populations of lysosomes from *Atp13a2* null tissue (Figure 3.3B). The abnormality in cathepsin D processing raised the possibility that loss of *Atp13a2* may compromise lysosomal acidification, as cathepsin maturation is a pH-dependent process (Zaidi et al., 2008). However, contrary to the increase in the intermediate form of cathepsin D observed in total lysates, levels of this intermediate form were reduced in the two groups of secondary lysosomes from *Atp13a2* null mice (Figure 3.3A). These findings suggest that rather than a problem of cathepsin D processing within lysosomes, the reduced levels in mature cathepsin D were mainly a consequence of compromised trafficking of this cathepsin to lysosomes. Several other findings support the selectivity of the cathepsin D defect and argue against a global disruption of the lysosomal pH gradient in these organelles. I observed no changes in the maturation of other cathepsins (Figure 3.3B), and no differences in the total proteolytic activity (Figure 3.3B) or the activity of other lysosomal hydrolases (hexosaminidase shown in Figure 3.3C). In addition, despite a previous report of pH neutralization in lysosomes of *ATP13A2* mutant fibroblasts (Dehay et al. 2012), I observed no difference in lysosomal pH in *Atp13a2* null mouse embryonic fibroblasts as measured by Oregon Green-dextran ratio (Figure 3.3D; $\text{pH}_{\text{wild type}} = 4.30 \pm 0.22$, $n = 174$ cells; $\text{pH}_{\text{Atp13a2 null}} = 4.26 \pm 0.33$, $n = 154$ cells; $t = 1.16$, d.f. = 326, $p = 0.25$).

Figure 3.3. Isolated lysosomes from *Atp13a2* null tissue have decreased cathepsin D levels, but normal proteolytic activity. Lysosomes were isolated from 2 pooled brains of 18-month-old wild type or *Atp13a2* null mice and probed for endolysosomal proteins and substrates. **A**, Western blotting of the indicated proteins of lysosomal compartments preferentially related with either chaperone-mediated autophagy (CMA) or with macroautophagy (MA). Protein levels were determined by densitometry (bottom). **B**, Proteolytic activity of freshly isolated lysosomes. Proteolysis was measured by incubating a pool of radiolabeled cytosolic proteins with the two subpopulations of lysosomes after disruption of their membranes by a hypotonic shock. Results are expressed as percent degradation per μg protein and are the average values of triplicate samples from 4 samples pooled from 8 brains of either wild type or *Atp13a2* null mice. **C**, Hexosaminidase activity in total homogenates and the two subpopulations of lysosomes isolated from the same animals as in **B**. Values are expressed as percentage of those in wild type control samples. **D**, Lysosomal pH, measured by ratiometric imaging following uptake of Oregon Green dextran. Calibration curve (above) was generated by holding wild type cells at set pH values, and allowed the conversion of C2/C1 ratio to pH (bottom) for wild type and *Atp13a2* null fibroblasts. $n = 174$ cells for wild type, 151 cells for *Atp13a2* null cells. Statistically significant differences are indicated (* $p < 0.05$). Error bars indicate SEM. Panels **A-C** in collaboration with Cuervo lab.

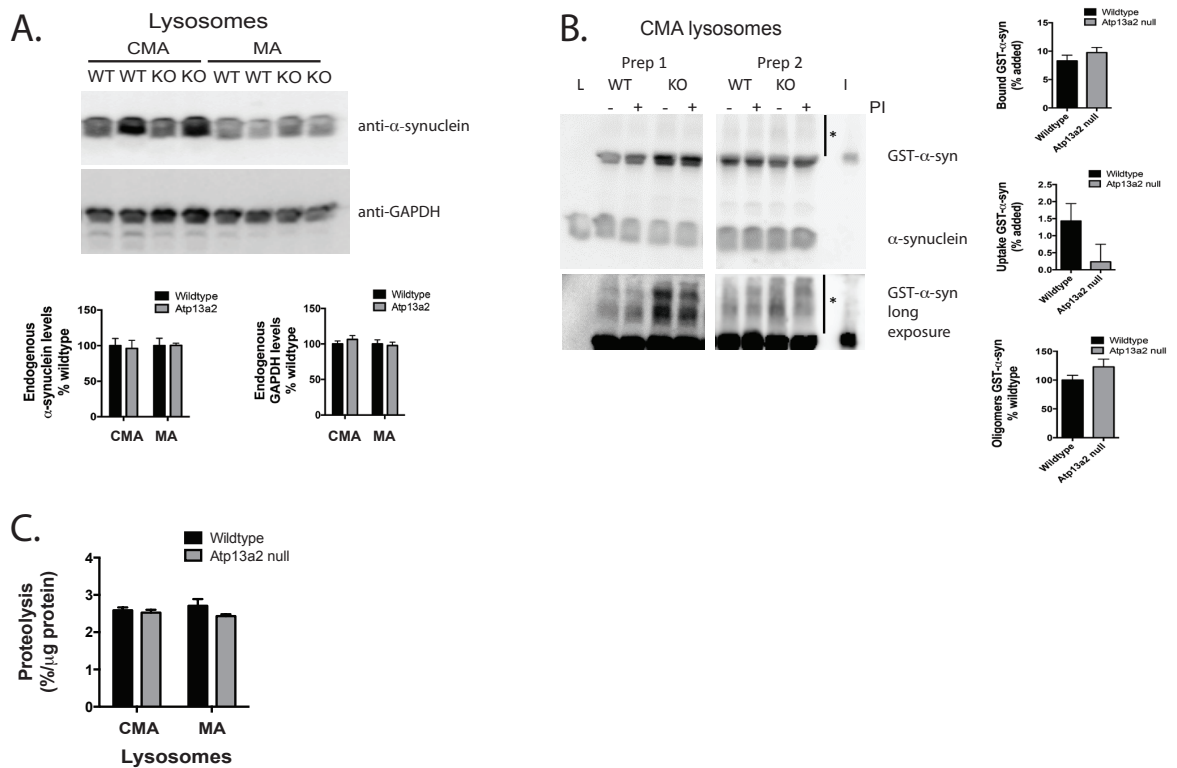


In light of the previously described lysosomal degradation of α -synuclein by both macroautophagy and CMA (Webb et al., 2003; Cuervo et al., 2004; Martinez-Vicente et al., 2008) and of the disruption of this process in other PD models, I next analyzed the association of α -synuclein with the isolated lysosomal fractions. Similar amounts of endogenous α -synuclein

were detected in wild type and *Atp13a2* null lysosomes and α -synuclein was more abundant in the subgroup of lysosomes with higher CMA activity (Figure 3.4A), as described previously (Martinez-Vicente et al., 2008). Levels of other well-characterized CMA substrate proteins such as GAPDH were also comparable in wild type and *Atp13a2* null lysosomes (Figure 3.4B).

To directly analyze the ability of *Atp13a2* null lysosomes to take up α -synuclein via CMA, we incubated CMA active lysosomes with GST-tagged α -synuclein (Figure 3.4C). While results varied somewhat between samples preparations, *Atp13a2* loss was not associated with reduced lysosomal uptake of α -synuclein or increased formation of oligomeric forms of α -synuclein. These findings are in contrast to such changes reported with the PD-related genes α -synuclein and LRRK2 (Martinez-Vicente et al., 2008; Orenstein et al., 2013). The normal ability of *Atp13a2* null lysosomes to internalize and degrade a mixture of radiolabeled proteins (Figure 3.4D), together with the normal lysosomal levels of both α -synuclein and GAPDH, provide substantial evidence indicating that lysosomal uptake and degradation of protein functions normally in the absence of *Atp13a2*.

Figure 3.4. Isolated lysosomes from *Atp13a2* null tissue have normal proteolysis of α -synuclein. **A**, Endogenous levels of α -synuclein and GAPDH in intact lysosomes from brains of wild type or *Atp13a2* null mice. Levels of the indicated proteins were calculated by densitometry (bottom). **B**, Association of recombinant GST- α -synuclein with CMA active lysosomes previously incubated or not with protease inhibitors (PI) to determine binding and uptake via CMA. L indicates lysosomes incubated without GST- α -synuclein and I indicates input (1/10 of added protein). Samples correspond to lysosomes isolated on two different days. Bottom shows high exposure of the high molecular region of the immunoblot to highlight oligomeric forms of GST- α -synuclein not present in the lysosomes alone or in the input. Percentage of monomeric GST- α -synuclein bound and taken up by lysosomes or associated to lysosomes as oligomers is shown on the right. **C**, Degradation of a pool of radiolabeled cytosolic proteins by the two subpopulations of lysosomes isolated from brains of wild type or *Atp13a2* null mice was performed as in Figure 3.3B but using intact, instead of disrupted lysosomes. In collaboration with Cuervo lab.



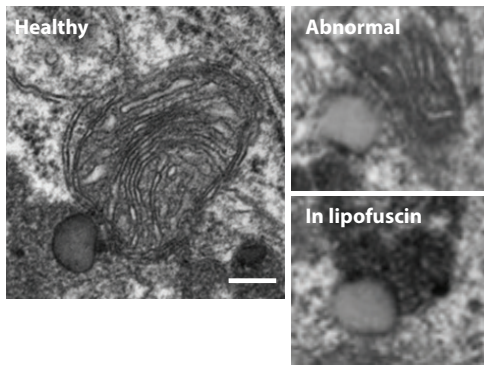
*No mitochondrial defects with loss of *Atp13a2**

Defective mitophagy is implicated in multiple forms of familial PD and knockdown of ATP13A2 in cell culture causes mitochondrial structural abnormalities, increased oxygen consumption rates, and the increase oxidized mitochondria and reactive oxygen species

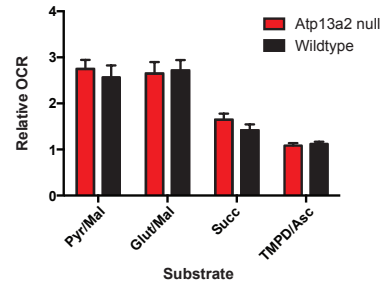
(Grunewald et al., 2012; Gusdon et al., 2012). During our electron microscopy study, we incidentally noticed abnormalities in mitochondria in close association with lipofuscin deposits (Figure 3.5A), suggestive that abnormal mitophagy may account for the CNS neuropathology observed in *Atp13a2* null mice. We assessed the oxygen consumption rate (OCR) of mitochondria isolated from cortical lysates of aged mice (12 to 18 months old) using the Seahorse XF24 Analyzer (Figure 3.5B, C). The Seahorse XF24 Analyzer allows the rapid screening of the bioenergetic profiles of mitochondria using different substrates and inhibitors to assess the state of each complex in the mitochondrial respiratory chain (Gusdon et al., 2012; Park et al., 2013). Mitochondria from aged *Atp13a2* null mice had a comparable OCR to wild type mitochondria both during basal conditions and during maximal oxygen consumption (state 4, FCCP). Fluorescence studies of mitochondria from wild type and *Atp13a2* null mouse embryonic fibroblasts using MitoTracker and MitoSox showed no change in overall mitochondrial levels, localization, or amount of oxidized mitochondria (Figure 3.5D). These studies suggest that while subtle alterations to mitochondrial morphology may occur, mitochondrial abnormalities are not a driving cause of CNS dysfunction in *Atp13a2* null mice.

Figure 3.5. Mitochondria from *Atp13a2* null CNS tissue have normal oxygen consumption rates. **A**, Transmission electron microscope images of mitochondria in association with lipid droplets in 18-month-old *Atp13a2* null mouse cortex. **Left**: healthy mitochondria in close proximity to lipid droplet, **right top**: abnormal mitochondria with widened cristae, **right bottom**: partially degraded mitochondria contained within lipofuscin deposit. **B**, Relative oxygen consumption rates (OCR) of mitochondria isolated from wild type or *Atp13a2* null mouse cortex (12- to 18-months-old) with substrates that enter the electron transport chain via different complexes. Relative OCR is defined as the ratio of state 3 consumption rate (ADP) to state 4 consumption rate (oligomycin). **C**, OCR of mitochondria during different respiratory states. Bottom graphs are representative OCR of wild type (red/pink) or *Atp13a2* null (blue/teal) mitochondria from one preparation while bar graphs are the average relative OCR of five independent experiments performed in quadruplicate on a littermate wild type/null pair. **D**, Immunofluorescence of normal and oxidized mitochondria (MitoTracker and MitoSox respectively) in wild type or *Atp13a2* null mouse embryonic fibroblasts. Average cellular fluorescence was quantified as in Figure 2.4D for 20 cells/experiment in three independent experiments. Statistically significant differences are shown. Error bars indicate SEM. Scale bars: **A**, 500 nm, **D**, 20 μ m. Panels **B**, **C** in collaboration with Jeongsoon Park, Lombard lab.

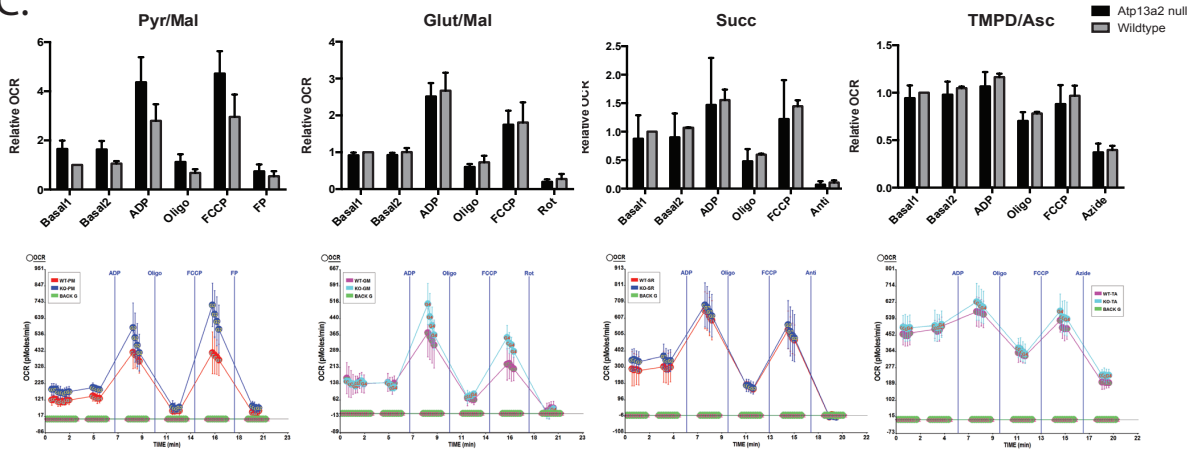
A.



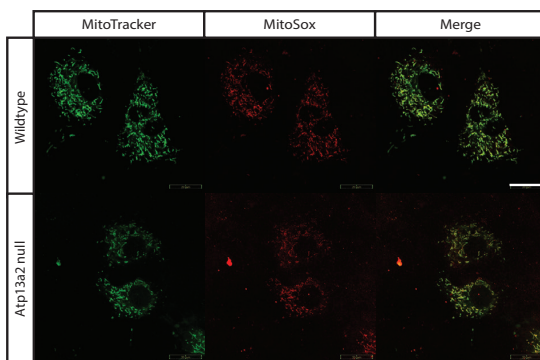
B.



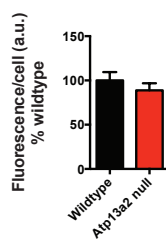
C.



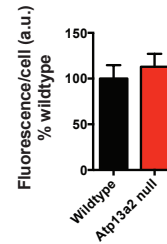
D.



MitoTracker



MitoSox



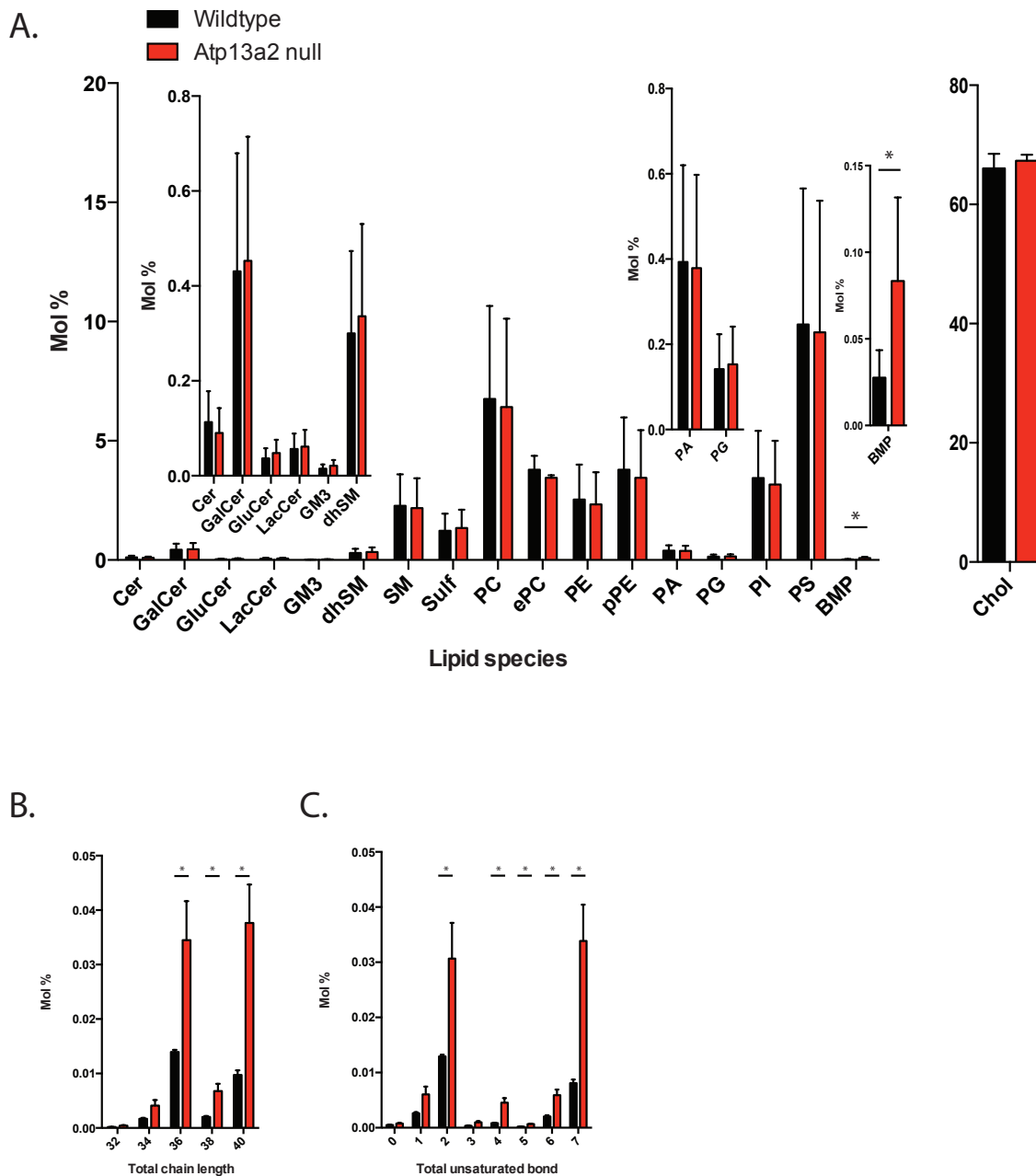
Selective alterations in BMP in Atp13a2 null cortex by lipidomic analysis

Our observation of prominent lipid droplets in multiple brain regions of *Atp13a2* null mice (Figure 2.4) suggested that *Atp13a2* may directly or indirectly affect the cell's lipid profile. We therefore conducted an unbiased lipidomics study of cortical lipid extracts from 18-month-old wild type or *Atp13a2* null mice, examining over 500 lipid species from 31 lipid subclasses. Both wild type and *Atp13a2* null lipid extracts showed similar lipid profiles to other lipidomic studies from mouse cortex (Chan et al., 2012). Free cholesterol levels occupied the bulk of the measured lipidome (WT: 66%, KO: 67%; Figure 3.6A), with the remainder comprised of bulk glycerophospholipids such as phosphatidylserine (PS; WT: 9.9%, KO: 9.6%), phosphatidylcholine (PC; WT: 6.8%, KO 6.4%), phosphatidylethanolamine (PE; WT: 2.5%, KO: 2.3%), plasmalogen phosphatidylethanolamine (pPE; WT: 3.8%, KO: 3.5%), phosphatidylinositol (PI; WT: 3.4%, KO: 3.2%), cholesterol esters (CE; WT: 1.6%, KO: 1.7%) and sphingolipids like sphingomyelin (SM; WT: 2.3%, KO: 2.2%) and sulfatide (Sulf; WT: 1.2%, KO: 1.3%). Contributing less than 4% of the total lipidome were a range of other lipids (Figure 3.6A). Despite increased lipid droplets by ultrastructural analysis, there were no changes to lipids commonly found in lipid droplets (Triglycerides: wild type mol. % = 0.049 ± 0.002 %, *Atp13a2* null mol. % = 0.053 ± 0.003 %, $t = 1.085$, d.f. = 4, $p = 0.34$; cholesterol esters: wild type mol. % = 1.635 ± 0.577 %, *Atp13a2* null mol. % = 1.694 ± 0.272 %, $t = 0.092$, d.f. = 4, $p = 0.93$).

Atp13a2 null cortical lipid extracts had a selective increase of the lysosomal/late endosomal lipid BMP (BMP_{wild type} mol % = 0.0276 ± 0.0015 %, BMP_{*Atp13a2* null} mol % = 0.0834 ± 0.0017 %, $t = 3.335$, d.f. = 4, $p = 0.02$; Figure 3.6A), consistent with selective perturbations to the lysosomal compartment. Further examination of specific BMP lipid species showed an increase in medium (36C) and long-chain fatty acyl chains composed of 38 or more carbon lengths rather

than short-chain (<34C; Figure 3.6B). Corresponding to the long fatty acid chain length, *Atp13a2* null cortical lipid extracts had increased polyunsaturated phospholipids (Figure 3.6C).

Figure 3.6. Selective increase in late endosome/lysosome lipid BMP in cortical lipid extracts of *Atp13a2* null tissue. **A**, Lipid profiles of wild type or *Atp13a2* null cortical lysates. Lipid subclasses are expressed as mean mol % of all lipid species measured. **B**, **C**, Analyses of BMP mean mol % based on the total number of carbon atoms in the fatty acid moieties (**B**) or the number of unsaturated bonds (**C**). Error bars indicate SEM. In collaboration with Di Paolo lab.



Discussion

I sought to understand how loss of endolysosomal Atp13a2 causes the neuropathological and behavioral abnormalities described in chapter 2 through detailed studies of autophagy and lysosomal function, mitochondrial oxygen consumption, and lipid profiles in aged mice. Because many of the pathological changes were age-dependent and did not arise until late in the mouse lifespan (>12 months), I utilized techniques that allowed the analysis of mitochondrial and lysosomal compartments isolated from aged mice. In contrast to *in vitro* reports of widespread autophagy and mitophagy disruption (Dehay et al., 2012; Gusdon et al., 2012; Usenovic et al., 2012), my studies show that loss of Atp13a2 *in vivo* caused highly selective changes to lysosomal function. I observed increased accumulation of p62 in multiple brain regions, consistent with the presence of ubiquitinated aggregates in the cortex and hippocampus of aged *Atp13a2* null mice. I also find selective abnormalities in cathepsin D trafficking. Despite increased overall levels of cathepsin D, less cathepsin D is trafficked to the lysosome and cleaved into its mature form (Figure 3.2, 3.3). This abnormal trafficking appears to be specific to this protease, as other cathepsins (B and L; Figure 3.2B) and other digestive enzymes (hexosaminidase; Figure 3.3C) are unaltered. How loss of Atp13a2 causes such a selective defect in cathepsin D trafficking is unclear, but could suggest that Atp13a2 is a necessary cofactor in the delivery of cathepsin D to the lysosome.

Similar to histopathological and genetic studies, biochemical studies suggest that Atp13a2 does not change α -synuclein proteostasis. *Atp13a2* null lysosomes were able to bind, uptake, and degrade α -synuclein to the same extent as wild type lysosomes (Figure 3.4B). Cathepsin D is known to degrade α -synuclein (Qiao et al., 2008; Sevlever et al., 2008; Cullen et

al., 2009). Complete loss of cathepsin D, as seen in cathepsin D null mice, results in much earlier onset of lipofuscin accumulation (Koike et al., 2000), glial activation, and neurotoxicity (Partanen et al., 2008). While cathepsin D null mice show increased levels of insoluble α -synuclein (Cullen et al., 2009), heterozygous mice do not show changes to α -synuclein levels (Crabtree et al., 2013), consistent with our finding that α -synuclein does not change in the presence of partial loss of lysosomal cathepsin D.

Studies of mitochondrial function and lipidomics revealed similarly selective changes to these cellular compartments. Incidental findings of abnormal mitochondrial morphology prompted us to investigate the OCR of mitochondria derived from aged mice. Mitochondria derived from aged *Atp13a2* null mice showed no changes in basal or maximal OCR utilizing different substrates (Figure 3.5B, C). Slight abnormalities in mitochondrial structure, which need to be confirmed, may be secondary to primary lysosomal deficits and are likely not a driving force of neuronal dysfunction in *Atp13a2* null mice. Similarly, lipidomics studies showed selective alterations to lysosomal compartments. Cortical lipid extracts showed increased levels of the lysosome/late endosome lipid BMP, confirming the upregulation of lysosome associated proteins like LAMP1 and LAMP2 in aged *Atp13a2* null mice. Despite prominent lipid droplets in the cortex at 18 months, lipidomics showed no other subclass of lipid elevated in *Atp13a2* null mice, possibly because the lipids contained within lipid droplets were diluted out by total cortical lipids. This result does not rule out ATP13A2 functioning as a lysosomal lipid flippase as these studies did not distinguish between the different sides of the phospholipid bilayer. It does suggest, however, that loss of *Atp13a2* is not profoundly changing the lipid profile in contrast to models of Niemann Pick type C or AD (Chevallier et al., 2008; Chan et al., 2012).

In contrast to *in vitro* studies, I show that loss of *Atp13a2* *in vivo* causes selective disruption of lysosomal function, specifically leading to alterations in cathepsin D processing and accumulation of p62. With increasing emphasis on disruptions in the endolysosomal system causing PD and related neurodegenerative diseases, it is important to understand how changes to intracellular trafficking cause disease pathogenesis. I present, for the first time, a mouse model of PD in which neuropathological and behavioral abnormalities occur with specific changes to the lysosomal compartment, such as increases in lysosomal proteins and lipids, accumulation of autophagy substrates like p62, ubiquitin, and lipid droplets, and selective trafficking defects in cathepsin D. This selectivity is in contrast to the working model of PD and autophagy in which PD genes cause neurotoxicity through widespread autophagy deficits and the accumulation of neurotoxic α -synuclein. Indeed, I see no accumulation of α -synuclein, nor alterations to α -synuclein's ability to bind or be degraded by *Atp13a2* null lysosomes. These studies therefore prompt a deeper inquiry into endolysosomal dysfunction in the context of PD-related genetic insults.

Materials and Methods

Antibodies and materials. The following antibodies were used: cathepsin B (1:500; Santa Cruz Biotechnology Inc. #sc-6493), cathepsin D (1:300; Santa Cruz Biotechnology Inc. #sc-6486), cathepsin L (1:200; Santa Cruz Biotechnology Inc. #sc-10778), EEA1 (1:5000; BD Biosciences #610456), GAPDH (1:3000; Abcam #AB8245), LAMP2A (1:1000; Invitrogen #51-2200), LC3 (1:5000; Novus Biologicals #NB100-2220), p62/SQSTM1 (WB: 1:10,000; AbNova #H00008878-01; IHC: 1:1000; American Research Products #03-GP62-C), Rab9 (1:3000; Santa Cruz Biotechnology Inc. #sc-28573), α -synuclein (1:10,000; Santa Cruz Biotechnology Inc. #sc-

5587 or 1:500; BD Biosciences #610786), and Vps4 (1:2000; Sigma-Aldrich, #SAB4200025). OregonGreen Dextran, MitoTracker, and MitoSox were from Invitrogen Corp.

Tissue homogenization and Western blot. To prepare brain lysates, microdissected frozen brains were homogenized with a Dounce homogenizer in an appropriate volume of ice-cold RIPA buffer (50mM Tris-HCl, pH 7.4, 150 mM NaCl, 0.1% SDS, 0.5% SDOC, and 1% NP-40) containing protease inhibitors (Roche Molecular Biochemicals). The samples were then sonicated to solubilize all proteins. Protein concentrations were determined using the BCA assay (Pierce Biotechnology). Proteins were separated by SDS-PAGE using Tris-HCl 4-20% gradient gels (BioRad) and transferred onto PVDF membranes (BioRad). Membranes were blocked in 5% non-fat milk in TBS-T (TBS plus 0.1% (v/v) Tween 20) for 1 hour, followed by overnight incubation at 4°C in primary antibodies in 5% non-fat milk in TBS-T. After a 1-hour incubation in an HRP-conjugated secondary antibody, immunoreactive bands were visualized on film by enhanced chemiluminescence (SuperSignal West Pico).

Immunocytochemistry. Wild type and *Atp13a2* null male mice at the indicated ages were anesthetized with a lethal dose of xylazine and ketamine HCl and transcardially perfused with a 0.9% saline solution followed by 4% paraformaldehyde in phosphate buffer. Whole brains were post-fixed overnight, equilibrated in 30% sucrose, and embedded in O.C.T. (Tissue-Tek). 40 µm frozen sagittal sections were collected on a Leica CM1850 cryostat (Leica Biosystems). For immunofluorescence, sections were blocked in 5% Normal Donkey Serum (NDS) in PBS-Tx (PBS plus 0.01% TritonX-100). Following overnight incubation at 4°C in primary antibodies in 1.5% NDS/PBS-Tx, sections were incubated in an AlexaFluor 488- or 555-conjugated secondary

(Invitrogen), incubated with 0.3% Sudan Black in 70% ethanol to quench autofluorescence, and mounted using ProLong Gold. For DAB immunohistochemistry, the following modifications were made to the above protocol. Prior to block, sections were first subjected to 30 min in 0.3% H₂O₂ in PBS to quench endogenous peroxidase activity. After a 1-hour incubation in a biotinylated secondary antibody (Jackson ImmunoResearch), sections were incubated in ABC for 1 hour (Vector Laboratories) followed by DAB reaction (Sigma-Aldrich). Images were acquired with a Zeiss Axioskop microscope (Carl Zeiss Group). Confocal images were acquired on an Olympus FluoView 500 (Olympus America) in the University of Michigan Microscopy and Image Analysis Laboratory. For each experiment, a representative image was selected after examination of four to ten animals.

Mouse embryonic fibroblast culture. Mouse embryos from an E12.5 female were dissected into ice-cold PBS. The head, liver, and heart were removed and the remaining tissue was trypsinized (0.25% trypsin in HBSS) at 37°C for 10 min. Trypsinized tissue was centrifuged (300 x g for 5 min), and washed two times with HBSS. The pelleted cells were resuspended in media (DMEM + 10% fetal bovine serum) and plated on 10 cm dishes. For mitochondrial studies, MitoTracker and MitoSox were used according to manufacturer instructions.

Lysosomal isolation. Two different lysosomal populations preferentially involved in chaperone-mediated autophagy (CMA) or in macroautophagy (MA) were isolated by centrifugation from a light mitochondrial/lysosomal fraction of a pool of 2 mice brains in a discontinuous metrizamide density gradient as reported before (Cuervo et al., 1997). Lysosomal integrity was verified after

isolation by measuring β -hexosaminidase latency and only preparations with more than 90% intact lysosomes were used.

Degradation of substrate proteins by lysosomes in vitro. Intact freshly isolated lysosomal subpopulations isolated as described above were incubated with a pool of radiolabeled proteins in 3-(N-morpholino)propanesulfonic acid (MOPS) buffer (10 mM MOPS, pH 7.3, 0.3 M sucrose, 1 mM dithiothreitol and 5.4 μ M cysteine) for 30 min at 37°C as described before (Kaushik and Cuervo, 2009). Reactions were stopped with 20% TCA, filtered through a Millipore Multiscreen Assay System (Millipore, Billerica, MA) and detected in a liquid scintillation analyzer (PerkinElmer Wallac, Gaithersburg, MD). Proteolysis was measured as the percentage of the initial acid-insoluble radioactivity (protein) transformed into acid-soluble radioactivity (peptides and free aminoacids). To analyze total proteolytic activity this assay was performed instead with lysosomes whose membrane had been disrupted by a hypotonic shock and addition of 0.1% Triton X-100.

Binding and uptake of α -synuclein as a CMA substrate by isolated lysosomes. Freshly isolated intact CMA active lysosomes were incubated with the substrate protein α -synuclein in MOPS buffer at 37°C for 20 min. Where indicated, lysosomes were preincubated with a cocktail of protease inhibitors for 10 min at 0°C to inhibit degradation of the substrate inside the lysosomes as described before (Cuervo et al., 2004). Lysosomes were collected by centrifugation, washed with MOPS buffer and subjected to SDS-PAGE, and immunoblotted for α -synuclein. Binding was calculated from the densitometric analysis as the amount of substrate protein bound to the lysosomal membrane in the absence of protease inhibitors. Uptake was calculated by subtracting

the amount of protein associated with lysosomes in the presence (protein bound to the lysosomal membrane and taken up by lysosomes) and absence (protein bound to the lysosomal membrane) of protease inhibitors.

Lysosomal pH. Lysosomal pH was determined using ratiometric imaging of endocytosed Oregon Green Dextran as described (Elrick et al., 2012). Oregon Green Dextran has both a pH-independent (440nm) and pH-dependent (492 nm) excitation maximum, with a pKa of 4.7, allowing the measurement of pH in living cells. Briefly, mouse embryonic fibroblasts grown on glass coverslips were pulsed overnight with 150 µg/mL Oregon Green Dextran in culture medium, which was then chased into lysosomes by washing 3 times and incubating in regular medium for 3-5 hours. Cells were then rinsed and imaged in Ringer's buffer (155 mM NaCl, 5 mM KCl, 2 mM CaCl₂, 1 mM MgCl₂, 2 mM NaH₂PO₄, 10 mM HEPES, and 10 mM glucose) using a Nikon TE300 inverted microscope with two filter pairs (Excitation/emission wavelengths - C1: 436/535 nm; C2: 492/535 nm). Calibration was performed as described (Elrick et al., 2012). Using GraphPad Prism 5.0, the standards were fit to a sigmoidal curve by the least squares method, and unknown pH values were interpolated from this curve.

Transmission electron microscopy. 12-month-old *Atp13a2* null or wild type mice were prepared for ultrastructural analysis as previously described (Goodchild et al., 2005). Briefly, mice were transcardially perfused with 4% paraformaldehyde/2.5% glutaraldehyde in 100 mM sodium phosphate buffer (pH 7.4), followed by overnight postfixation in the same solution. Samples were postfixated with 1% osmium tetroxide in 0.1 M cacodylate buffer (pH 7.4) for 1 hour, followed by treatment with 3% uranyl acetate, dehydration with alcohol, propylene oxide

treatment, and embedding in Embed 812 (Electron Microscopy Sciences, Fort Washington, PA). The resin was polymerized in a 60°C oven for 2 days and sections were cut with a Dupont diamond knife on a Reichart Ultracut-E microtome (Leica), collected on copper grids, and double stained with saturated aqueous uranyl acetate and lead citrate. Images were taken using a Philips CM-100 transmission electron microscope (Philips Research) and AMTV540 image capture software (Advanced Microscopy Techniques) in the University of Michigan Microscopy and Image Analysis Laboratory.

Mitochondrial respiration. Respiration of isolated mitochondria was measured with a Seahorse XF-24 Analyzer (Seahorse Bioscience, North Billerica, MA USA) as previously described (Park et al., 2013). Cortices were isolated from 18-month old *Atp13a2* null or wild type mice and gently homogenized in hypotonic buffer (10 mM HEPES pH 7.9, 10 mM KCl, 0.1 mM EDTA) containing protease inhibitors (Roche) for 15 min on ice with a Dounce homogenizer. Mitochondria were isolated by centrifugation at 800 x g for 5 min at 4°C to pellet nuclei. The resulting supernatant was centrifuged at 6200 x g for 10 min at 4°C to pellet mitochondria. Mitochondria were diluted to 0.2 mg/ml in BSA-free LM (70 mM sucrose, 220 mM mannitol, 1 mM EGTA, 2 mM HEPES, 1% w/v defatted BSA, pH 7.2; Mailloux et al., 2013). 10 µg mitochondria (except for ascorbate/TMPD where 5 µg was used) was loaded into Seahorse tissue culture plate wells and centrifuged at 2000 x g for 10 min at 4°C to attach mitochondria to the plate. OCR was first measured under state 2 conditions (substrate only: 10 mM pyruvate and 5 mM malate, or 5 mM succinate and 2 µM rotenone, or 5 mM glutamate and 5 mM malate, or 1 mM TMPD and 100 mM ascorbate). State 3, state 4 (proton leak-dependent respiration), maximal respiration, and respiration independent of the respiratory chain were tested by the

sequential injection of 0.1 mM ADP (state 3), 2.5 µg/mL oligomycin (state 4), 2 µM FCCP (maximal respiration), and 5 mM fluoropyruvate or 2 µM rotenone or 4 µM antimycin A or sodium azide (respiration independent of the respiratory chain) respectively. Relative OCR was defined as the ratio of OCR during State 3 to State 4 respiration. Four independent measurements, in triplicate, were recorded at baseline, and after the addition of each compound. Mitochondria isolated from five mice were analyzed separately and averaged together to obtain final values.

Lipid analysis using high performance liquid chromatography-mass spectrometry. Lipid extracts were prepared from 18-month-old cortical lysates using a modified Bligh/Dyer extraction procedure as previously described (Chan et al., 2012). Samples were analyzed using an Agilent Technologies 6490 Ion Funnel LC/MS Triple Quadrupole system with front end 1260 Infinity HPLC. Phospholipids and sphingolipids were separated by normal phase HPLC while neutral lipids were separated using reverse phase HPLC. For normal phase analysis, lipids were separated on an Agilent Rx-Sil column (i.d. 2.1 x 100 mm) using a gradient consisting of A: chloroform/methanol/ammonium hydroxide (89.9:10:0.1) and B: chloroform/methanol/water/ammonium hydroxide (55:39:5.9:0.1), starting at 5% B and ramping to 70% B over a 20 min period before returning back to 5% B. Neutral lipids were separated on an Agilent Zorbax XDB-C18 column (i.d. 4.6 x 100 mm) using an isocratic mobile phase chloroform:methanol:0.1M ammonium acetate (100:100:4) at a flow rate of 300 µL/min. Multiple reaction monitoring (MRM) transitions were set up for quantitative analysis of different lipid species and their corresponding internal standards as described previously (Chan et al., 2012). Lipid levels for each sample were calculated relative to the spiked internal standards and then normalized to the

total amount of all lipid species measured and presented as relative mol %. Data are presented as mean mol % for 3 samples of each genotype.

Statistics. Results were analyzed using GraphPad Prism 5.0. Data were first examined for equal variance and then subjected to student's *t*-tests as indicated. In all studies, n indicates the number of samples per group and a critical value of $p \leq 0.05$ was used. Data are plotted as means \pm SEM.

Chapter 4

Association between LRRK2 and microtubules enhanced by Parkinson disease

mutations and kinase inhibition by LRRK2-IN-1²

Abstract

Dominant missense mutations in leucine-rich repeat kinase 2 (LRRK2) are the most common genetic causes of Parkinson disease (PD) and genome-wide association studies identify LRRK2 sequence variants as risk factors for sporadic PD. Intact kinase function appears critical for toxicity of LRRK2 PD mutants, yet our understanding of how LRRK2 causes neurodegeneration remains limited. I find that most LRRK2 PD mutants abnormally enhance LRRK2 oligomerization, causing it to form filamentous structures in transfection of cell lines or primary neuronal cultures. Strikingly, ultrastructural analyses, including immuno-electron microscopy and electron microscopic tomography, demonstrate that these filaments consist of LRRK2 recruited onto part of the cellular microtubule network in a well-ordered, periodic fashion. Like LRRK2-related neurodegeneration, microtubule association is abolished with the introduction of kinase-dead mutations or mutations that remove the WD40 domain, potentially linking microtubule binding and neurodegeneration. Treatment with the inhibitor LRRK2-IN-1 caused increased filament formation in both wild type and G2019S-LRRK2 transfected cells, suggesting

² Most of this chapter was originally published as: Kett LR*, Boassa D*, Ho CC*, Rideout HJ, Hu J, Terada M, Ellisman M, and Dauer WT. 2012. LRRK2 Parkinson disease mutations enhance its microtubule association. Hum Mol Genet 21(4):890-899. (* These authors contributed equally to the publication.)

that LRRK2-microtubule association may be a normal physiological process that is enhanced with PD mutations or kinase inhibition. These observations identify a novel effect of LRRK2 PD mutations and highlight a potential role for microtubules in the pathogenesis of LRRK2-related neurodegeneration.

Introduction

The currently understood biology of leucine-rich repeat kinase 2 (LRRK2) suggests that studies of this protein may provide new insights into neurodegeneration that are broadly relevant to sporadic Parkinson disease (PD) and amenable to therapeutic targeting. Genome-wide association studies demonstrate that common variation around the locus that encodes LRRK2 segregates with increased risk for PD (Satake et al., 2009; Simon-Sanchez et al., 2009) and missense mutations in LRRK2 cause a clinical and neuropathological syndrome indistinguishable from typical-appearing sporadic PD (Zimprich et al., 2004). LRRK2 contains GTPase and kinase domains, as well as leucine-rich repeat (LRR) and WD40 protein-protein interaction domains (Figure 4.1A). Many potentially pathogenic sequence alterations have been identified in LRRK2, but only five missense mutations (Figure 4.1A) clearly segregate with PD in large family studies (Bonifati, 2007). Two of these mutations (R1441G, R1441C) are located in the GTPase domain (termed Ras of complex proteins, or ‘Roc’ domain), a third (Y1699C) falls in a region between the GTPase and kinase domains (termed the C-terminal of Roc, or ‘COR’ domain) and two other mutations (G2019S and I2020T) are in the kinase domain.

LRRK2 appears to exist as a dimer (Greggio et al., 2006; Deng et al., 2008; Jorgensen et al., 2009), and studies of fragments of LRRK2 or its prokaryotic homolog indicate that dimerization occurs in the Roc-COR region (Deng et al., 2008). Structural analyses of these

fragments indicate that the R1441C PD mutation (or mutation of the analogous residue in the prokaryotic protein) can destabilize the dimer formed by these fragments (Deng et al., 2008; Gotthardt et al., 2008). Yet, available data do not define the functional significance of LRRK2 self-association and it is unclear whether this property is altered in PD mutant forms of the full-length protein. One possibility is that LRRK2 self-association regulates its kinase activity, but only the G2019S mutation clearly increases kinase activity (by ~3-5-fold), whereas the other mutations appear to have little or no effect on kinase function (Greggio et al., 2006; MacLeod et al., 2006; Smith et al., 2006; Jaleel et al., 2007; West et al., 2007), at least in the *in vitro* assays used thus far. Intact kinase function does appear necessary for LRRK2 toxicity *in vitro* and *in vivo* (Greggio et al., 2006; Smith et al., 2006; Lee et al., 2010). LRRK2-induced neurodegeneration of primary neuronal cultures is caspase-dependent, and may involve activation of the fas-associated protein with death domain (FADD)-caspase-8 pathway (Ho et al., 2009). One site of LRRK2 toxicity may be in neuronal processes, as overexpression of LRRK2 *in vitro* or *in vivo* causes neurite shortening, whereas the loss of LRRK2 function leads to increased neuron length and branching (MacLeod et al., 2006). The molecular details that underlie LRRK2 effects in neuronal processes are not clear, but may involve interactions with the cytoskeleton or cytoskeletal-related molecules (Jaleel et al., 2007; Gandhi et al., 2008; Gillardon, 2009; Parisiadou et al., 2009).

Here, I present evidence that four PD mutations (R1441C, R1441G, Y1699C, I2020T) cause LRRK2 to decorate microtubules in a well-ordered periodic fashion, as evidenced by immunofluorescence, immuno-electron microscopy (EM) and EM tomographic studies. Microtubule-associated LRRK2 appears as filamentous structures in transfected cell lines or primary neuronal cultures, and the frequency of these structures increases with microtubule

stabilization (taxol) and decreases with microtubule dissolution (nocodazole). Similar to LRRK2-induced neurodegeneration, filament formation returns to baseline in LRRK2 mutants containing kinase-dead mutations or mutants lacking the WD40 domain, potentially linking LRRK2-microtubule association to neurodegeneration. Similar filament formation occurs rapidly in wild type and G2019S-LRRK2 transfected cells following treatment with LRRK2 kinase inhibitors, potentially implicating improper LRRK2 signaling in its microtubule association. These observations identify a novel effect of LRRK2 PD mutations, and provide a platform to further dissect LRRK2-related signals by identifying factors that modulate the interaction between LRRK2 and microtubules.

Results

LRRK2 mutations enhance filament formation

In multiple cell lines (including Cath.a-differentiated (CAD), human embryonic kidney (HEK293T), and HeLa) transfected with wild type (WT) LRRK2, LRRK2 adopted a primarily diffuse cytosolic distribution, but we also observed LRRK2-positive aggregates and a distinct pattern of filament formation (Figure 4.1B). These patterns were observed with different epitope tags (e.g. GFP and V5) as well as with untagged protein (data not shown). To determine whether PD mutations alter the subcellular distribution of LRRK2, we quantified the frequency of these patterns (diffuse, aggregate or filament) for WT and all PD mutant alleles (Figure 4.1C and E). This analysis was performed in the neuronal catecholaminergic CAD cell line because of the robust transfection efficiency possible with this system. The percentage of cells with punctate aggregates was not increased by any of the PD mutant alleles (Figure 4.1C), so these structures likely represent a non-specific effect of LRRK2 overexpression. In contrast, filament formation

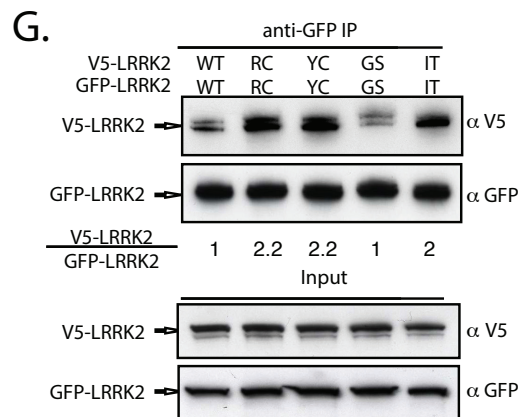
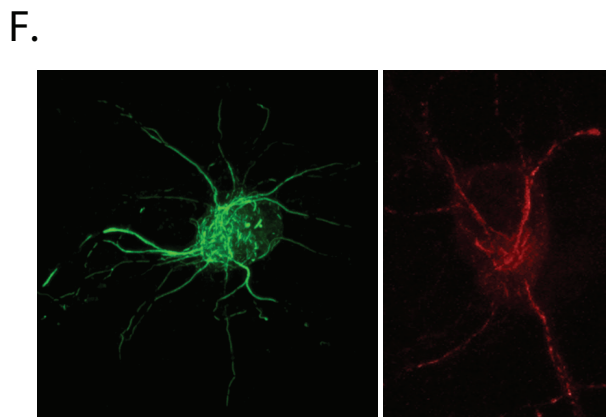
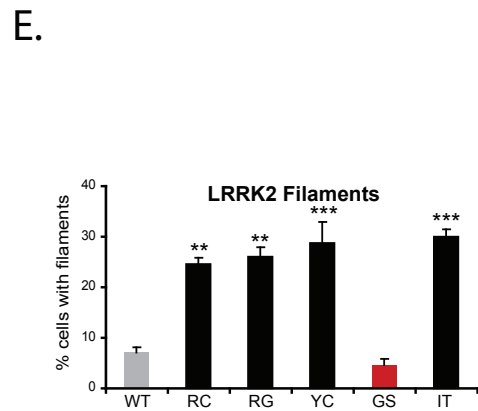
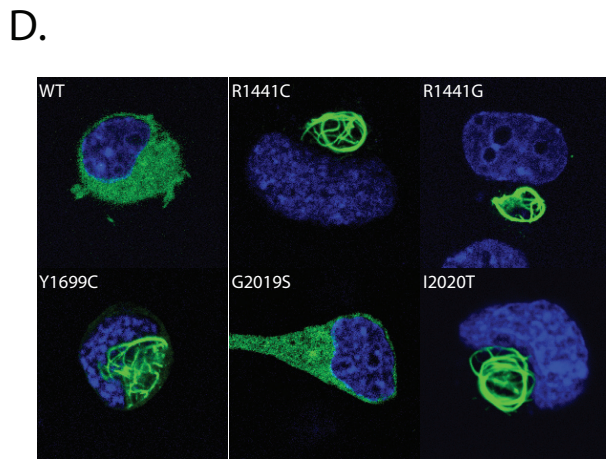
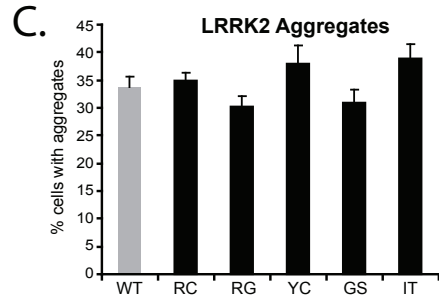
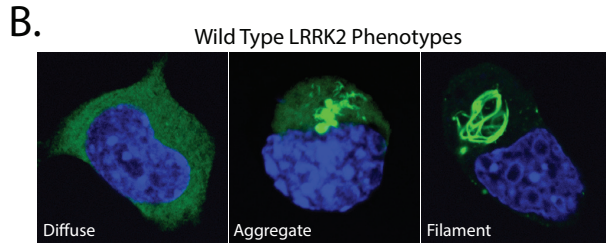
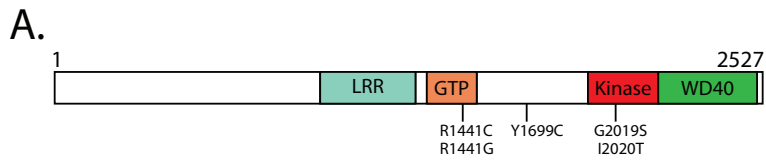
was enhanced by all LRRK2 PD mutations that do not consistently enhance kinase function (Greggio et al., 2006; Smith et al., 2006; Jaleel et al., 2007), whereas no effect on filament formation was observed for the single mutant, G2019S, that consistently increases kinase activity (Figure 4.1D and E; Greggio et al., 2006; Smith et al., 2006; Jaleel et al., 2007). Notably, steady-state protein levels of WT and PD mutant LRRK2 are similar (data not shown), so these filament-forming mutations do not appear to act by altering LRRK2 stability. Morphologically, these filaments are reminiscent of death-effector filaments formed by FADD, caspase-8, tumor necrosis factor receptor type 1-associated death domain protein, and BCL10 (Siegel et al., 1998; Guiet and Vito, 2000; Fotin-Mleczek et al., 2002). All of these filament-forming proteins participate in cell death-related signaling, potentially providing a clue to LRRK2 function relevant to neurodegeneration. LRRK2 filaments also occur in LRRK2-transfected primary neurons, both in the cell body and in neurites, and with both yellow fluorescent protein (YFP)-tagged as well as untagged protein (Figure 4.1F).

For previously characterized filament-forming proteins, filament formation reflects a homotypic protein-protein interaction that is required for their normal signaling function (Guiet and Vito, 2000; Fotin-Mleczek et al., 2002; Muppidi et al., 2006). Oligomerization is also a signaling mechanism employed by RIP1 and RIP2 kinases (Inohara et al., 2000), close phylogenetic relatives of LRRK2. These facts led to the hypothesis that the filaments represent enhanced LRRK2 oligomerization. To investigate the extent to which LRRK2 oligomerizes, we co-expressed GFP- and V5-LRRK2 in CAD cells and tested whether they co-immunoprecipitate (co-IP). Lysates were immunoprecipitated with a GFP antibody and probed for associated V5-LRRK2. Differentially tagged WT-LRRK2 molecules did co-purify (Figure 4.1G), indicating that LRRK2 can oligomerize. Moreover, LRRK2 oligomerization was clearly enhanced by

filament-forming PD mutations (R1441C, Y1699C, I2020T), whereas the non-filament-inducing mutant (G2019S) did not differ from the WT-LRRK2 control (Figure 4.1G). The oligomerization status of LRRK2 mutants therefore correlates with the level of filament formation, indicating that the cytosolic filaments are related to the oligomerization aspect of LRRK2 biology.

LRRK2 filaments appear similar to cytoskeletal structures, suggesting that LRRK2 was either templating onto existing cytoskeletal elements or forming novel ‘LRRK2 only’ structures. To determine which, if any, cytoskeletal structures LRRK2 may interact with, I examined cells transfected with FLAG-LRRK2-I2020T with both anti-FLAG and a panel of antibodies against the major cytoskeletal elements, as well as with MitoTracker and caspase-8, since mitochondria exist in filamentous strands and caspase-8 has been shown to associate with LRRK2 (Ho et al., 2009). However, LRRK2 filaments staining did not colocalize with any of these markers (data not shown).

Figure 4.1. Multiple pathogenic mutations enhance LRRK2 oligomerization and filament formation in a kinase-dependent manner. **A**, Domain structure and Parkinson's disease mutations of LRRK2. LRR, leucine-rich repeat; GTP, GTPase domain (also called Roc domain, Ras of complex proteins). Five PD-causing missense mutations are shown. **B-E**, The formation of LRRK2 filaments is enhanced by multiple PD mutations. Cath.a-differentiated (CAD) cells were transfected with WT (**B**) or PD mutant forms (**D**; R1441C, R1441G, Y1699C, G2019S, I2020T) of GFP-tagged LRRK2. WT-LRRK2 adopted either a diffuse, aggregated or filamentous pattern of subcellular localization (**B**; labeled using anti-GFP antibody). The frequency of cells bearing LRRK2 aggregates or filaments was quantified 48 hour after transfection (**C** and **E**). Multiple PD mutations increased the percentage of cells with LRRK2 filaments (labeled using anti-GFP antibody). Data are means \pm S.E.M. of four to five independent experiments (** $p < 0.01$, *** $p < 0.001$, n.s., non-significant; ANOVA with Tukey's test). **F**, Expression of LRRK2 in neuronal processes. Yellow fluorescent protein (YFP)-LRRK2-Y1699C was transfected into primary cortical neurons and imaged by confocal microscopy (left image, YFP fluorescence shown in green). A similar pattern of filament formation was observed in neurites in primary neurons transfected with untagged LRRK2-I2020T (right image, labeled using an anti-LRRK2 antibody shown in red). **G**, WT LRRK2 oligomerizes and multiple LRRK2 PD mutations enhance its oligomerization. V5-LRRK2 was co-expressed in CAD cells with GFP or GFP-LRRK2. Lysates were immunoprecipitated with anti-GFP 48 hour after transfection, and the immunoprecipitates were analyzed with anti-V5 and anti-GFP immunoblots. The oligomeric state of LRRK2 is shown as a relative ratio of co-purified V5-LRRK2 to GFP-LRRK2, normalized to the WT-LRRK2 ratio. In collaboration with C.C. Ho, H. Rideout, Dauer lab.



LRRK2 decorates microtubules in an organized manner

To further explore the nature of LRRK2 filaments, we employed EM to define the ultrastructure of these structures. A correlated light and EM study was conducted by transfecting HEK293T cells with YFP-LRRK2-I2020T, using YFP fluorescence to identify filament-bearing cells, and then processed the same samples for EM to obtain high-resolution information on LRRK2 distribution in specific subcellular domains. Figure 4.2 shows filament formation identified by YFP fluorescence (Figure 4.2A-C) and the corresponding low-magnification electron micrograph of a thin section from the same area (Figure 4.2D). Increasing magnifications (Figure 4.2E and F) reveal filamentous structures organized in parallel arrays. The filaments consist of microtubules, identified by their characteristic structure in high-resolution EM as well as the correlated immunofluorescence, and these consist of LRRK2 apparently recruited onto parts of these unusually arrayed microtubules (Figure 4.2F and G). Areas of naked microtubules (indicated by black arrows in Figure 4.2G) were interrupted by bundles of microtubules decorated by electron densities around them (indicated by black arrowheads in Figure 4.2G). Immuno-EM using a specific antibody against LRRK2 confirmed the specificity of LRRK2 densities around the microtubules (Figure 4.3A). To further examine the organization of the filaments, we performed electron tomography on 250 nm thick sections. The tomograms show that LRRK2 appears to interact closely with the microtubules in a well-ordered, periodic fashion (Figure 4.3B-E).

Figure 4.2. Pattern of expression of LRRK2 using correlated light and EM. (A–C) The distribution of LRRK2 filaments was revealed in HEK293T cells expressing YFP-LRRK2-I2020T by the YFP fluorescence, (D) correlated image at low-power EM and (E–G) intermediate magnifications. Intermediate magnification of filaments (G) shows areas of naked microtubules (arrows) as well as electron densities (arrowheads) around them. In collaboration with D. Boassa, Ellisman lab.

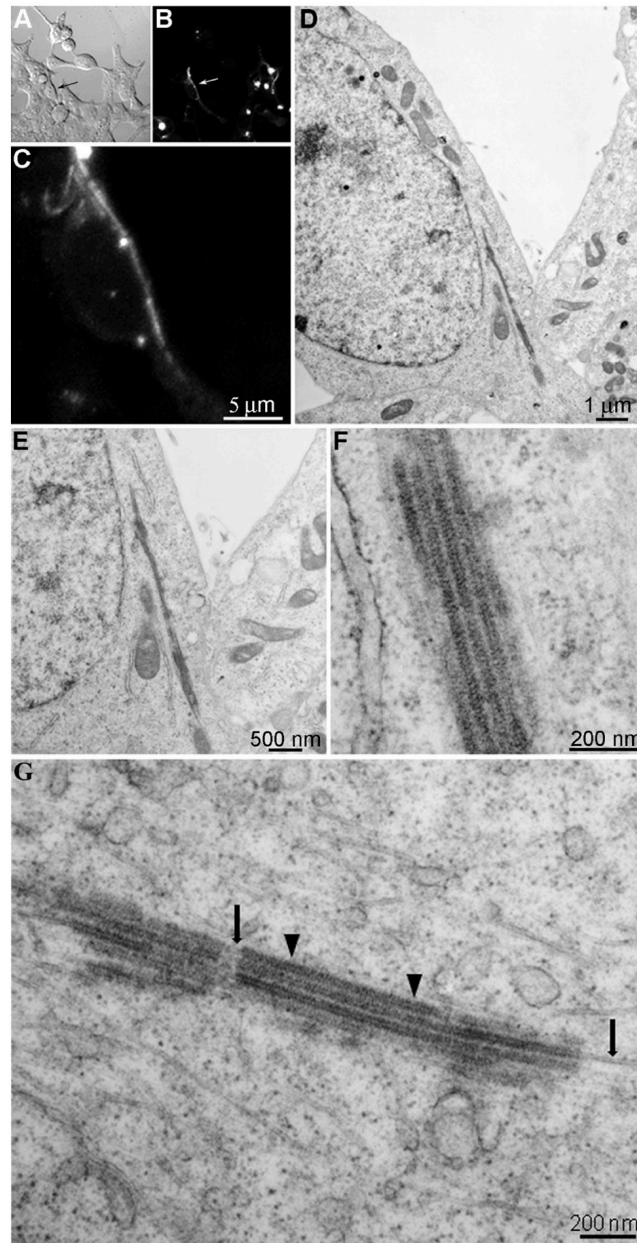
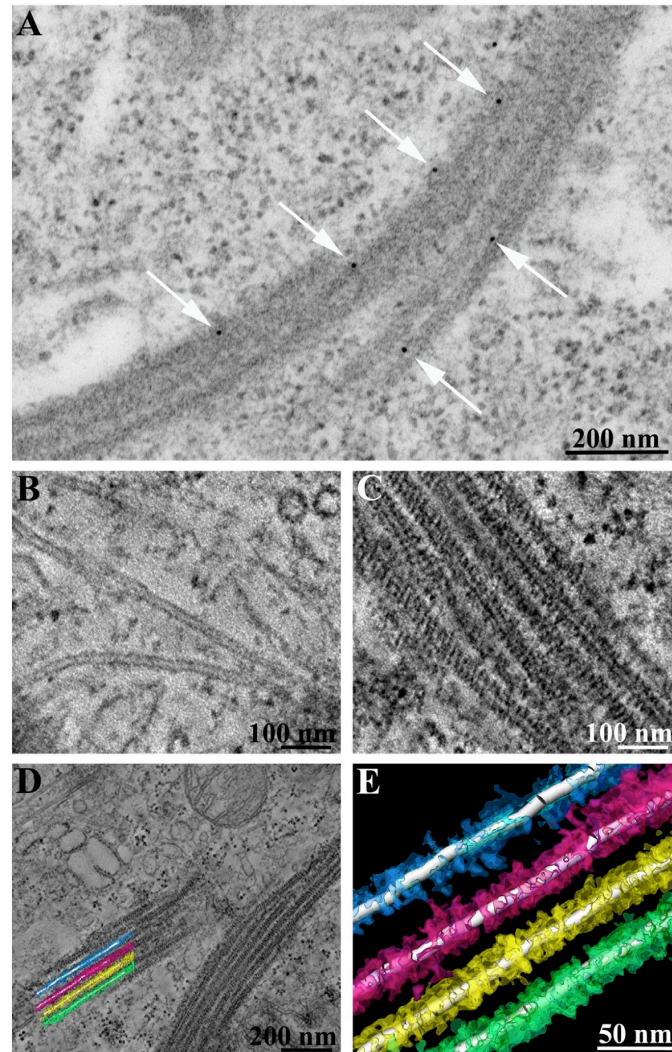


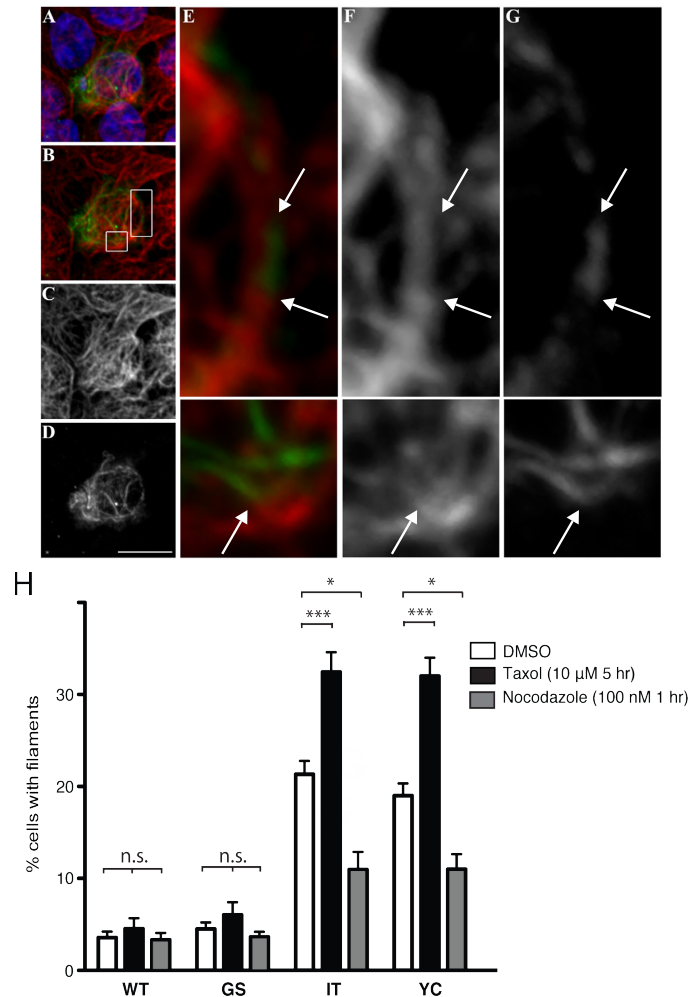
Figure 4.3. Immuno-EM and electron tomography of LRRK2 filaments. **A**, Immuno-EM was performed with a LRRK2-specific antibody. Immuno-gold signals appear as black dots (indicated by white arrows) on bundles of microtubules. **B-E**, Electron tomography of LRRK2 filaments. Higher magnification images of non-decorated tubules (**B**) and decorated microtubules (**C**) from electron tomograms are shown as well as a low power field from the area reconstructed by electron tomography (**D**) from which a graphical reconstruction was produced using Amira (**E**). In collaboration with D. Boassa, Ellisman lab.



The tomographic data showing LRRK2 ‘coating’ microtubules suggested that masking of the tubulin epitope by LRRK2 could explain the lack of co-localization between tubulin and LRRK2 immunofluorescence. Indeed a re-examination of individual Z-images from the immunofluorescent staining (rather than the maximal intensity projection) showed distinct

regions in which LRRK2 filaments appear as direct continuations of microtubules (Figure 4.4A-G). I further explored the LRRK2-microtubule association by testing whether the frequency of filament formation was altered by microtubule stability. To accomplish this, I treated LRRK2-transfected CAD cells with the microtubule-stabilizing drug taxol (10 μ M for 5 hours), the microtubule-destabilizing drug nocodazole (100 nM for 1 hour), or vehicle [dimethyl sulfoxide (DMSO)] control. An examiner blinded to genotype and drug treatment then counted the proportion of cells with filaments. Analysis of filament proportion showed an effect of genotype, drug treatment, and the interaction between the two [two-way analysis of variance (ANOVA): $F = 14.36$, $P < 0.0001$]. In cells transfected with either GFP-LRRK2-I2020T or Y1699C, taxol increased the percentage of filament-bearing cells, whereas this percentage was decreased by nocodazole (Figure 4.4H). In contrast, taxol or nocodazole did not change the percentage of filament-bearing cells transfected with GFP-LRRK2-WT or G2019S. This distinction between the behavior of the G2019S and the other PD mutations is similar to that observed for their kinase activity (Greggio et al., 2006; MacLeod et al., 2006; Smith et al., 2006; Jaleel et al., 2007; West et al., 2007). Taken together with the observations of LRRK2-coating microtubules by EM tomography, these data further indicate that multiple LRRK2 PD mutations (but not G2019S) enhance its ability to associate with microtubules under normal cellular conditions. As cellular stressors, it is possible that taxol and nocodazole treatment alter LRRK2 behavior through indirect mechanisms, although the fact that they modulate filament formation in opposite directions makes it unlikely.

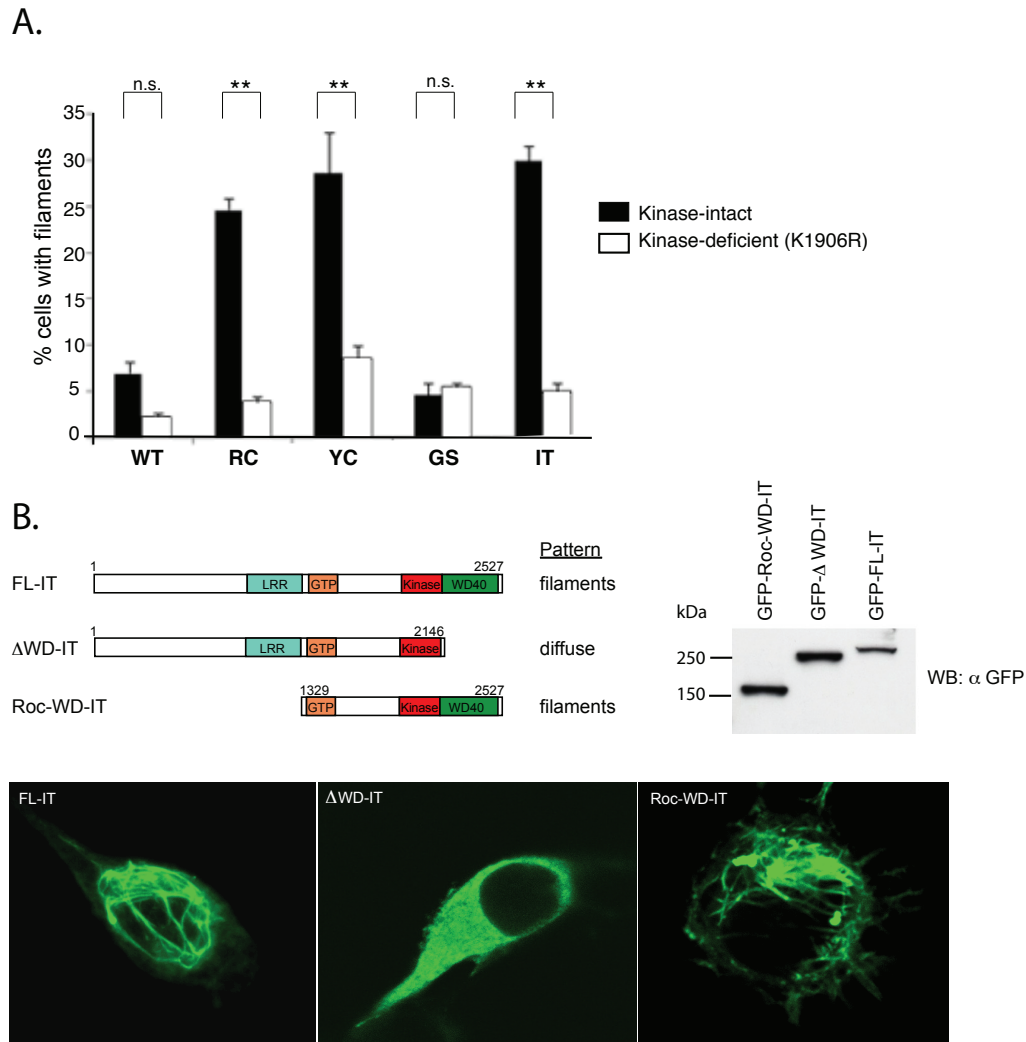
Figure 4.4. LRRK2 filaments associate with microtubules and are modified by microtubule-altering drugs. **A-G**, LRRK2 filaments localize to microtubules. HEK293T cells transfected with FLAG-LRRK2-I2020T were double labeled with anti-FLAG (**D** and **G**) and anti-alpha tubulin (**C** and **F**) antibodies. LRRK2 filaments appear as continuations of microtubules (**A**, **B**, and **E**, merged images showing tubulin in red, LRRK2-FLAG in green and nuclei in blue; insets in **B** are shown in **E**, **F**, and **G**). Arrows denote portions of microtubules positive for LRRK2 staining, but lacking tubulin staining. Scale bar is 10 μm . **H**, Treatment with microtubule-altering drugs changed the filament proportion. CAD cells were transfected with WT or PD mutant forms (G2019S, I2020T or Y1699C) of GFP-LRRK2. Forty-eight hours post-transfection, cells were treated with the microtubule-stabilizing drug taxol (10 μM for 5 hours), the microtubule-destabilizing drug nocodazole (100 nM for 1 hour) or dimethyl sulfoxide (DMSO) control. Following drug treatment, cells were fixed, stained for GFP and the frequency of cells with filaments was quantified. Data are means + SE of three independent experiments. (* $p < 0.05$, *** $p < 0.001$, n.s. non-significant; two-way analysis of variance (ANOVA) with post-hoc Tukey's test).



LRRK2-microtubule association affected by kinase-dead mutations and requires the WD40 domain

Kinase-dead mutants prevent the neurotoxicity of LRRK2 PD mutants (Greggio et al., 2006; Smith et al., 2006) and may therefore prevent the enhanced microtubule association caused by LRRK2 PD mutations. Consistent with the neurotoxicity data, blocking kinase activity by introducing a second mutation in the kinase domain, K1906R, completely abolished the effect of LRRK2 PD mutations on microtubule association (Figure 4.5A). To further elucidate the mechanism whereby LRRK2 PD mutations provoke enhanced microtubule association, we attempted to define a microtubule association domain by performing a structure-function study, testing which regions of LRRK2 are required (or are dispensable) for filament formation. The I2020T mutant was used as a representative mutation for these studies because the behavior of this mutant does not differ from R1441C or Y1699C (Figure 4.1 and 4.4). This analysis demonstrated that the WD40 domain was necessary for filament formation (Figure 4.5B), whereas the entire N-terminus, prior to the LRR domain, is dispensable for microtubule binding. Jorgensen et al. reported previously that Δ WD40-LRRK2 is unable to autophosphorylate yet retains the ability to trans-phosphorylate the model substrate MBP, suggesting a potential relationship between autophosphorylation and microtubule association (Jorgensen et al., 2009). Such a relationship could contribute to an explanation of why blocking kinase function through the presence of the K1906R kinase dead mutant virtually abolishes microtubule association (Figure 4.5A).

Figure 4.5. Kinase dead mutations and loss of the WD40 domain disrupt LRRK2-microtubule association. **A**, The microtubule-association effect of LRRK2 PD mutations is diminished by the kinase-dead mutant K1906R. Blocking LRRK2 kinase function blocks the effect of filament formation caused by PD mutations. CAD cells were transfected with WT LRRK2-GFP or ‘double mutant’ constructs containing a LRRK2 PD mutation and a kinase-deficient mutation (K1906R) and stained for filaments with an anti-GFP antibody. Quantification of filament formation was done as in Figure 4.1E. Data are means + S.E.M. of three independent experiments (** $p < 0.01$, n.s.: non-significant; ANOVA with Tukey’s test). **B**, Filament formation requires the WD40 domain of LRRK2. CAD cells were transfected with full-length GFP-LRRK2-I2020T (FL-IT), GFP-LRRK2-I2020T lacking the WD40 domain (Δ WD40) or the Roc and WD40 domains of LRRK2-I2020T (Roc-WD-IT). Forty-eight hours after transfection, the cells were assessed for filament formation. Anti-GFP immunoblot of transfected cell lysate demonstrates that truncated proteins are produced at the same or greater level of expression as full-length LRRK2. In collaboration with C.C. Ho, H. Rideout, Dauer lab.



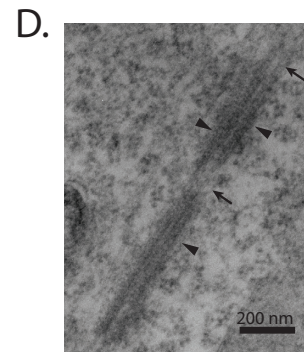
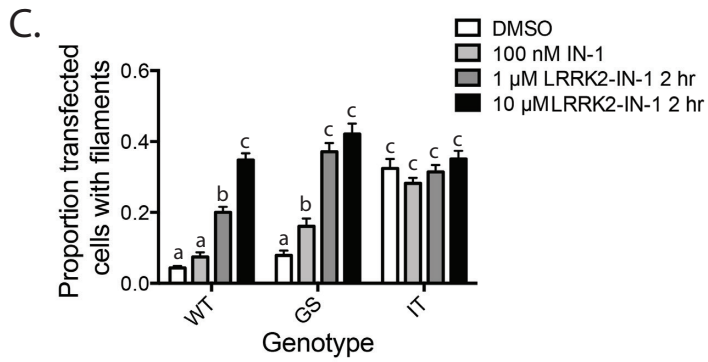
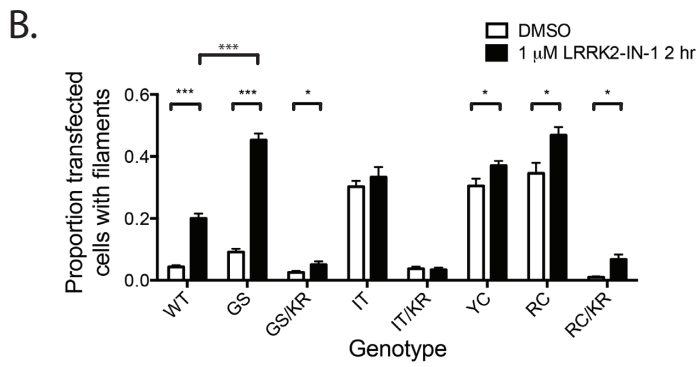
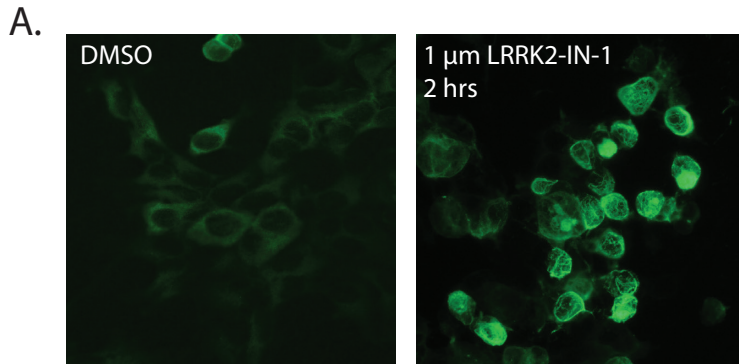
Kinase inhibition with LRRK2-IN-1 increases filament formation in WT- and G2019S-LRRK2-GFP transfected cells

To better understand the apparent kinase-dependent nature of filament formation, I utilized a recently described LRRK2-specific inhibitor (LRRK2-IN-1: Deng et al., 2011). Pharmacological kinase inhibitors, in comparison to the K1906R kinase-dead mutation, allow the rapid inhibition of LRRK2 kinase as well as abrogate the need for multiple mutations in the LRRK2 protein, reducing the likelihood of abnormal, non-physiological folding. Deng et al. (2011) reported filaments following treatment with LRRK2-IN-1 that appeared similar to those observed, suggesting discrepancies between the kinase-dead, K1906R mutations and chemical kinase inhibition. To clarify this difference between chronic, genetic kinase inhibition and acute, chemical kinase inhibition, I treated CAD cells transfected with WT, PD mutant, or kinase-dead ‘double mutants’ with 1 μ M LRRK2-IN-1 for 2 hours, a dose that achieves near-complete LRRK2 kinase inhibition and was used previously to induce filaments similar to those observed (Deng et al., 2011). Following treatment, I fixed and stained transfected cells for GFP. An observer blinded to genotype quantified the proportion of cells with filaments. Similar to Deng et al. (2011), I observed dramatic LRRK2 filamentation in LRRK2-IN-1-treated cells in G2019S-LRRK2-GFP cells (Figure 4.6A), the only PD mutant that does not show a high proportion of filaments in basal conditions. Filament proportion also increased with LRRK2-IN-1 treatment of WT-LRRK2-GFP transfected cells (Figure 4.6B). The relative increase in filamentation differed between WT and G2019S-LRRK2-transfected cells, suggesting that kinase inhibition affected the PD mutant more than wild type. In other PD mutants (I2020T, Y1699C, R1441C) that already have a high proportion of filaments under basal conditions, LRRK2-IN-1 had a lesser effect on filamentation (Figure 4.6B). This result likely reflects a ceiling effect of filamentation

for these PD mutants rather than reduced efficacy of LRRK2-IN-1. These mutants already have filaments in 30-40% of cells and the proportion of filaments never exceeded 50% of cells in all conditions and experiments. Lastly, I treated cells transfected with LRRK2 ‘double mutants’ containing both a PD mutation and the kinase-dead mutation, K1906R, which prevents filament formation under basal conditions (Figure 4.5A). Similar to basal conditions, the presence of the K1906R reduced the proportion of filaments in all mutants (Figure 4.6B) and reflects profound differences between genetic and chemical inhibition of LRRK2.

I was interested in the differential response to kinase inhibition between WT and PD mutant LRRK2 and so performed a dose-response study using ten-fold changes in LRRK2-IN-1 concentration and WT-, G2019S-, and I2020T-LRRK2-GFP, with I2020T as a representative filament-forming PD mutant. Both WT- and G2019S-LRRK2-transfected cells showed increased filamentation with increasing concentrations of LRRK2-IN-1 (Figure 4.6C). Consistent with the initial study, G2019S-LRRK2 transfected cells had increased sensitivity to LRRK2-IN-1 compared to WT-LRRK2 cells. At both 100 nM and 1 μ M LRRK2-IN-1, G2019S-LRRK2 cells had a greater proportion of filaments than WT-LRRK2 transfected cells, before reaching an apparent ceiling at 10 μ M LRRK2-IN-1 (Two-way ANOVA: $F_{\text{genotype}}(2,140) = 70.06$, $p < 0.0001$; $F_{\text{treatment}}(3,140) = 86.33$, $p < 0.0001$; $F_{\text{interaction}}(6,140) = 16.62$, $p < 0.0001$; followed by post-hoc Tukey’s tests corrected for multiple comparisons). A correlated light and EM study of G2019S-LRRK2-GFP cells treated with 1 μ M LRRK2-IN-1 for 2 hours confirmed that these filaments were similar to filaments previously described (Figure 4.1-4.5). Similar to those in Figure 4.2, LRRK2-IN-1-induced filaments showed electron dense material around microtubules (Figure 4.6D), reinforcing that the two filaments are of similar composition.

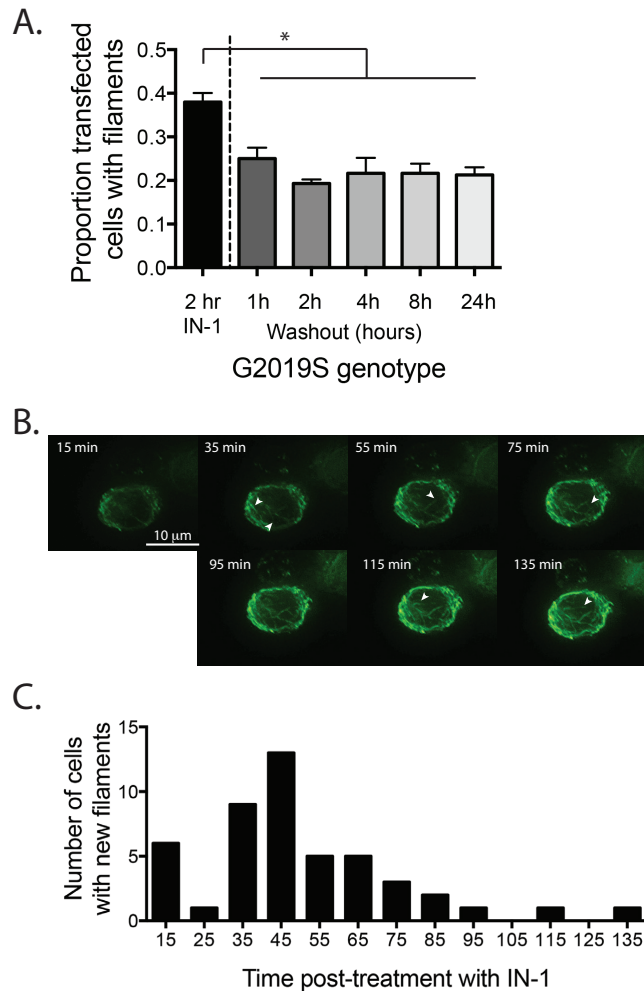
Figure 4.6. Inhibition of kinase activity by LRRK2-IN-1 increases LRRK2-microtubule association. **A**, Treatment of cells transfected with G2019S-LRRK2-GFP with 1 μ M LRRK2-IN-1 for 2 hours (right) resulted in increased LRRK2 filamentation. DMSO-treated cells shown as control (left). **B**, Quantitation of LRRK2-IN-1-induced filamentation. CAD cells were transfected with WT LRRK2-GFP, LRRK2 PD mutant constructs, or ‘double mutant’ constructs containing a LRRK2 PD mutation and a kinase-deficient mutation (K1906R). 48 hours post-transfection, cells were treated with either 1 μ M LRRK2-IN-1 or DMSO control and stained for filaments with an anti-GFP antibody. Quantification of filament formation was done as in Figure 4.1E. Data are means + S.E.M. of three independent experiments (* $p < 0.05$, *** $p < 0.001$, n.s.: non-significant; 2-way ANOVA with post-hoc Tukey’s tests controlled for multiple comparisons). **C**, Dose-response of LRRK2-IN-1 filamentation in WT, G2019S, or I2020T LRRK2-GFP transfected CAD cells. 48 hours post-transfection, cells were treated with either 100 nM, 1 μ M, or 100 μ M LRRK2-IN-1 or DMSO control for 2 hours and stained for filaments with an anti-GFP antibody. Quantification of filament formation was done as in Figure 4.1E. Data are means + S.E.M. of three independent experiments (statistically different conditions are indicated with different letters (a, b, c); 2-way ANOVA with post-hoc Tukey’s tests controlled for multiple comparisons). **D**, Correlated light and EM of LRRK2-IN-1-induced filaments in G2019S-LRRK2-GFP transfected cells show similar ultrastructure to I2020T-LRRK2-GFP filaments shown in Figure 4.2. G2019S-LRRK2-GFP transfected HEK293T cells were treated with 1 μ M LRRK2-IN-1 for 2 hours and processed for correlated light and EM. LRRK2-IN-1 treated cells showed similar undecorated microtubules (arrows) and electron densities (arrowheads) to I2020T-LRRK2-GFP transfected cells (Figure 4.2).



The rapid induction of filamentation following LRRK2-IN-1 treatment led me to probe the dynamics of LRRK2 filamentation, specifically how stable filaments are, how rapidly they form, and the kinetics of their formation. To examine stability, I induced filaments by treating G2019S-LRRK2-GFP transfected CAD cells with 1 μ M LRRK2-IN-1 for 2 hours. After filament induction, the cells were washed and incubated in media lacking LRRK2-IN-1 for a variable time (one hour to 24 hours). Within one hour of drug removal, the proportion of cells with filaments decreased by approximately half (Figure 4.7); however, the proportion then remained unchanged up to 24 hours after drug treatment, suggesting that while filament turnover can occur rapidly, the association between LRRK2 and microtubules is quite stable once formed.

I next examined filament formation by live cell imaging using the Deltavision-RT Live Cell Imaging System (University of Michigan Microscopy and Image Analysis Laboratory). CAD cells transfected with G2019S-LRRK2-GFP were identified by fluorescence and confirmed visually to contain no filaments. Media containing 1 μ M LRRK2-IN-1 was added to the cells and cells were repeatedly imaged every 10 minutes starting 15 minutes after drug treatment. During five independent experiments, forty-seven of 140 imaged cells developed filaments. Image series were then examined for the frame at which filament formation began (Figure 4.7B). While variable in terms of filament onset, the majority of filaments started forming between 35 to 65 minutes after drug treatment (Figure 4.7C), confirming that filament formation can occur rapidly following kinase inhibition. Furthermore, examination of individual filaments across images revealed extension of filaments over time (see arrowheads, Figure 4.7C), rather than the instantaneous formation of complete LRRK2 filaments.

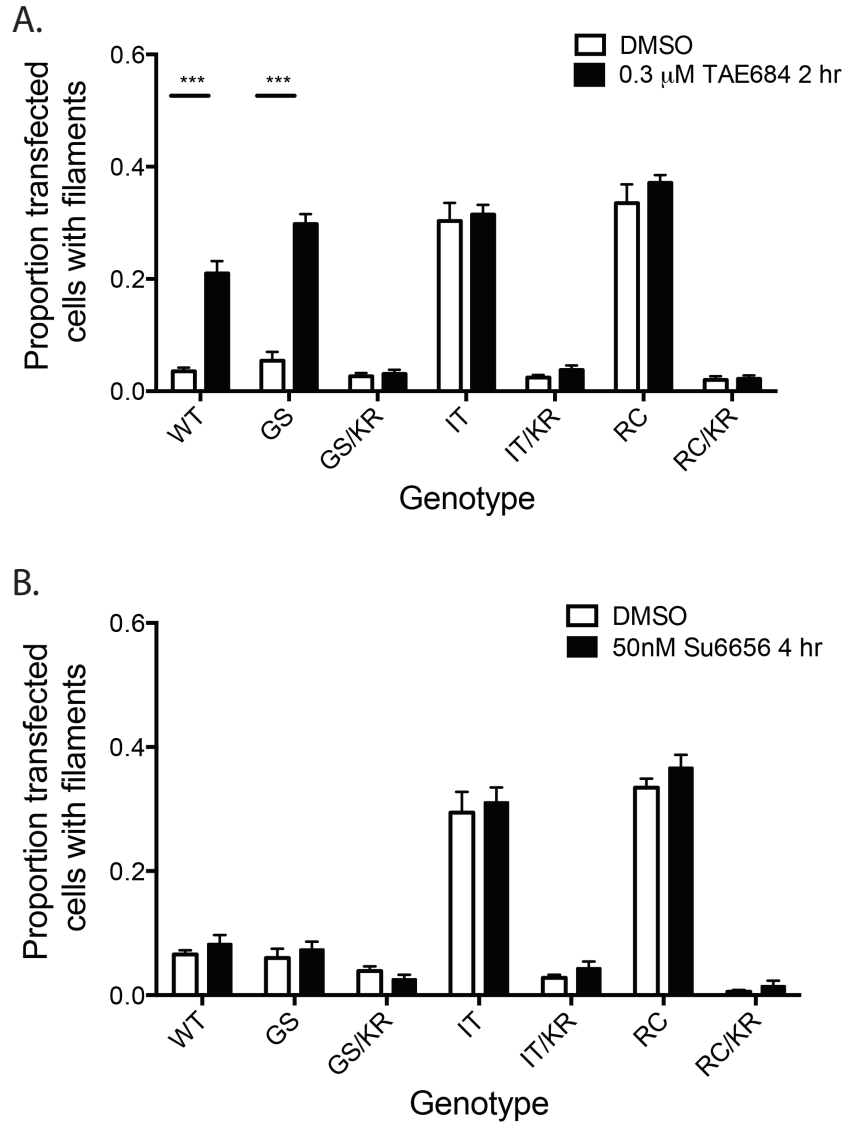
Figure 4.7. Kinetics of LRRK2-IN-1 induced filamentation in LRRK2-G2019S transfected cells. **A**, Washout of LRRK2-IN-1 demonstrates that a portion of filaments are stable up to 24 h after drug treatment. Forty-eight hours after transfection with G2019S-LRRK2-GFP, CAD cells were treated with 1 μ M LRRK2-IN-1 for 2 h. Cells were then washed three times and incubated in media without drug. Frequency of LRRK2 filaments was quantified. Data are mean \pm S.E.M. of three independent experiments, done in triplicate (* $p < 0.05$; ANOVA with Tukey's test). **B-C**, Live cell imaging of LRRK2-IN-1 induced filaments in G2019S-LRRK2-GFP transfected cells. CAD cells were transfected with G2019S-LRRK2-GFP. Forty-eight hours post-transfection, LRRK2-GFP-positive cells without filaments were identified by fluorescence. Media was replaced with DMEM/F12 containing 1 μ M LRRK2-IN-1 and images were captured of identified cells every 10 minutes starting 15 minutes after drug treatment. **B**, Example of transfected cell with filament formation. Arrowheads indicate locations of filament growth not present at previous time point. **C**, Histogram of number of new filaments identified at each time point after drug addition. Data are from five independent experiments with 20-30 cells identified and followed in each experiment.



Variability in the effects of kinase inhibitors on LRRK2 filamentation

Dzamko *et al.* reported similar appearing filaments following LRRK2 inhibition with H-1152 (Dzamko *et al.*, 2010). In addition, LRRK2-IN-1 has been reported to have many off-target effects (Luerman *et al.*, 2013). To understand the specificity of filamentation following kinase inhibition, I examined LRRK2 filament formation in transfected CAD cells treated with two additional LRRK2-specific kinase inhibitors [TAE684: (Zhang *et al.*, 2012); Su6656: Y. Peng, Dauer lab, data not shown]. For both drugs, I first conducted a dose-response curve and time-course to ascertain a dose with no cellular toxicity, but well above the *in vitro* IC₅₀ values for the two inhibitors [IC₅₀ for TAE684: 7.8 nM (Zhang *et al.*, 2012); IC₅₀ for Su6656: < 5 nM, Y. Peng, data not shown]. Once optimal doses were established with WT-LRRK2-GFP and G2019S-LRRK2-GFP, I treated CAD cells transfected with WT, PD mutant, and ‘double mutant’ forms of LRRK2-GFP with 300 nM TAE684 for 2 h, 50 nM Su6656 for 4 h, or DMSO. TAE684 promoted filamentation in WT- and G2019S-LRRK2 transfected cells (Figure 4.8A), but Su6656 did not (Figure 4.8B). These results suggested that different LRRK2 kinase inhibitors have variable effects on filamentation in WT and G2019S-transfected cells, though whether from variability in off-target effects or on structural changes to LRRK2 is not currently known.

Figure 4.8. LRRK2 kinase inhibitors show variable effect on LRRK2-microtubule association. The formation of LRRK2 filaments in WT-LRRK2 or G2019S-LRRK2 is enhanced by treatment with the kinase inhibitor TAE684, but not Su6656. CAD cells were transfected with WT, PD mutant forms, or ‘double mutants’ containing a PD mutation and kinase-dead, K1906R mutation. Forty-eight hours after transfection, cells were treated with either 0.3 μ M TAE684 for 2 hours (A) or 50 nM Su6656 for 4 hours (B). The frequency of cells with LRRK2 filaments was quantified. Data are mean \pm S.E.M. of three independent experiments (***) $p < 0.001$; ANOVA with Tukey’s test).



Discussion

This study is the first to provide evidence that multiple PD mutations enhance the association of LRRK2 with microtubules. Several characteristics of this interaction indicate that it may contribute to LRRK2-dependent neurodegeneration. First, similar to LRRK2 neurotoxicity, this effect requires the WD40 domain (Jorgensen et al., 2009) and is abolished by the presence of kinase-dead mutations (Greggio et al., 2006; Smith et al., 2006; Jorgensen et al., 2009; Lee et al., 2010). Secondly, the colocalization and ultrastructural analyses show that LRRK2 interacts closely with microtubules in a well-ordered, periodic fashion, suggesting the existence of a LRRK2-binding site on microtubules or microtubule-bound proteins. Conversely, the specific requirement of the WD40 domain (but not the N-terminus) for microtubule binding indicates that specific regions of LRRK2 mediate microtubule association, recently confirmed to be in the Roc-COR region of LRRK2 (Law et al., 2014). Our studies also show that LRRK2 filaments appear similar to linear arrays of electron dense structures observed in human post-mortem substantia nigra tissue from a patient carrying the filament-forming Y1699C mutation (Wszolek et al., 1997). With the development of better LRRK2 antibodies for immunohistochemical studies, it will be interesting to see if similar filaments are observed in the brains of PD patients with LRRK2 mutations.

The link between visible microtubule association (filaments) and toxicity mirrors those observed for protein aggregates seen with α -synuclein and other neurodegenerative-related proteins: neurotoxicity occurs in the population of LRRK2-transfected neurons, whereas visible filaments are seen in a minority of cells. In all of these cases, the visible protein lesions (filaments or aggregates) appear to reflect toxic events that also occur in soluble (and therefore not visualizable) protein. The co-IP results (Figure 4.1G) support such a scenario since these

studies, which assess the entire cell population (including untransfected cells), show a markedly increased association for filament-forming LRRK2 PD mutations.

Similar filaments have been reported by Alegre-Abarregui *et al.* (2009) for R1441C-LRRK2. That report suggested that LRRK2 filaments were a form of multivesicular bodies, yet used a LRRK2 antibody for immuno-EM that has not been validated using LRRK2 knockout tissue, and no multivesicular body markers were shown to colocalize with LRRK2 filaments. In contrast, we used a validated LRRK2 antibody for detection (as well as an epitope tag), and employed correlated light and EM to ensure that the ultrastructural features reflected the same structures visualized by immunofluorescence. Membrane was never observed in association with LRRK2 filaments, either by EM or using membrane dyes on LRRK2-transfected cells (data not shown).

The discrepancy in filament formation between LRRK2 chemical inhibition (Figure 4.6-4.8) and genetic inhibition (Figure 4.5) has larger implications for our understanding of LRRK2 biology. Our laboratory and others have relied predominantly on genetic mutations that disrupt the binding of ATP to LRRK2 and thereby disrupt kinase function. These genetic ‘kinase-dead’ mutants have implicated LRRK2 kinase function in autophagy, neurite outgrowth, the interaction between the kinase and GTPase domains, and neurotoxicity (Greggio *et al.*, 2006; West *et al.*, 2007; Plowey *et al.*, 2008; Greggio *et al.*, 2009; Jorgensen *et al.*, 2009; Skibinski *et al.*, 2014). Yet, in contrast to LRRK2 ‘kinase-dead’ mutations, which diminish filament formation (Figure 4.5), the LRRK2-specific kinase inhibitors LRRK2-IN-1 and TAE684 [and H-1152 (Dzamko *et al.*, 2010)] result in an increase in filament formation. Most likely, the introduction of a second, non-physiological mutation causes abnormalities in LRRK2 protein folding, despite normal protein levels (data not shown). With the development of more specific LRRK2 kinase

inhibitors, it will be vital to use chemical inhibition to revisit the role of kinase activity in LRRK2 function. The kinase inhibitor Su6656 had no effect on filamentation, suggesting that the location of binding to LRRK2 kinase may alter secondary structure and allow for microtubule binding. Substantial off-target effects of LRRK2-IN-1 have been reported (Luerman et al., 2013), raising the possibility that inhibition of another kinase has secondary effects on LRRK2-microtubule association. Finally, it is possible that chronic, genetic inhibition results in secondary effects within the cell that differ from acute, chemical inhibition.

The interaction of LRRK2 with microtubules could affect microtubule dynamics or microtubule-related transport, or microtubules could serve as a scaffold to concentrate LRRK2 signaling events such as the recruitment of the FADD/caspase-8 complex. *In vitro*, LRRK2 can bind alpha/beta-tubulin heterodimers (Gandhi et al., 2008), and can phosphorylate beta-tubulin (Gillardon, 2009). Active (but not kinase dead) LRRK2 enhances the polymerization of tubulin (isolated from bovine brain) in the presence of microtubule-associated proteins (Gillardon, 2009). More recent work has suggested microtubule binding to the Roc-COR domain (Law et al., 2014) and that binding enhances GTPase activity (Caesar et al., 2013). Further support for a LRRK2 interaction with the cytoskeleton includes the findings of deficient microtubule associated protein tau phosphorylation in brain lysates from LRRK2 null mice (Gillardon, 2009), and multiple reports of alterations of neurite length and branching in situations of LRRK2 deficiency or overexpression (MacLeod et al., 2006; Plowey et al., 2008; Cookson, 2010; Dachselt et al., 2010; Lin et al., 2010).

In light of an emerging role for endolysosomal dysfunction in PD, LRRK2 may act on microtubules to facilitate vesicular transport via the recruitment of necessary proteins. Microtubules are the major conduit for long-distance movement within the cell. Rab proteins, the

small GTPases that function to identify and sort specific vesicles within the endolysosomal system, interact with microtubules to coordinate both forward and retrograde movement (Stenmark, 2009; Horgan and McCaffrey, 2011). LRRK2 also physically interacts with multiple Rab proteins like Rab5, Rab7, and Rab7L1 (Shin et al., 2008; Heo et al., 2010; Dodson et al., 2012; MacLeod et al., 2013; Beilina et al., 2014) to coordinate intracellular vesicular localization. Enhanced microtubule association of mutant LRRK2 may promote the recruitment of Rabs and other signaling molecules to alter vesicle movement. LRRK2 is reported to signal via the FADD/caspase-8 pathway (Ho et al., 2009), and in olfactory receptor neurons, degeneration of the axon and soma require synaptically activated caspase-8 that is retrogradely transported along microtubules (Carson et al., 2005). LRRK2 might therefore modulate the axonal transport of caspase-8 or other cargo, a notion consistent with the potentially central role of axonal degeneration in PD (Cheng et al., 2010). Alternately, LRRK2 was recently reported to form a co-complex with Rab7L1, BAG5, GAK, and/or retromer that alters trafficking of vesicles between the early endosome and *trans*-Golgi network (MacLeod et al., 2013; Beilina et al., 2014). LRRK2 recruitment to microtubules may provide the scaffold upon which these other proteins are brought together.

One potential mechanism for the enhanced microtubule association of mutant LRRK2 is that PD mutations may directly enhance the affinity of LRRK2 for microtubules or microtubule-bound proteins. Alternatively, PD mutations may enhance LRRK2 homo-oligomerization or complex formation with other cytosolic proteins like Rab7L1 or retromer, and these homo-oligomers or protein complexes may themselves have enhanced affinity for microtubules. Our data provide evidence that multiple pathogenic mutations enhance LRRK2-LRRK2 interactions, an effect abrogated by kinase-dead mutations and correlated with filament formation. Studies

from Wittinghofer and colleagues (Gotthardt et al., 2008) suggest that the COR domain is important for LRRK2 dimerization, and data from Cookson and colleagues (Deng et al., 2008) suggest that PD mutations that replace the arginine at position 1441 with either cysteine or glycine (which cause filaments) weaken the interaction in the Roc-COR region. The structural alteration produced by weakening of this interaction may expose a protein-protein interaction domain, providing a potential mechanism for how PD mutations enhance LRRK2-microtubule association. The fact that all PD mutations provoke LRRK2 filaments, either in basal conditions or in the presence of LRRK2 kinase inhibitors, indicates that other insults, such as those that occur in idiopathic PD, might also promote abnormal LRRK2 association with microtubules.

Materials and Methods

Plasmids. LRRK2 cDNA from HEK293T cells was cloned in pCMS-EGFP (Clontech Laboratories Inc., Mountain View, CA), pcDNA-DEST53 and -DEST40 (Invitrogen). All subsequent mutants were generated using site-directed mutagenesis and all mutant clones were re-sequenced to confirm their accuracy.

Cell lines and primary cortical neuron cultures. CAD cells were grown in Dulbecco's modified eagle medium (DMEM)/F12 (Gibco, Grand Island, NY) supplemented with 8% fetal bovine serum. HEK293T cells were grown in DMEM (Gibco) with 10% serum. Cells were transfected with Lipofectamine 2000 (Invitrogen) according to the manufacturer's instructions. Cultures of cortical neurons from E16 mice were maintained in Neurobasal medium containing B-27 supplements (Gibco), and transfected with Lipofectamine 2000 four days after being plated. Primary neurons were transfected with LRRK2 expression constructs and pCMS-EGFP at 10:1

ratio. Each experiment was performed on cover slips in triplicate three times, with >100 cells on each cover slip being quantified.

Antibodies. We used the following antibodies: rabbit anti-GFP (Abcam, Cambridge, MA, #ab6656); mouse anti-GFP (Roche Applied Science, #11814460001); mouse anti-V5 (Invitrogen, #R960-25); rabbit monoclonal anti-LRRK2 (Epitomics, Burlingame, CA, #3514-1); mouse monoclonal anti-alpha tubulin (Sigma-Aldrich, #T6074); and rabbit polyclonal anti-FLAG (Abnova, Taipei City, Taiwan, #PAB0900). The rabbit anti-LRRK2 used to immunostain untagged LRRK2 was a kind gift from Dr. Benoit Giasson (University of Pennsylvania, Philadelphia, PA).

Cell preparation for EM. HEK293T cells transfected with YFP-LRRK2-IT or GFP-LRRK2-GS were fixed for 30 min in 2% glutaraldehyde in 0.1M sodium cacodylate buffer (pH 7.4) on ice. After washes in 0.1M cacodylate buffer, cells were post-fixed with 1% osmium tetroxide for 30 min, stained with 2% uranyl acetate and then dehydrated and embedded in Curcupan epoxy resin. Sections were cut using a diamond knife at a thickness of 70-90 nm for thin sections and 250 nm for thick sections. Post-staining of grids was done with 2% uranyl acetate for 5 min and lead citrate for 1 min. Thin sections were examined using a JEOL 1200 FX1 operated at 120 kV.

Electron tomography. Colloidal gold particles (10 nm diameter) were deposited on opposite sides of the thick epoxy sections to serve as fiducial markers. For stability in the beam, the section was coated with carbon on both sides. For reconstruction, a triple series of images at regular tilt (angular increments of 2° from -60° to +60° increments) was collected with a JEOL

4000EX intermediate-voltage electron microscope operated at 400 kV. The specimens were irradiated before initiating a tilt series to limit anisotropic specimen thinning during image collection. Tilt series were recorded using a slow-scan CCD camera. The pixel dimensions of the CCD camera were 4000 x 4000 and the pixel resolution was 0.754 nm. Fine alignment and reconstruction were performed using the TxBR software package (Lawrence et al., 2006).

Post-embedding immuno-EM. For ultrastructural analysis of the filaments, we used an anti-LRRK2 antibody using 10 nm gold particles to identify the LRRK2 protein around the microtubules. After labeling, grids were washed and post-stained with 2% uranyl acetate for 5 min and lead citrate for 1 min.

Immunofluorescent labeling. Forty-eight hours after transfection, methanol- or 4% paraformaldehyde-fixed HEK293T or CAD cells on poly-D-lysine coated glass cover slips were blocked in phosphate buffered saline (PBS) containing 0.3% Triton X-100 and 5% bovine serum albumin. Cover slips were then incubated overnight at 4°C in primary antibodies diluted in block solution. The next day, cover slips were washed, incubated with Alexa488-, Alexa555-, or Alexa647-conjugated antibodies (Invitrogen) and washed in PBS before mounting using ProLong Gold antifade reagent with 4',6-diamidino-2-phenylindole (Invitrogen). Data was done with an Olympus FluoView1000 laser-scanning confocal microscope (Olympus Inc., Center Valley, PA), using a 60X1.42 NA lens or with a 100x oil-immersion objective with a Zeiss LSM510 2-photon confocal microscope (Carl Zeiss Microscopy, Thornwood, NY). Image analysis of z-scan was done using the Imaris Software (Bitplane AG, St. Paul, MN) and the Image J software (rsb.info.nih.gov/ij).

Live cell imaging. Forty-eight hours after transfection with GFP-LRRK2-G2019S, cells grown on glass coverslips on 35 mm dishes (MatTek Corp., Ashland, MA) were imaged using Deltavision-RT Live Cell Imaging System with a Photometrics CoolSNAP HQ camera. GFP-positive cells without filaments were identified and then 1 μ M LRRK2-IN-1 was added to fresh media (DMEM/F12 without phenol red, Gibco). Images of the identified cells were acquired using a 60x Olympus PlanApo N oil immersion objective, NA of 1.42, with images being collected every 10 min starting 15 min after drug was added. Images were subsequently deconvolved using softWoRx 3.5.1 software (GE Healthcare, Issaquah, WA). Image series were then studied in ImageJ to identify time points at which filaments first appeared.

Drug treatment. Forty-eight hours after transfection, cells on coverslips were treated with taxol (10 μ M in DMSO for 5 h; Sigma), nocodazole (100 nM in DMSO for 1 h; Sigma) or DMSO. For kinase inhibitor experiments, forty-eight hours after transfection, cells were treated with LRRK2-IN-1 (EMD Millipore, Billerica, MA), Su6656 (Sigma), TAE684 (SelleckChem, Houston, TX), or DMSO. Concentrations and incubation times are indicated in the relevant figures and text.

Co-IP analysis. HEK293T or CAD cells transfected with various expression constructs were Dounce homogenized in lysis buffer (20 mM 4-(2-hydroxyethyl)-1-piperzaineethanesulfonic acid, pH 7.4, 150 mM NaCl, 0.1-0.5% NP40, 2 mM ethylene glycol tetraacetic acid, 2 mM MgCl₂, 10% glycerol, 1 mM sodium orthovanadate, 10 mM NaF, 25 mM β -glycerophosphate, pH 7.2 and protease inhibitors). Following centrifugation at 20,000 x g for 15 min, the supernatants were pre-cleared with protein-A agarose (Roche) for 30 min. Lysates containing 2

mg total protein were immunoprecipitated with rabbit anti-GFP for 1 h – overnight followed by incubation with protein-A beads for 2 h at 4°C.

Western blotting. Cellular lysates were prepared by homogenizing confluent transfected HEK293T or CAD cells with a Dounce homogenizer in an appropriate volume of ice-cold RIPA buffer (10mM Tris-HCl, 150 mM NaCl, 0.1% SDS, 0.1% SDOC, and 0.01% Triton-X 100) containing protease inhibitors (Roche). The samples were then sonicated to solubilize all proteins. Protein concentrations were determined using the BCA assay (Pierce Biotechnology). Proteins were separated by SDS-PAGE using Tris-HCl 4-20% gradient gels (BioRad) and transferred onto PVDF membranes (BioRad). Membranes were blocked in 5% non-fat milk in TBS-T (TBS plus 0.1% (v/v) Tween 20) for 1 hour, followed by overnight incubation at 4°C in primary antibodies in 5% non-fat milk in TBS-T. After a 1-hour incubation in an HRP-conjugated secondary antibody, immunoreactive bands were visualized on film by enhanced chemiluminescence (SuperSignal West Pico, Pierce Biotechnology).

Chapter 5

Conclusions

Considerable data implicate endolysosomal dysfunction as a key feature of PD pathogenesis. Based on these data, and genetic studies linking parkinsonism to ATP13A2, a protein localized to this pathway, I generated and characterized a novel *Atp13a2* null mouse model of PD-related neurodegeneration. The goal of these studies was: 1) to generate a model of PD-related neurotoxicity linked to endolysosomal dysfunction, and 2) to exploit this model to identify key events by which endolysosomal dysfunction causes neurodegeneration. *Atp13a2* null mice develop early gliosis and lysosomal changes followed by aggregation of autophagy substrates and behavioral abnormalities. In contrast to the prevailing theory suggesting a crucial role for α -synuclein, I demonstrated these changes are not significantly altered by α -synuclein levels, emerging at the same time and progressing to a similar extent following loss or overexpression of α -synuclein. Furthermore, in contrast to previous reports, I showed that *in vivo* loss of *Atp13a2* caused minimal alterations to lysosomal function, without broad deficits in proteolysis, mitophagy, or lipid profiles. Loss of *Atp13a2* does cause selective perturbations in the trafficking of cathepsin D, a lysosomal protease linked to other neurodegenerative disorders and a putative cellular synucleinase. Together, these results are among the first to examine how primary endolysosomal dysfunction *in vivo* results in PD-related neurodegeneration and

challenges the assumption that loss of *Atp13a2* causes parkinsonism through autophagy deficits and α -synuclein aggregation.

In cell biological studies, I probe the interactions between LRRK2 and microtubules, structures critical for normal endolysosomal function. I demonstrated that PD-mutant forms of LRRK2 closely associate with microtubules and that loss of LRRK2 kinase activity affects this interaction. As microtubules are necessary for the movement of vesicles within the endolysosomal system, LRRK2 may act as an important signaling molecule on microtubules during vesicular movement. Enhanced association with microtubules may then alter the signaling of PD mutant forms of LRRK2. In the remainder of this chapter, I will discuss my findings in the context of current views of PD pathogenesis, highlighting aspects of this work that challenge current views, questions this work prompts, and fruitful directions for future study.

Endolysosomal dysfunction in PD

To understand the mechanism underlying pathogenesis in *Atp13a2* null mice, I undertook detailed studies of lysosomal function *in vivo*, especially with respect to autophagy and mitophagy. Loss of key autophagy genes in the SNpC causes accumulation of α -synuclein (Ahmed et al., 2012; Friedman et al., 2012) and mice lacking key lysosomal enzymes like glucocerebrosidase or cathepsin D develop α -synuclein aggregation (Cullen et al., 2009; Mazzulli et al., 2011) and mitochondrial abnormalities (Osellame et al., 2013). Loss of *Atp13a2* did not cause α -synuclein aggregation, but did result in accumulation of other autophagy substrates including ubiquitin, p62, and lipofuscin. P62 and ubiquitin aggregation has been identified in virtually every neurodegenerative disease and likely represents a cellular stress response (Zatloukal et al., 2002; Komatsu and Ichimura, 2010). Lipofuscin deposits are similarly

found in many neurodegenerative disorders, most notably the neuronal ceroid lipofuscinoses (Palmer et al., 2013), but also AD (Hirai et al., 2001). Yet, despite having prominent deposits throughout the cortex, detailed study of cortical lysosomal function revealed abnormalities limited to cathepsin D maturation. Indeed, examination of lysosomes isolated from the cortex of *Atp13a2* null mice showed normal function in assays of bulk proteolysis and chaperone-mediated autophagy, but did show decreased levels of cathepsin D. These studies point to a selective deficit in cathepsin D trafficking.

How *Atp13a2* selectively affects cathepsin D processing and if cathepsin D loss alone is responsible for other pathological changes in *Atp13a2* null mice is unknown. Cathepsin D abnormalities occurred after the onset of reactive astrocytosis and the accumulation of lysosomal proteins and lipids (Figure 2.10), suggesting that cathepsin D trafficking deficits may be a later and, therefore, more distal sequela of *Atp13a2* loss. Yet, cathepsin D abnormalities occurred in a similar time frame to the onset of lipofuscinosis, p62 and ubiquitin aggregation, and prior to behavioral changes in *Atp13a2* null mice. Furthermore, alterations to cathepsin D are increasingly identified in genetic forms of PD. Cathepsin D is known to degrade α -synuclein (Qiao et al., 2008; Sevelever et al., 2008; Cullen et al., 2009). Complete loss of cathepsin D, as seen in cathepsin D null mice, results in much earlier onset of lipofuscin accumulation (Koike et al., 2000), glial activation, and neurotoxicity (Partanen et al., 2008), potentially linking cathepsin D loss to the pathological changes observed in *Atp13a2* null mice. While cathepsin D null mice show increased levels of insoluble α -synuclein (Cullen et al., 2009), heterozygous mice do not show changes to α -synuclein levels (Crabtree et al., 2013), consistent with my finding that α -synuclein does not change in the presence of partial loss of lysosomal cathepsin D. Similarly, cell biological studies showed that the D620N mutation in VPS35 also decreases the trafficking

of cathepsin D to the lysosome, presumably through defects in the trafficking of the cation-independent mannose-6-phosphate receptor (CI-MPR; Follett et al., 2014). Such alterations in lysosomal cathepsin D could contribute to selective neurodegeneration, which my work suggests occurs independent of α -synuclein.

Another possible explanation is that the selective deficits in cathepsin D processing reflect larger upstream alterations to endolysosomal vesicle trafficking. Follett et al. recently showed that the D620N mutation in VPS35 leads to defects in endosome maturation and distribution within the cell. Improper retrograde trafficking of the CI-MPR in VPS35 D620N cells led to decreased delivery of CI-MPR substrates to the lysosomes (Follett et al., 2014). Similar trafficking defects of CI-MPR occurred with loss or mutation of LRRK2 or Rab7L1 (MacLeod et al., 2013). I also observed increases in early endosome (EEA-positive) and lysosome number in the cell body and proximal dendrites of primary neurons isolated from *Atp13a2* null mice (data not shown), and accumulation of lysosomal proteins and lipids preceded altered cathepsin D processing in *Atp13a2* null mice. Perhaps lysosomal upregulation is not in response to improper degradation of autophagy substrates, but instead reflects compensation for abnormal movement of vesicles along microtubules or improper maturation of late endosomes/lysosomes. Further study of the effect of PD-related proteins on vesicle movement and the trafficking of specific cargo proteins will shed valuable light on these possibilities.

Endolysosomal dysfunction has been studied longer in the context of AD pathogenesis. In early endosomes, β -secretase cleaves amyloid precursor protein (APP) to initiate the amyloidogenic cascade (Small and Gandy, 2006). Mutations that increase the early endosomal pool or enhance substrate time within early endosomes promote this cleavage and amyloidogenesis. For example, increases in synaptojanin 1, as seen in individuals with Down

Syndrome, almost all of whom go on to develop AD, increase the uptake of cell surface proteins like APP and β -secretase into the endosome (Cossec et al., 2012). Hemizyosity of *Synj1* in mice rescues AD behavioral and synaptic phenotypes (McIntire et al., 2012), likely by altering the flux of APP away from the endosome and towards lysosomal degradation (Zhu et al., 2013). Conversely, retromer proteins are decreased in post-mortem tissue from AD patients (Small et al., 2005), causing increased retention of APP within the endosome and its subsequent cleavage into amyloid- β . As multiple endolysosomal proteins are linked to PD pathogenesis, it is tempting to look for similar patterns, especially with respect to α -synuclein. However, PD mutations cluster in several distinct parts of the endolysosomal system: the lysosome, clathrin-mediated endocytosis, and retromer trafficking. It is not immediately clear what effect most of these mutations have on these various compartments and there is not yet a clear locus in which pathogenic events converge.

α -Synuclein in PD-related neurodegeneration

Considerable attention has focused on the hypothesis that in PD, endolysosomal dysfunction causes neurodegeneration by increasing α -synuclein levels. In contrast to previous work *in vivo* (Schultheis et al., 2013), I find that *Atp13a2* null mice do not develop changes in α -synuclein solubility, despite exhibiting abnormal accumulation of ubiquitinated protein aggregates. This absence of α -synuclein pathology differs from *in vitro* studies which report a modest increase in α -synuclein levels in cells following *ATP13A2* knockdown or mutation (Dehay et al., 2012; Usenovic et al., 2012) and is in clear contrast with other cell and mouse models of PD where autophagic-lysosomal dysfunction seems to cause neurotoxicity and elevated α -synuclein levels (Mazzulli et al., 2011; Ahmed et al., 2012; Friedman et al., 2012).

These findings could not exclude the possibility that soluble toxic forms of α -synuclein not detected by our methods might contribute to the abnormalities in *Atp13a2* null mice. To explore this possibility, I genetically altered α -synuclein levels by crossing *Atp13a2* null mice to either mice lacking or overexpressing α -synuclein. In these double mutants, I observed no change in the onset or extent of neuropathology seen in *Atp13a2* null mice, even up to 9 months of age. My findings dissociate alterations in α -synuclein homeostasis from neuropathological and behavioral abnormalities in a model of endolysosomal dysfunction similar to that causing L-DOPA-responsive parkinsonism in humans. My results emphasize that, even in the context of a PD-related insult, endolysosomal dysfunction and defective α -synuclein proteostasis are not synonymous. These findings highlight the importance of broadly considering the consequences of endolysosomal dysfunction that may contribute to neurodegeneration in PD. The endolysosomal system tightly regulates the intracellular and extracellular fate of many proteins. Endolysosomal dysfunction, therefore, may cause a host of cellular abnormalities any of which may contribute to cellular injury and death independent of α -synuclein. As more genetic mutations in endolysosomal proteins are found to increase disease risk, it will be crucial to know if patients with these mutations accumulate α -synuclein. Behavioral and pathological study of animal models of these genes similar to the work presented here will allow further dissection of the sequence of pathological changes both with respect to and independent of α -synuclein. At the same time, more detailed examination of protein trafficking, secretion, and degradation in the context of PD-related mutations is necessary to understand how endolysosomal dysfunction contributes to neurodegeneration.

Relatively little is known about the precise mechanism by which α -synuclein causes neurotoxicity. An understudied component of α -synuclein proteostasis is its impact on the

endolysosomal system. Yeast studies show that overexpression of α -synuclein causes broad dysfunction on vesicular trafficking (Cooper et al., 2006; Gitler et al., 2009; Soper et al., 2011) and α -synuclein is known to bind not only to membranes, but also multiple members of the Rab family (Sung et al., 2001; Dalfo et al., 2004; Liu et al., 2009). Higher molecular weight α -synuclein species interact more tightly with Rab3 (Dalfo et al., 2004), suggesting a potential gain of function in disease state. Perhaps part of α -synuclein-mediated toxicity occurs through perturbations in endolysosomal trafficking or signaling. Future experiments that more closely reflect *in vivo* conditions will be needed to determine the endolysosomal compartments that are affected by α -synuclein function in normal and disease states.

***Atp13a2* null mice as a new model of PD-related neurodegeneration**

Despite increased understanding of the genetic mutations underlying PD risk, PD-related research has suffered from the lack of genetic mouse models that display the hallmarks of disease: age-related motor abnormalities, progressive neurodegeneration, SNpC cell loss, and α -synuclein aggregation (Dawson et al., 2010). Without reliable animal models, it is difficult to reconstruct the sequence of events leading to neurodegeneration or develop novel therapeutics to halt early events in pathogenesis. I generated a novel mouse model where loss of a PD-related gene causes age-related lysosomal abnormalities, protein aggregation, gliosis, and ultimately motor deficits. Similar to PD, in which up to 80% of dopaminergic cells are lost prior to the onset of symptoms, neuropathological changes in *Atp13a2* null mice precede behavioral abnormalities by many months. This delay in behavioral changes provides a prolonged time period during which therapeutic intervention may halt or reverse the lysosomal dysfunction. Similar to other genetic mouse models of PD, *Atp13a2* null mice do not lose dopaminergic SNpC

neurons, potentially reflecting important differences in the susceptibility to selective neurodegeneration between mouse and human dopaminergic neurons. It may be valuable to explore how the SNpC in *Atp13a2* null mice remains relatively immune to lysosomal accumulation, gliosis, and neuronal injury. In contrast to transgenic and knockout mouse lines, viral injection of α -synuclein and mutant LRRK2 into the SNpC does cause neuronal cell death (Lo Bianco et al., 2002; Kirik et al., 2003; Lee et al., 2010; Dusanchet et al., 2011). This difference in outcome may arise from compensatory mechanisms during development that allow the mouse SNpC to counteract increased α -synuclein or loss of *Atp13a2*, for example. Use of our *Atp13a2*-flx line would allow the excision of *Atp13a2* in adulthood, causing a more abrupt hit to the lysosomal system, and perhaps more pronounced pathology.

LRRK2, microtubules, and the endolysosomal system

The work in this dissertation is among the first to show that multiple PD mutations enhance the binding of LRRK2 to microtubules. Subsequent work has proposed a binding site for β -tubulin in the GTPase domain of LRRK2 (Law et al., 2014), a location that may be altered by the PD mutations that are located in the both the GTPase domain (R1441G, R1441C) and the nearby COR domain (Y1699C). The association between LRRK2 and microtubules is dependent on LRRK2 enzymatic activity; chemical kinase inhibition causes increased filamentation in both wild type and G2019S-LRRK2. LRRK2 kinase inhibitors have been heavily pursued as therapeutic agents, but my studies suggest that kinase inhibitors have consequences such as enhanced binding to microtubules that may promote unanticipated toxicity. Further understanding of the precise role of the GTPase and kinase domains in normal LRRK2 function is clearly needed, as is identification of *in vivo* substrates.

The normal cellular function of LRRK2 remains unknown. LRRK2 has been implicated in diverse cellular pathways (reviewed in Kett and Dauer, 2012), including regulation of transcription (Kanao et al., 2010), translation (Imai et al., 2008), apoptosis (Ho et al., 2009), and mitochondrial function (Smith et al., 2005). LRRK2 most consistently localizes to intracellular membranous structures including mitochondria (West et al., 2005; Biskup et al., 2006; Gloeckner et al., 2006; Hatano et al., 2007), endolysosomal membranes (Alegre-Abarrategui et al., 2009), endoplasmic reticulum (ER; Gloeckner et al., 2006; Vitte et al., 2010), and Golgi (Biskup et al., 2006; Gloeckner et al., 2006; Hatano et al., 2007). The localization of LRRK2 to microtubules under both physiological and pathological conditions may help explain the varied reports of LRRK2 function. Microtubules serve as major conduits for the long-distance movement of vesicles and organelles within the cell (Stenmark, 2009). Microtubules could serve as a scaffold to concentrate LRRK2 signaling events such as the recruitment of the FADD/caspase-8 complex (Ho et al., 2009). LRRK2 may exist in a complex with the PD-related proteins Rab7L1, GAK, BAG5 and/or retromer to mediate the shuttling of cargo between the *trans*-Golgi network and early endosomes (MacLeod et al., 2013; Beilina et al., 2014). LRRK2's association with microtubules may provide the necessary platform to mediate the recruitment of the other proteins in this co-complex and facilitate the movement of vesicles to/from the Golgi. Follow up to these studies will help delineate how LRRK2 interacts with the endolysosomal system, via microtubules or other protein-protein complexes, its cellular function, and the effect of PD mutations.

With the identification of more genetic mutations linked to PD, a major question is whether all of these mutations converge on a common cellular pathway. This question is particularly pressing for α -synuclein and LRRK2, the two most important proteins in both

familial and sporadic disease. It is notable that while *SNCA* mutations are nearly 85% penetrant (in one study), *LRRK2* mutations are associated with much lower penetrance (Polymeropoulos et al., 1997; Healy et al., 2008). One potential reason for reduced penetrance is the presence of genetic modifiers, possibly of other endolysosomal proteins, that decrease disease risk in known *LRRK2* mutation carriers. Enhanced genetic techniques will permit the study of such genetic modifiers. An example of this type of study came with the identification of *RAB7L1* as a modifier of *LRRK2* risk in sporadic disease (MacLeod et al., 2013). Whole exome sequencing has recently identified three additional genetic mutations in familial forms of PD (Edvardson et al., 2012; Krebs et al., 2013; Vilarino-Guell et al., 2013).

Parkinson disease is a devastating disorder that affects millions of patients with profound impairment and morbidity. Medical treatment of PD remains focused on symptom management, because of a lack of understanding of the mechanisms responsible for PD-related neurodegeneration. Over the past 15 years, genetic advancements have profoundly shifted our comprehension of underlying pathogenesis, but have yielded disappointing therapeutic results. A new wave of genetic, biochemical, and animal studies is revealing the complexity of endolysosomal dysfunction in PD. The work in this dissertation captures this complexity and provides advancement in our understanding of the normal and pathological effects of two PD-related proteins, *ATP13A2* and *LRRK2*. I hope that this work will contribute to a broader understanding of the cellular mechanisms occurring in PD, with the ultimate goal of developing novel therapeutic targets that will finally be able to halt or even reverse the neurodegenerative process.

References

- Aasly JO, Vilarino-Guell C, Dachsel JC, Webber PJ, West AB, Haugarvoll K, Johansen KK, Toft M, Nutt JG, Payami H, Kachergus JM, Lincoln SJ, Felic A, Wider C, Soto-Ortolaza AI, Cobb SA, White LR, Ross OA, Farrer MJ (2010) Novel pathogenic LRRK2 p.Asn1437His substitution in familial Parkinson's disease. *Mov Disord*, 25:2156–2163.
- Aharon-Peretz J, Rosenbaum H, Gershoni-Baruch R (2004) Mutations in the glucocerebrosidase gene and Parkinson's disease in Ashkenazi Jews. *N Engl J Med*, 351:1972–1977.
- Ahlskog JE (2009) Parkin and PINK1 parkinsonism may represent nigral mitochondrial cytopathies distinct from Lewy body Parkinson's disease. *Parkinsonism Relat Disord*, 15:721–727.
- Ahmed I, Liang Y, Schools S, Dawson VL, Dawson TM, Savitt JM (2012) Development and characterization of a new Parkinson's disease model resulting from impaired autophagy. *J Neurosci*, 32:16503–16509.
- Ahn TB, Kim SY, Kim JY, Park SS, Lee DS, Min HJ, Kim YK, Kim SE, Kim JM, Kim HJ, Cho J, Jeon BS (2008) alpha-Synuclein gene duplication is present in sporadic Parkinson disease. *Neurology*, 70:43–49.
- Alegre-Abarrategui J, Christian H, Lufino MM, Mutihac R, Venda LL, Ansorge O, Wade-Martins R (2009) LRRK2 regulates autophagic activity and localizes to specific membrane microdomains in a novel human genomic reporter cellular model. *Hum Mol Genet*, 18:4022–4034.
- Alvarez-Erviti L, Seow Y, Schapira AH, Gardiner C, Sargent IL, Wood MJ, Cooper JM (2011) Lysosomal dysfunction increases exosome-mediated alpha-synuclein release and transmission. *Neurobiol Dis*, 42:360–367.
- Amo T, Sato S, Saiki S, Wolf AM, Toyomizu M, Gautier CA, Shen J, Ohta S, Hattori N (2011) Mitochondrial membrane potential decrease caused by loss of PINK1 is not due to proton leak, but to respiratory chain defects. *Neurobiol Dis*, 41:111–118.
- Annesi G, Savettieri G, Pugliese P, D'Amelio M, Tarantino P, Ragonese P, La Bella V, Piccoli T, Civitelli D, Annesi F, Fierro B, Piccoli F, Arabia G, Caracciolo M, Ciro Candiano IC, Quattrone A (2005) DJ-1 mutations and parkinsonism-dementia-amyotrophic lateral sclerosis complex. *Ann Neurol*, 58:803–807.
- Ariga H, Takahashi-Niki K, Kato I, Maita H, Niki T, Iguchi-Ariga SM (2013) Neuroprotective function of DJ-1 in Parkinson's disease. *Oxid Med Cell Longev*, 2013:683920.
- Assayag K, Yakunin E, Loeb V, Selkoe DJ, Sharon R (2007) Polyunsaturated fatty acids induce alpha-synuclein-related pathogenic changes in neuronal cells. *Am J Pathol*, 171:2000–2011.
- Banerjee R, Starkov AA, Beal MF, Thomas B (2009) Mitochondrial dysfunction in the limelight of Parkinson's disease pathogenesis. *Biochim Biophys Acta*, 1792:651–663.

- Barcelo-Coblijn G, Golovko MY, Weinhofer I, Berger J, Murphy EJ (2007) Brain neutral lipids mass is increased in alpha-synuclein gene-ablated mice. *J Neurochem*, 101:132–141.
- Behrens MI et al. (2010) Clinical spectrum of Kufor-Rakeb syndrome in the Chilean kindred with ATP13A2 mutations. *Mov Disord*, 25:1929–1937.
- Beilina A et al. (2014) Unbiased screen for interactors of leucine-rich repeat kinase 2 supports a common pathway for sporadic and familial Parkinson disease. *Proc Natl Acad Sci U S A*, 111:2626–2631.
- Bendor JT, Logan TP, Edwards RH (2013) The function of alpha-synuclein. *Neuron*, 79:1044–1066.
- Berman DE, Dall’Armi C, Voronov SV, McIntire LB, Zhang H, Moore AZ, Staniszewski A, Arancio O, Kim TW, Di Paolo G (2008) Oligomeric amyloid-beta peptide disrupts phosphatidylinositol-4,5-bisphosphate metabolism. *Nat Neurosci*, 11:547–554.
- Bertoncini CW, Fernandez CO, Griesinger C, Jovin TM, Zweckstetter M (2005) Familial mutants of alpha-synuclein with increased neurotoxicity have a destabilized conformation. *J Biol Chem*, 280:30649–30652.
- Bible E, Gupta P, Hofmann SL, Cooper JD (2004) Regional and cellular neuropathology in the palmitoyl protein thioesterase-1 null mutant mouse model of infantile neuronal ceroid lipofuscinosis. *Neurobiol Dis*, 16:346–359.
- Biskup S, Moore DJ, Celsi F, Higashi S, West AB, Andrabi SA, Kurkinen K, Yu SW, Savitt JM, Waldvogel HJ, Faull RL, Emson PC, Torp R, Ottersen OP, Dawson TM, Dawson VL (2006) Localization of LRRK2 to membranous and vesicular structures in mammalian brain. *Ann Neurol*, 60:557–569.
- Bonifati V (2007) LRRK2 low-penetrance mutations (Gly2019Ser) and risk alleles (Gly2385Arg)-linking familial and sporadic Parkinson’s disease. *Neurochem Res*, 32:1700–1708.
- Bonifati V (2014) Genetics of Parkinson’s disease--state of the art, 2013. *Parkinsonism Relat Disord*, 20 Suppl 1:S23–S28.
- Bonifati V, Rizzu P, van Baren MJ, Schaap O, Breedveld GJ, Krieger E, Dekker MC, Squitieri F, Ibanez P, Joosse M, van Dongen JW, Vanacore N, van Swieten JC, Brice A, Meco G, van Duijn CM, Oostra BA, Heutink P (2003) Mutations in the DJ-1 gene associated with autosomal recessive early-onset parkinsonism. *Science*, 299:256–259.
- Braak H, Rub U, Gai WP, Del Tredici K (2003) Idiopathic Parkinson’s disease: possible routes by which vulnerable neuronal types may be subject to neuroinvasion by an unknown pathogen. *J Neural Transm*, 110:517–536.
- Bras J, Verloes A, Schneider SA, Mole SE, Guerreiro RJ (2012) Mutation of the parkinsonism gene ATP13A2 causes neuronal ceroid-lipofuscinosis. *Hum Mol Genet*, 21:2646–2650.
- Bruggemann N, Hagenah J, Reetz K, Schmidt A, Kasten M, Buchmann I, Eckerle S, Bahre M, Munchau A, Djarmati A, van der Vegt J, Siebner H, Binkofski F, Ramirez A, Behrens MI, Klein C (2010) Recessively inherited parkinsonism: effect of ATP13A2 mutations on the clinical and neuroimaging phenotype. *Arch Neurol*, 67:1357–1363.
- Burchell VS, Nelson DE, Sanchez-Martinez A, Delgado-Camprubi M, Ivatt RM, Pogson JH, Randle SJ, Wray S, Lewis PA, Houlden H, Abramov AY, Hardy J, Wood NW, Whitworth AJ, Laman H, Plun-Favreau H (2013) The Parkinson’s disease-linked proteins Fbxo7 and Parkin interact to mediate mitophagy. *Nat Neurosci*, 16:1257–1265.
- Burke RE, Dauer WT, Vonsattel JP (2008) A critical evaluation of the Braak staging scheme for Parkinson’s disease. *Ann Neurol*, 64:485–491.

- Caesar M, Zach S, Carlson CB, Brockmann K, Gasser T, Gillardon F (2013) Leucine-rich repeat kinase 2 functionally interacts with microtubules and kinase-dependently modulates cell migration. *Neurobiol Dis*, 54:280–288.
- Canet-Aviles RM, Wilson MA, Miller DW, Ahmad R, McLendon C, Bandyopadhyay S, Baptista MJ, Ringe D, Petsko GA, Cookson MR (2004) The Parkinson's disease protein DJ-1 is neuroprotective due to cysteine-sulfinic acid-driven mitochondrial localization. *Proc Natl Acad Sci U S A*, 101:9103–9108.
- Carson C, Saleh M, Fung FW, Nicholson DW, Roskams AJ (2005) Axonal dynactin p150Glued transports caspase-8 to drive retrograde olfactory receptor neuron apoptosis. *J Neurosci*, 25:6092–6104.
- Cataldo AM, Barnett JL, Pieroni C, Nixon RA (1997) Increased neuronal endocytosis and protease delivery to early endosomes in sporadic Alzheimer's disease: neuropathologic evidence for a mechanism of increased beta-amyloidogenesis. *J Neurosci*, 17:6142–6151.
- Chan RB, Oliveira TG, Cortes EP, Honig LS, Duff KE, Small SA, Wenk MR, Shui G, Di Paolo G (2012) Comparative lipidomic analysis of mouse and human brain with Alzheimer disease. *J Biol Chem*, 287:2678–2688.
- Chang M, Cooper JD, Sleat DE, Cheng SH, Dodge JC, Passini MA, Lobel P, Davidson BL (2008) Intraventricular enzyme replacement improves disease phenotypes in a mouse model of late infantile neuronal ceroid lipofuscinosis. *Mol Ther*, 16:649–656.
- Chartier-Harlin MC et al. (2011) Translation initiator EIF4G1 mutations in familial Parkinson disease. *Am J Hum Genet*, 89:398–406.
- Chartier-Harlin MC, Kachergus J, Roumier C, Mouroux V, Douay X, Lincoln S, Levecque C, Larvor L, Andrieux J, Hulihan M, Waucquier N, Defebvre L, Amouyel P, Farrer M, Destee A (2004) Alpha-synuclein locus duplication as a cause of familial Parkinson's disease. *Lancet*, 364:1167–1169.
- Cheng F, Li X, Li Y, Wang C, Wang T, Liu G, Baskys A, Ueda K, Chan P, Yu S (2011) alpha-Synuclein promotes clathrin-mediated NMDA receptor endocytosis and attenuates NMDA-induced dopaminergic cell death. *J Neurochem*, 119:815–825.
- Cheng HC, Ulane CM, Burke RE (2010) Clinical progression in Parkinson disease and the neurobiology of axons. *Ann Neurol*, 67:715–725.
- Chevallier J, Chamoun Z, Jiang G, Prestwich G, Sakai N, Matile S, Parton RG, Gruenberg J (2008) Lysobisphosphatidic acid controls endosomal cholesterol levels. *J Biol Chem*, 283:27871–27880.
- Chien HF, Bonifati V, Barbosa ER (2011) ATP13A2-related neurodegeneration (PARK9) without evidence of brain iron accumulation. *Mov Disord*, 26:1364–1365.
- Chinta SJ, Mallajosyula JK, Rane A, Andersen JK (2010) Mitochondrial alpha-synuclein accumulation impairs complex I function in dopaminergic neurons and results in increased mitophagy in vivo. *Neurosci Lett*, 486:235–239.
- Clark IE, Dodson MW, Jiang C, Cao JH, Huh JR, Seol JH, Yoo SJ, Hay BA, Guo M (2006) *Drosophila pink1* is required for mitochondrial function and interacts genetically with parkin. *Nature*, 441:1162–1166.
- Cookson MR (2005) The biochemistry of Parkinson's disease. *Annu Rev Biochem*, 74:29–52.
- Cookson MR (2010) The role of leucine-rich repeat kinase 2 (LRRK2) in Parkinson's disease. *Nat Rev Neurosci*, 11:791–797.
- Cookson MR (2012) Cellular effects of LRRK2 mutations. *Biochem Soc Trans*, 40:1070–1073.

- Cookson MR, van der Brug M (2008) Cell systems and the toxic mechanism(s) of alpha-synuclein. *Exp Neurol*, 209:5–11.
- Cooper AA, Gitler AD, Cashikar A, Haynes CM, Hill KJ, Bhullar B, Liu K, Xu K, Strathern KE, Liu F, Cao S, Caldwell KA, Caldwell GA, Marsischky G, Kolodner RD, Labaer J, Rochet JC, Bonini NM, Lindquist S (2006) Alpha-synuclein blocks ER-Golgi traffic and Rab1 rescues neuron loss in Parkinson's models. *Science*, 313:324–328.
- Cossec JC, Lavaur J, Berman DE, Rivals I, Hoischen A, Stora S, Ripoll C, Mircher C, Grattau Y, Olivomarin JC, de Chaumont F, Lecourtois M, Antonarakis SE, Veltman JA, Delabar JM, Duyckaerts C, Di Paolo G, Potier MC (2012) Trisomy for synaptojanin1 in Down syndrome is functionally linked to the enlargement of early endosomes. *Hum Mol Genet*, 21:3156–3172.
- Costa Mdo C, Paulson HL (2012) Toward understanding Machado-Joseph disease. *Prog Neurobiol*, 97:239–257.
- Covy JP, Waxman EA, Giasson BI (2012) Characterization of cellular protective effects of ATP13A2/PARK9 expression and alterations resulting from pathogenic mutants. *J Neurosci Res*, 90:2306–2316.
- Crabtree D, Dodson M, Ouyang X, Boyer-Guittaut M, Liang Q, Ballestas ME, Fineberg N, Zhang J (2013) Over-expression of an inactive mutant cathepsin D increases endogenous alpha-synuclein and cathepsin B activity in SH-SY5Y cells. *J Neurochem*,
- Cuervo AM, Dice JF, Knecht E (1997) A population of rat liver lysosomes responsible for the selective uptake and degradation of cytosolic proteins. *J Biol Chem*, 272:5606–5615.
- Cuervo AM, Stefanis L, Fredenburg R, Lansbury PT, Sulzer D (2004) Impaired degradation of mutant alpha-synuclein by chaperone-mediated autophagy. *Science*, 305:1292–1295.
- Cullen V, Lindfors M, Ng J, Paetau A, Swinton E, Kolodziej P, Boston H, Saftig P, Woulfe J, Feany MB, Myllykangas L, Schlossmacher MG, Tyynela J (2009) Cathepsin D expression level affects alpha-synuclein processing, aggregation, and toxicity in vivo. *Mol Brain*, 2:5.
- Dachsel JC, Behrouz B, Yue M, Beevers JE, Melrose HL, Farrer MJ (2010) A comparative study of Lrrk2 function in primary neuronal cultures. *Parkinsonism Relat Disord*, 16:650–655.
- Dagda RK, Cherra SJ, Kulich SM, Tandon A, Park D, Chu CT (2009) Loss of PINK1 function promotes mitophagy through effects on oxidative stress and mitochondrial fission. *J Biol Chem*, 284:13843–13855.
- Dalfo E, Barrachina M, Rosa JL, Ambrosio S, Ferrer I (2004) Abnormal alpha-synuclein interactions with rab3a and rabphilin in diffuse Lewy body disease. *Neurobiol Dis*, 16:92–97.
- Danzer KM, Haasen D, Karow AR, Moussaud S, Habeck M, Giese A, Kretschmar H, Hengerer B, Kostka M, Danzer KM, Krebs SK, Wolff M, Birk G, Hengerer B (2007) Different species of alpha-synuclein oligomers induce calcium influx and seeding.
- Seeding induced by alpha-synuclein oligomers provides evidence for spreading of alpha-synuclein pathology. *J Neurosci J Neurochem*, 27:9220–9232.
- Danzer KM, Kranich LR, Ruf WP, Cagsal-Getkin O, Winslow AR, Zhu L, Vanderburg CR, McLean PJ (2012) Exosomal cell-to-cell transmission of alpha synuclein oligomers. *Mol Neurodegener*, 7:42.
- Danzer KM, Krebs SK, Wolff M, Birk G, Hengerer B (2009) Seeding induced by alpha-synuclein oligomers provides evidence for spreading of alpha-synuclein pathology. *J Neurochem*, 111:192–203.

- Dauer W, Kholodilov N, Vila M, Trillat AC, Goodchild R, Larsen KE, Staal R, Tieu K, Schmitz Y, Yuan CA, Rocha M, Jackson-Lewis V, Hersch S, Sulzer D, Przedborski S, Burke R, Hen R (2002) Resistance of alpha -synuclein null mice to the parkinsonian neurotoxin MPTP. *Proc Natl Acad Sci U S A*, 99:14524–14529.
- Dauer W, Przedborski S (2003) Parkinson's disease: mechanisms and models. *Neuron*, 39:889–909.
- Dawson TM, Ko HS, Dawson VL (2010) Genetic animal models of Parkinson's disease. *Neuron*, 66:646–661.
- de Rijk MC, Breteler MM, Graveland GA, Ott A, Grobbee DE, van der Meche FG, Hofman A (1995) Prevalence of Parkinson's disease in the elderly: the Rotterdam Study. *Neurology*, 45:2143–2146.
- Decressac M, Mattsson B, Weikop P, Lundblad M, Jakobsson J, Bjorklund A (2013) TFEB-mediated autophagy rescues midbrain dopamine neurons from alpha-synuclein toxicity. *Proc Natl Acad Sci U S A*, 110:E1817–E1826.
- Dehay B, Ramirez A, Martinez-Vicente M, Perier C, Cannon MH, Doudnikoff E, Vital A, Vila M, Klein C, Bezdard E (2012) Loss of P-type ATPase ATP13A2/PARK9 function induces general lysosomal deficiency and leads to Parkinson disease neurodegeneration. *Proc Natl Acad Sci U S A*, 109:9611–9616.
- Deng J, Lewis PA, Greggio E, Sluch E, Beilina A, Cookson MR (2008) Structure of the ROC domain from the Parkinson's disease-associated leucine-rich repeat kinase 2 reveals a dimeric GTPase. *Proc Natl Acad Sci U S A*, 105:1499–1504.
- Deng X, Dzamko N, Prescott A, Davies P, Liu Q, Yang Q, Lee JD, Patricelli MP, Nomanbhoy TK, Alessi DR, Gray NS (2011) Characterization of a selective inhibitor of the Parkinson's disease kinase LRRK2. *Nat Chem Biol*, 7:203–205.
- Devi L, Raghavendran V, Prabhu BM, Avadhani NG, Anandatheerthavarada HK (2008) Mitochondrial import and accumulation of alpha-synuclein impair complex I in human dopaminergic neuronal cultures and Parkinson disease brain. *J Biol Chem*, 283:9089–9100.
- Devine MJ, Gwinn K, Singleton A, Hardy J (2011) Parkinson's disease and alpha-synuclein expression. *Mov Disord*, 26:2160–2168.
- Di Fonzo A et al. (2007) ATP13A2 missense mutations in juvenile parkinsonism and young onset Parkinson disease. *Neurology*, 68:1557–1562.
- Di Fonzo A, Dekker MC, Montagna P, Baruzzi A, Yonova EH, Correia Guedes L, Szczerbinska A, Zhao T, Dubbel-Hulsman LO, Wouters CH, de Graaff E, Oyen WJ, Simons EJ, Breedveld GJ, Oostra BA, Horstink MW, Bonifati V (2009) FBXO7 mutations cause autosomal recessive, early-onset parkinsonian-pyramidal syndrome. *Neurology*, 72:240–245.
- Di Paolo G, Kim TW (2011) Linking lipids to Alzheimer's disease: cholesterol and beyond. *Nat Rev Neurosci*, 12:284–296.
- Dodson MW, Zhang T, Jiang C, Chen S, Guo M (2012) Roles of the Drosophila LRRK2 homolog in Rab7-dependent lysosomal positioning. *Hum Mol Genet*, 21:1350–1363.
- Dusonchet J, Kochubey O, Stafa K, Young SMJ, Zufferey R, Moore DJ, Schneider BL, Aebischer P (2011) A rat model of progressive nigral neurodegeneration induced by the Parkinson's disease-associated G2019S mutation in LRRK2. *J Neurosci*, 31:907–912.

- Dzamko N, Deak M, Hentati F, Reith AD, Prescott AR, Alessi DR, Nichols RJ (2010) Inhibition of LRRK2 kinase activity leads to dephosphorylation of Ser(910)/Ser(935), disruption of 14-3-3 binding and altered cytoplasmic localization. *Biochem J*, 430:405–413.
- Ebrahimi-Fakhari D, Cantuti-Castelvetri I, Fan Z, Rockenstein E, Masliah E, Hyman BT, McLean PJ, Unni VK (2011) Distinct roles in vivo for the ubiquitin-proteasome system and the autophagy-lysosomal pathway in the degradation of alpha-synuclein. *J Neurosci*, 31:14508–14520.
- Edvardson S, Cinnamon Y, Ta-Shma A, Shaag A, Yim YI, Zenvirt S, Jalas C, Lesage S, Brice A, Taraboulos A, Kaestner KH, Greene LE, Elpeleg O (2012) A deleterious mutation in DNAJC6 encoding the neuronal-specific clathrin-uncoating co-chaperone auxilin, is associated with juvenile parkinsonism. *PLoS One*, 7:e36458.
- Eiberg H, Hansen L, Korbo L, Nielsen IM, Svenstrup K, Bech S, Pinborg LH, Friberg L, Hjermand LE, Olsen OR, Nielsen JE (2012) Novel mutation in ATP13A2 widens the spectrum of Kufor-Rakeb syndrome (PARK9). *Clin Genet*, 82:256–263.
- Ejlerskov P, Rasmussen I, Nielsen TT, Bergstrom AL, Tohyama Y, Jensen PH, Vilhardt F (2013) Tubulin polymerization-promoting protein (TPPP/p25alpha) promotes unconventional secretion of alpha-synuclein through exophagy by impairing autophagosome-lysosome fusion. *J Biol Chem*, 288:17313–17335.
- El-Agnaf OM, Salem SA, Paleologou KE, Cooper LJ, Fullwood NJ, Gibson MJ, Curran MD, Court JA, Mann DM, Ikeda S, Cookson MR, Hardy J, Allsop D (2003) Alpha-synuclein implicated in Parkinson's disease is present in extracellular biological fluids, including human plasma. *FASEB J*, 17:1945–1947.
- El-Agnaf OM, Salem SA, Paleologou KE, Curran MD, Gibson MJ, Court JA, Schlossmacher MG, Allsop D (2006) Detection of oligomeric forms of alpha-synuclein protein in human plasma as a potential biomarker for Parkinson's disease. *FASEB J*, 20:419–425.
- Elrick MJ, Yu T, Chung C, Lieberman AP (2012) Impaired proteolysis underlies autophagic dysfunction in Niemann-Pick type C disease. *Hum Mol Genet*, 21:4876–4887.
- Emmanouilidou E, Melachroinou K, Roumeliotis T, Garbis SD, Ntzouni M, Margaritis LH, Stefanis L, Vekrellis K (2010) Cell-produced alpha-synuclein is secreted in a calcium-dependent manner by exosomes and impacts neuronal survival. *J Neurosci*, 30:6838–6851.
- Exner N, Treske B, Paquet D, Holmstrom K, Schiesling C, Gispert S, Carballo-Carbajal I, Berg D, Hoepken HH, Gasser T, Kruger R, Winklhofer KF, Vogel F, Reichert AS, Auburger G, Kahle PJ, Schmid B, Haass C (2007) Loss-of-function of human PINK1 results in mitochondrial pathology and can be rescued by parkin. *J Neurosci*, 27:12413–12418.
- Farias FH, Zeng R, Johnson GS, Winingar FA, Taylor JF, Schnabel RD, McKay SD, Sanders DN, Lohi H, Seppala EH, Wade CM, Lindblad-Toh K, O'Brien DP, Katz ML (2011) A truncating mutation in ATP13A2 is responsible for adult-onset neuronal ceroid lipofuscinosis in Tibetan terriers. *Neurobiol Dis*, 42:468–474.
- Farrer M, Chan P, Chen R, Tan L, Lincoln S, Hernandez D, Forno L, Gwinn-Hardy K, Petrucelli L, Hussey J, Singleton A, Tanner C, Hardy J, Langston JW (2001) Lewy bodies and parkinsonism in families with parkin mutations. *Ann Neurol*, 50:293–300.
- Farrer M, Kachergus J, Forno L, Lincoln S, Wang DS, Hulihan M, Maraganore D, Gwinn-Hardy K, Wszolek Z, Dickson D, Langston JW (2004) Comparison of kindreds with parkinsonism and alpha-synuclein genomic multiplications. *Ann Neurol*, 55:174–179.

- Follett J, Norwood SJ, Hamilton NA, Mohan M, Kovtun O, Tay S, Zhe Y, Wood SA, Mellick GD, Silburn PA, Collins BM, Bugarcic A, Teasdale RD (2014) The Vps35 D620N Mutation Linked to Parkinson's Disease Disrupts the Cargo Sorting Function of Retromer. *Traffic*, 15:230–244.
- Fong CY, Rolfs A, Schwarzbraun T, Klein C, O'Callaghan FJ (2011) Juvenile parkinsonism associated with heterozygous frameshift ATP13A2 gene mutation. *Eur J Paediatr Neurol*, 15:271–275.
- Fotin-Mleczech M, Henkler F, Samel D, Reichwein M, Hausser A, Parmryd I, Scheurich P, Schmid JA, Wajant H (2002) Apoptotic crosstalk of TNF receptors: TNF-R2-induces depletion of TRAF2 and IAP proteins and accelerates TNF-R1-dependent activation of caspase-8. *J Cell Sci*, 115:2757–2770.
- Friedman LG, Lachenmayer ML, Wang J, He L, Poulouse SM, Komatsu M, Holstein GR, Yue Z (2012) Disrupted autophagy leads to dopaminergic axon and dendrite degeneration and promotes presynaptic accumulation of alpha-synuclein and LRRK2 in the brain. *J Neurosci*, 32:7585–7593.
- Fuchs J, Tichopad A, Golub Y, Munz M, Schweitzer KJ, Wolf B, Berg D, Mueller JC, Gasser T (2008) Genetic variability in the SNCA gene influences alpha-synuclein levels in the blood and brain. *FASEB J*, 22:1327–1334.
- Gallala HD, Sandhoff K (2011) Biological function of the cellular lipid BMP-BMP as a key activator for cholesterol sorting and membrane digestion. *Neurochem Res*, 36:1594–1600.
- Gan-Or Z, Bar-Shira A, Dahary D, Mirelman A, Kedmi M, Gurevich T, Giladi N, Orr-Urtreger A (2012) Association of sequence alterations in the putative promoter of RAB7L1 with a reduced parkinson disease risk. *Arch Neurol*, 69:105–110.
- Gandhi PN, Wang X, Zhu X, Chen SG, Wilson-Delfosse AL (2008) The Roc domain of leucine-rich repeat kinase 2 is sufficient for interaction with microtubules. *J Neurosci Res*, 86:1711–1720.
- Gegg ME, Cooper JM, Chau KY, Rojo M, Schapira AH, Taanman JW (2010) Mitofusin 1 and mitofusin 2 are ubiquitinated in a PINK1/parkin-dependent manner upon induction of mitophagy. *Hum Mol Genet*, 19:4861–4870.
- Geisler S, Holmstrom KM, Skujat D, Fiesel FC, Rothfuss OC, Kahle PJ, Springer W (2010) PINK1/Parkin-mediated mitophagy is dependent on VDAC1 and p62/SQSTM1. *Nat Cell Biol*, 12:119–131.
- Giasson BI, Duda JE, Quinn SM, Zhang B, Trojanowski JQ, Lee VM (2002) Neuronal alpha-synucleinopathy with severe movement disorder in mice expressing A53T human alpha-synuclein. *Neuron*, 34:521–533.
- Gillardon F (2009) Leucine-rich repeat kinase 2 phosphorylates brain tubulin-beta isoforms and modulates microtubule stability--a point of convergence in parkinsonian neurodegeneration? *J Neurochem*, 110:1514–1522.
- Gitler AD, Chesi A, Geddie ML, Strathearn KE, Hamamichi S, Hill KJ, Caldwell KA, Caldwell GA, Cooper AA, Rochet JC, Lindquist S (2009) Alpha-synuclein is part of a diverse and highly conserved interaction network that includes PARK9 and manganese toxicity. *Nat Genet*, 41:308–315.
- Gloeckner CJ, Kinkl N, Schumacher A, Braun RJ, O'Neill E, Meitinger T, Kolch W, Prokisch H, Ueffing M (2006) The Parkinson disease causing LRRK2 mutation I2020T is associated with increased kinase activity. *Hum Mol Genet*, 15:223–232.

- Goker-Alpan O, Schiffmann R, LaMarca ME, Nussbaum RL, McInerney-Leo A, Sidransky E (2004) Parkinsonism among Gaucher disease carriers. *J Med Genet*, 41:937–940.
- Goodchild RE, Kim CE, Dauer WT (2005) Loss of the dystonia-associated protein torsinA selectively disrupts the neuronal nuclear envelope. *Neuron*, 48:923–932.
- Gotthardt K, Weyand M, Kortholt A, Van Haastert PJ, Wittinghofer A (2008) Structure of the Roc-COR domain tandem of *C. tepidum*, a prokaryotic homologue of the human LRRK2 Parkinson kinase. *EMBO J*, 27:2239–2249.
- Graham DG, Tiffany SM, Bell WRJ, Gutknecht WF (1978) Autoxidation versus covalent binding of quinones as the mechanism of toxicity of dopamine, 6-hydroxydopamine, and related compounds toward C1300 neuroblastoma cells in vitro. *Mol Pharmacol*, 14:644–653.
- Greggio E, Jain S, Kingsbury A, Bandopadhyay R, Lewis P, Kaganovich A, van der Brug MP, Beilina A, Blackinton J, Thomas KJ, Ahmad R, Miller DW, Kesavapany S, Singleton A, Lees A, Harvey RJ, Harvey K, Cookson MR (2006) Kinase activity is required for the toxic effects of mutant LRRK2/dardarin. *Neurobiol Dis*, 23:329–341.
- Greggio E, Taymans JM, Zhen EY, Ryder J, Vancraenenbroeck R, Beilina A, Sun P, Deng J, Jaffe H, Baekelandt V, Merchant K, Cookson MR (2009) The Parkinson's disease kinase LRRK2 autophosphorylates its GTPase domain at multiple sites. *Biochem Biophys Res Commun*, 389:449–454.
- Grunewald A, Arns B, Seibler P, Rakovic A, Munchau A, Ramirez A, Sue CM, Klein C (2012) ATP13A2 mutations impair mitochondrial function in fibroblasts from patients with Kufor-Rakeb syndrome. *Neurobiol Aging*, 33:1843.e1–1843.e7.
- Guiet C, Vito P (2000) Caspase recruitment domain (CARD)-dependent cytoplasmic filaments mediate bcl10-induced NF-kappaB activation. *J Cell Biol*, 148:1131–1140.
- Gupta A, Dawson VL, Dawson TM (2008) What causes cell death in Parkinson's disease? *Ann Neurol*, 64 Suppl 2:S3–15.
- Gupta P, Soyombo AA, Atashband A, Wisniewski KE, Shelton JM, Richardson JA, Hammer RE, Hofmann SL (2001) Disruption of PPT1 or PPT2 causes neuronal ceroid lipofuscinosis in knockout mice. *Proc Natl Acad Sci U S A*, 98:13566–13571.
- Gusdon AM, Zhu J, Van Houten B, Chu CT (2012) ATP13A2 regulates mitochondrial bioenergetics through macroautophagy. *Neurobiol Dis*, 45:962–972.
- Gwinn-Hardy K, Chen JY, Liu HC, Liu TY, Boss M, Seltzer W, Adam A, Singleton A, Koroshetz W, Waters C, Hardy J, Farrer M (2000a) Spinocerebellar ataxia type 2 with parkinsonism in ethnic Chinese. *Neurology*, 55:800–805.
- Gwinn-Hardy K, Mehta ND, Farrer M, Maraganore D, Muentner M, Yen SH, Hardy J, Dickson DW (2000b) Distinctive neuropathology revealed by alpha-synuclein antibodies in hereditary parkinsonism and dementia linked to chromosome 4p. *Acta Neuropathol*, 99:663–672.
- Gwinn-Hardy K, Singleton A, O'Suilleabhain P, Boss M, Nicholl D, Adam A, Hussey J, Critchley P, Hardy J, Farrer M (2001) Spinocerebellar ataxia type 3 phenotypically resembling parkinson disease in a black family. *Arch Neurol*, 58:296–299.
- Hagerman RJ, Leehey M, Heinrichs W, Tassone F, Wilson R, Hills J, Grigsby J, Gage B, Hagerman PJ (2001) Intention tremor, parkinsonism, and generalized brain atrophy in male carriers of fragile X. *Neurology*, 57:127–130.

- Hall DA, Howard K, Hagerman R, Leehey MA (2009) Parkinsonism in FMR1 premutation carriers may be indistinguishable from Parkinson disease. *Parkinsonism Relat Disord*, 15:156–159.
- Hamza TH, Zabetian CP, Tenesa A, Laederach A, Montimurro J, Yearout D, Kay DM, Doheny KF, Paschall J, Pugh E, Kusel VI, Collura R, Roberts J, Griffith A, Samii A, Scott WK, Nutt J, Factor SA, Payami H (2010) Common genetic variation in the HLA region is associated with late-onset sporadic Parkinson's disease. *Nat Genet*, 42:781–785.
- Hansen C, Angot E, Bergstrom AL, Steiner JA, Pieri L, Paul G, Outeiro TF, Melki R, Kallunki P, Fog K, Li JY, Brundin P (2011) alpha-Synuclein propagates from mouse brain to grafted dopaminergic neurons and seeds aggregation in cultured human cells. *J Clin Invest*, 121:715–725.
- Hao LY, Giasson BI, Bonini NM (2010) DJ-1 is critical for mitochondrial function and rescues PINK1 loss of function. *Proc Natl Acad Sci U S A*, 107:9747–9752.
- Hardy J (2010) Genetic analysis of pathways to Parkinson disease. *Neuron*, 68:201–206.
- Harold D et al. (2009) Genome-wide association study identifies variants at CLU and PICALM associated with Alzheimer's disease. *Nat Genet*, 41:1088–1093.
- Hasegawa K, Stoessel AJ, Yokoyama T, Kowa H, Wszolek ZK, Yagishita S (2009) Familial parkinsonism: study of original Sagami-hara PARK8 (I2020T) kindred with variable clinicopathologic outcomes. *Parkinsonism Relat Disord*, 15:300–306.
- Hatano T, Kubo S, Imai S, Maeda M, Ishikawa K, Mizuno Y, Hattori N (2007) Leucine-rich repeat kinase 2 associates with lipid rafts. *Hum Mol Genet*, 16:678–690.
- Hauser DN, Hastings TG (2013) Mitochondrial dysfunction and oxidative stress in Parkinson's disease and monogenic parkinsonism. *Neurobiol Dis*, 51:35–42.
- Hayflick SJ, Westaway SK, Levinson B, Zhou B, Johnson MA, Ching KH, Gitschier J (2003) Genetic, clinical, and radiographic delineation of Hallervorden-Spatz syndrome. *N Engl J Med*, 348:33–40.
- Healy DG et al. (2008) Phenotype, genotype, and worldwide genetic penetrance of LRRK2-associated Parkinson's disease: a case-control study. *Lancet Neurol*, 7:583–590.
- Heo HY, Kim KS, Seol W (2010) Coordinate Regulation of Neurite Outgrowth by LRRK2 and Its Interactor, Rab5. *Exp Neurol*, 19:97–105.
- Hierro A, Rojas AL, Rojas R, Murthy N, Effantin G, Kajava AV, Steven AC, Bonifacino JS, Hurley JH (2007) Functional architecture of the retromer cargo-recognition complex. *Nature*, 449:1063–1067.
- Hirai K, Aliev G, Nunomura A, Fujioka H, Russell RL, Atwood CS, Johnson AB, Kress Y, Vinters HV, Tabaton M, Shimohama S, Cash AD, Siedlak SL, Harris PL, Jones PK, Petersen RB, Perry G, Smith MA (2001) Mitochondrial abnormalities in Alzheimer's disease. *J Neurosci*, 21:3017–3023.
- Hjermind LE, Johannsen LG, Blau N, Wevers RA, Lucking CB, Hertz JM, Friberg L, Regeur L, Nielsen JE, Sorensen SA (2006) Dopa-responsive dystonia and early-onset Parkinson's disease in a patient with GTP cyclohydrolase I deficiency? *Mov Disord*, 21:679–682.
- Ho CC, Rideout HJ, Ribe E, Troy CM, Dauer WT (2009) The Parkinson disease protein leucine-rich repeat kinase 2 transduces death signals via Fas-associated protein with death domain and caspase-8 in a cellular model of neurodegeneration. *J Neurosci*, 29:1011–1016.
- Horgan CP, McCaffrey MW (2011) Rab GTPases and microtubule motors. *Biochem Soc Trans*, 39:1202–1206.

- Houlden H, Singleton AB (2012) The genetics and neuropathology of Parkinson's disease. *Acta Neuropathol*, 124:325–338.
- Hutton M et al. (1998) Association of missense and 5'-splice-site mutations in tau with the inherited dementia FTDP-17. *Nature*, 393:702–705.
- Ibanez P, Bonnet AM, Debarges B, Lohmann E, Tison F, Pollak P, Agid Y, Durr A, Brice A (2004) Causal relation between alpha-synuclein gene duplication and familial Parkinson's disease. *Lancet*, 364:1169–1171.
- Ibanez P, Lesage S, Janin S, Lohmann E, Durif F, Destee A, Bonnet AM, Brefel-Courbon C, Heath S, Zelenika D, Agid Y, Durr A, Brice A (2009) Alpha-synuclein gene rearrangements in dominantly inherited parkinsonism: frequency, phenotype, and mechanisms. *Arch Neurol*, 66:102–108.
- Imai Y, Gehrke S, Wang HQ, Takahashi R, Hasegawa K, Oota E, Lu B (2008) Phosphorylation of 4E-BP by LRRK2 affects the maintenance of dopaminergic neurons in *Drosophila*. *EMBO J*, 27:2432–2443.
- Inohara N, Koseki T, Lin J, del Peso L, Lucas PC, Chen FF, Ogura Y, Nunez G (2000) An induced proximity model for NF-kappa B activation in the Nod1/RICK and RIP signaling pathways. *J Biol Chem*, 275:27823–27831.
- Irwin DJ, Lee VM, Trojanowski JQ (2013) Parkinson's disease dementia: convergence of alpha-synuclein, tau and amyloid-beta pathologies. *Nat Rev Neurosci*, 14:626–636.
- Jabs S, Quitsch A, Kakela R, Koch B, Tyynela J, Brade H, Glatzel M, Walkley S, Saftig P, Vanier MT, Braulke T (2008) Accumulation of bis(monoacylglycero)phosphate and gangliosides in mouse models of neuronal ceroid lipofuscinosis. *J Neurochem*, 106:1415–1425.
- Jacquemont S, Hagerman RJ, Leehey MA, Hall DA, Levine RA, Brunberg JA, Zhang L, Jardini T, Gane LW, Harris SW, Herman K, Grigsby J, Greco CM, Berry-Kravis E, Tassone F, Hagerman PJ (2004) Penetrance of the fragile X-associated tremor/ataxia syndrome in a premutation carrier population. *JAMA*, 291:460–469.
- Jaleel M, Nichols RJ, Deak M, Campbell DG, Gillardon F, Knebel A, Alessi DR (2007) LRRK2 phosphorylates moesin at threonine-558: characterization of how Parkinson's disease mutants affect kinase activity. *Biochem J*, 405:307–317.
- Jang A, Lee HJ, Suk JE, Jung JW, Kim KP, Lee SJ (2010) Non-classical exocytosis of alpha-synuclein is sensitive to folding states and promoted under stress conditions. *J Neurochem*, 113:1263–1274.
- Jin SM, Lazarou M, Wang C, Kane LA, Narendra DP, Youle RJ (2010) Mitochondrial membrane potential regulates PINK1 import and proteolytic destabilization by PARL. *J Cell Biol*, 191:933–942.
- Jorgensen ND, Peng Y, Ho CC, Rideout HJ, Petrey D, Liu P, Dauer WT (2009) The WD40 domain is required for LRRK2 neurotoxicity. *PLoS One*, 4:e8463.
- Kachergus J, Mata IF, Hulihan M, Taylor JP, Lincoln S, Aasly J, Gibson JM, Ross OA, Lynch T, Wiley J, Payami H, Nutt J, Maraganore DM, Czyzewski K, Styczynska M, Wszolek ZK, Farrer MJ, Toft M (2005) Identification of a novel LRRK2 mutation linked to autosomal dominant parkinsonism: evidence of a common founder across European populations. *Am J Hum Genet*, 76:672–680.
- Kalia LV, Kalia SK, McLean PJ, Lozano AM, Lang AE (2013) alpha-Synuclein oligomers and clinical implications for Parkinson disease. *Ann Neurol*, 73:155–169.

- Kanao T, Venderova K, Park DS, Unterman T, Lu B, Imai Y (2010) Activation of FoxO by LRRK2 induces expression of proapoptotic proteins and alters survival of postmitotic dopaminergic neuron in *Drosophila*. *Hum Mol Genet*, 19:3747–3758.
- Kann M, Jacobs H, Mohrmann K, Schumacher K, Hedrich K, Garrels J, Wieggers K, Schwinger E, Pramstaller PP, Breakefield XO, Ozelius LJ, Vieregge P, Klein C (2002) Role of parkin mutations in 111 community-based patients with early-onset parkinsonism. *Ann Neurol*, 51:621–625.
- Katz ML, Narfstrom K, Johnson GS, O'Brien DP (2005) Assessment of retinal function and characterization of lysosomal storage body accumulation in the retinas and brains of Tibetan Terriers with ceroid-lipofuscinosis. *Am J Vet Res*, 66:67–76.
- Katz ML, Sanders DN, Mooney BP, Johnson GS (2007) Accumulation of glial fibrillary acidic protein and histone H4 in brain storage bodies of Tibetan terriers with hereditary neuronal ceroid lipofuscinosis. *J Inher Metab Dis*, 30:952–963.
- Kaushik S, Cuervo AM (2009) Methods to monitor chaperone-mediated autophagy. *Methods Enzymol*, 452:297–324.
- Kaushik S, Cuervo AM (2012) Chaperone-mediated autophagy: a unique way to enter the lysosome world. *Trends Cell Biol*, 22:407–417.
- Kett LR, Dauer WT (2012) Leucine-rich repeat kinase 2 for beginners: six key questions. *Cold Spring Harb Perspect Med*, 2:a009407.
- Kilarski LL et al. (2012) Systematic review and UK-based study of PARK2 (parkin), PINK1, PARK7 (DJ-1) and LRRK2 in early-onset Parkinson's disease. *Mov Disord*, 27:1522–1529.
- Kirik D, Annett LE, Burger C, Muzyczka N, Mandel RJ, Bjorklund A (2003) Nigrostriatal alpha-synucleinopathy induced by viral vector-mediated overexpression of human alpha-synuclein: a new primate model of Parkinson's disease. *Proc Natl Acad Sci U S A*, 100:2884–2889.
- Kisos H, Ben-Gedalya T, Sharon R (2014) The Clathrin-Dependent Localization of Dopamine Transporter to Surface Membranes Is Affected by alpha-Synuclein. *J Mol Neurosci*, 52:167–176.
- Kitada T, Asakawa S, Hattori N, Matsumine H, Yamamura Y, Minoshima S, Yokochi M, Mizuno Y, Shimizu N (1998) Mutations in the parkin gene cause autosomal recessive juvenile parkinsonism. *Nature*, 392:605–608.
- Klein RJ, Zeiss C, Chew EY, Tsai JY, Sackler RS, Haynes C, Henning AK, SanGiovanni JP, Mane SM, Mayne ST, Bracken MB, Ferris FL, Ott J, Barnstable C, Hoh J (2005) Complement factor H polymorphism in age-related macular degeneration. *Science*, 308:385–389.
- Kobayashi T, Stang E, Fang KS, de Moerloose P, Parton RG, Gruenberg J (1998) A lipid associated with the antiphospholipid syndrome regulates endosome structure and function. *Nature*, 392:193–197.
- Koga H, Kaushik S, Cuervo AM (2010) Altered lipid content inhibits autophagic vesicular fusion. *FASEB J*, 24:3052–3065.
- Koike M, Nakanishi H, Saftig P, Ezaki J, Isahara K, Ohsawa Y, Schulz-Schaeffer W, Watanabe T, Waguri S, Kametaka S, Shibata M, Yamamoto K, Kominami E, Peters C, von Figura K, Uchiyama Y (2000) Cathepsin D deficiency induces lysosomal storage with ceroid lipofuscin in mouse CNS neurons. *J Neurosci*, 20:6898–6906.

- Komatsu M, Ichimura Y (2010) Physiological significance of selective degradation of p62 by autophagy. *FEBS Lett*, 584:1374–1378.
- Kong SM, Chan BK, Park JS, Hill KJ, Aitken JB, Cottle L, Farghaian H, Cole AR, Lay PA, Sue CM, Cooper AA (2014) Parkinson's disease-linked human PARK9/ATP13A2 maintains zinc homeostasis and promotes alpha-Synuclein externalization via exosomes. *Hum Mol Genet*.
- Kopra O, Vesa J, von Schantz C, Manninen T, Minye H, Fabritius AL, Rapola J, van Diggelen OP, Saarela J, Jalanko A, Peltonen L (2004) A mouse model for Finnish variant late infantile neuronal ceroid lipofuscinosis, CLN5, reveals neuropathology associated with early aging. *Hum Mol Genet*, 13:2893–2906.
- Kordower JH, Chu Y, Hauser RA, Freeman TB, Olanow CW (2008a) Lewy body-like pathology in long-term embryonic nigral transplants in Parkinson's disease. *Nat Med*, 14:504–506.
- Kordower JH, Chu Y, Hauser RA, Olanow CW, Freeman TB (2008b) Transplanted dopaminergic neurons develop PD pathologic changes: a second case report. *Mov Disord*, 23:2303–2306.
- Koroglu C, Baysal L, Cetinkaya M, Karasoy H, Tolun A (2013) DNAJC6 is responsible for juvenile parkinsonism with phenotypic variability. *Parkinsonism Relat Disord*, 19:320–324.
- Krebs CE, Karkheiran S, Powell JC, Cao M, Makarov V, Darvish H, Di Paolo G, Walker RH, Shahidi GA, Buxbaum JD, De Camilli P, Yue Z, Paisan-Ruiz C (2013) The Sac1 domain of SYNJ1 identified mutated in a family with early-onset progressive Parkinsonism with generalized seizures. *Hum Mutat*, 34:1200–1207.
- Kruer MC, Hiken M, Gregory A, Malandrini A, Clark D, Hogarth P, Grafe M, Hayflick SJ, Woltjer RL (2011) Novel histopathologic findings in molecularly-confirmed pantothenate kinase-associated neurodegeneration. *Brain*, 134:947–958.
- Kruger R, Kuhn W, Muller T, Woitalla D, Graeber M, Kosel S, Przuntek H, Epplen JT, Schols L, Riess O (1998) Ala30Pro mutation in the gene encoding alpha-synuclein in Parkinson's disease. *Nat Genet*, 18:106–108.
- Lambert JC et al. (2009) Genome-wide association study identifies variants at CLU and CR1 associated with Alzheimer's disease. *Nat Genet*, 41:1094–1099.
- Langston JW, Ballard P, Tetrud JW, Irwin I (1983) Chronic Parkinsonism in humans due to a product of meperidine-analog synthesis. *Science*, 219:979–980.
- Law BM, Spain VA, Leinster VH, Chia R, Beilina A, Cho HJ, Taymans JM, Urban MK, Sancho RM, Ramirez MB, Biskup S, Baekelandt V, Cai H, Cookson MR, Berwick DC, Harvey K (2014) A Direct Interaction between Leucine-rich Repeat Kinase 2 and Specific beta-Tubulin Isoforms Regulates Tubulin Acetylation. *J Biol Chem*, 289:895–908.
- Lawrence A, Bouwer JC, Perkins G, Ellisman MH (2006) Transform-based backprojection for volume reconstruction of large format electron microscope tilt series. *J Struct Biol*, 154:144–167.
- Lazarou M, Jin SM, Kane LA, Youle RJ (2012) Role of PINK1 binding to the TOM complex and alternate intracellular membranes in recruitment and activation of the E3 ligase Parkin. *Dev Cell*, 22:320–333.
- Lee BD, Shin JH, VanKampen J, Petrucelli L, West AB, Ko HS, Lee YI, Maguire-Zeiss KA, Bowers WJ, Federoff HJ, Dawson VL, Dawson TM (2010) Inhibitors of leucine-rich repeat kinase-2 protect against models of Parkinson's disease. *Nat Med*, 16:998–1000.

- Lee HJ, Cho ED, Lee KW, Kim JH, Cho SG, Lee SJ (2013) Autophagic failure promotes the exocytosis and intercellular transfer of alpha-synuclein. *Exp Mol Med*, 45:e22.
- Lee HJ, Patel S, Lee SJ (2005) Intravesicular localization and exocytosis of alpha-synuclein and its aggregates. *J Neurosci*, 25:6016–6024.
- Lee HJ, Suk JE, Bae EJ, Lee SJ (2008) Clearance and deposition of extracellular alpha-synuclein aggregates in microglia. *Biochem Biophys Res Commun*, 372:423–428.
- Lee MK, Stirling W, Xu Y, Xu X, Qui D, Mandir AS, Dawson TM, Copeland NG, Jenkins NA, Price DL (2002) Human alpha-synuclein-harboring familial Parkinson's disease-linked Ala-53 --> Thr mutation causes neurodegenerative disease with alpha-synuclein aggregation in transgenic mice. *Proc Natl Acad Sci U S A*, 99:8968–8973.
- Lee VM, Trojanowski JQ (2006) Mechanisms of Parkinson's disease linked to pathological alpha-synuclein: new targets for drug discovery. *Neuron*, 52:33–38.
- Lees AJ, Hardy J, Revesz T (2009) Parkinson's disease. *Lancet*, 373:2055–2066.
- Leroy E, Boyer R, Auburger G, Leube B, Ulm G, Mezey E, Harta G, Brownstein MJ, Jonnalagada S, Chernova T, Dehejia A, Lavedan C, Gasser T, Steinbach PJ, Wilkinson KD, Polymeropoulos MH (1998) The ubiquitin pathway in Parkinson's disease. *Nature*, 395(6701):451–452.
- Lesage S, Durr A, Tazir M, Lohmann E, Leutenegger AL, Janin S, Pollak P, Brice A (2006) LRRK2 G2019S as a cause of Parkinson's disease in North African Arabs. *N Engl J Med*, 354(4):422–423.
- Lesage S, Leutenegger AL, Ibanez P, Janin S, Lohmann E, Durr A, Brice A (2005) LRRK2 haplotype analyses in European and North African families with Parkinson disease: a common founder for the G2019S mutation dating from the 13th century. *Am J Hum Genet*, 77:330–332.
- Li A, Paudel R, Johnson R, Courtney R, Lees AJ, Holton JL, Hardy J, Revesz T, Houlden H (2012a) Pantothenate kinase-associated neurodegeneration is not a synucleinopathy. *Neuropathol Appl Neurobiol*,
- Li J, Kanekiyo T, Shinohara M, Zhang Y, LaDu MJ, Xu H, Bu G (2012b) Differential regulation of amyloid-beta endocytic trafficking and lysosomal degradation by apolipoprotein E isoforms. *J Biol Chem*, 287:44593–44601.
- Li JY, Englund E, Holton JL, Soulet D, Hagell P, Lees AJ, Lashley T, Quinn NP, Rehncrona S, Bjorklund A, Widner H, Revesz T, Lindvall O, Brundin P (2008) Lewy bodies in grafted neurons in subjects with Parkinson's disease suggest host-to-graft disease propagation. *Nat Med*, 14:501–503.
- Li Y, Liu W, Oo TF, Wang L, Tang Y, Jackson-Lewis V, Zhou C, Geghman K, Bogdanov M, Przedborski S, Beal MF, Burke RE, Li C (2009) Mutant LRRK2(R1441G) BAC transgenic mice recapitulate cardinal features of Parkinson's disease. *Nat Neurosci*, 12:826–828.
- Lin CH, Tsai PI, Wu RM, Chien CT (2010) LRRK2 G2019S mutation induces dendrite degeneration through mislocalization and phosphorylation of tau by recruiting autoactivated GSK3ss. *J Neurosci*, 30:13138–13149.
- Liu J, Zhang JP, Shi M, Quinn T, Bradner J, Beyer R, Chen S, Zhang J (2009) Rab11a and HSP90 regulate recycling of extracellular alpha-synuclein. *J Neurosci*, 29:1480–1485.
- Lo Bianco C, Ridet JL, Schneider BL, Deglon N, Aebischer P (2002) alpha-Synucleinopathy and selective dopaminergic neuron loss in a rat lentiviral-based model of Parkinson's disease. *Proc Natl Acad Sci U S A*, 99:10813–10818.

- Lucking CB, Durr A, Bonifati V, Vaughan J, De Michele G, Gasser T, Harhangi BS, Meco G, Deneffe P, Wood NW, Agid Y, Brice A (2000) Association between early-onset Parkinson's disease and mutations in the parkin gene. *N Engl J Med*, 342:1560–1567.
- Luerman GC, Nguyen C, Samaroo H, Loos P, Xi H, Hurtado-Lorenzo A, Needle E, Stephen Noell G, Galatsis P, Dunlop J, Geoghegan KF, Hirst WD (2013) Phosphoproteomic evaluation of pharmacological inhibition of leucine-rich repeat kinase 2 reveals significant off-target effects of LRRK2-IN-1. *J Neurochem*,
- Luk KC, Kehm V, Carroll J, Zhang B, O'Brien P, Trojanowski JQ, Lee VM (2012a) Pathological alpha-synuclein transmission initiates Parkinson-like neurodegeneration in nontransgenic mice. *Science*, 338:949–953.
- Luk KC, Kehm VM, Zhang B, O'Brien P, Trojanowski JQ, Lee VM (2012b) Intracerebral inoculation of pathological alpha-synuclein initiates a rapidly progressive neurodegenerative alpha-synucleinopathy in mice. *J Exp Med*, 209:975–986.
- Luk KC, Song C, O'Brien P, Stieber A, Branch JR, Brunden KR, Trojanowski JQ, Lee VM (2009) Exogenous alpha-synuclein fibrils seed the formation of Lewy body-like intracellular inclusions in cultured cells. *Proc Natl Acad Sci U S A*, 106:20051–20056.
- Lutz AK, Exner N, Fett ME, Schlehe JS, Kloos K, Lammermann K, Brunner B, Kurz-Drexler A, Vogel F, Reichert AS, Bouman L, Vogt-Weisenhorn D, Wurst W, Tatzelt J, Haass C, Winklhofer KF (2009) Loss of parkin or PINK1 function increases Drp1-dependent mitochondrial fragmentation. *J Biol Chem*, 284:22938–22951.
- Lwin A, Orvisky E, Goker-Alpan O, LaMarca ME, Sidransky E (2004) Glucocerebrosidase mutations in subjects with parkinsonism. *Mol Genet Metab*, 81:70–73.
- Lynch T, Sano M, Marder KS, Bell KL, Foster NL, Defendini RF, Sima AA, Keohane C, Nygaard TG, Fahn S, et al (1994) Clinical characteristics of a family with chromosome 17-linked disinhibition-dementia-parkinsonism-amyotrophy complex. *Neurology*, 44:1878–1884.
- Macauley SL, Wozniak DF, Kielar C, Tan Y, Cooper JD, Sands MS (2009) Cerebellar pathology and motor deficits in the palmitoyl protein thioesterase 1-deficient mouse. *Exp Neurol*, 217:124–135.
- MacLeod D, Dowman J, Hammond R, Leete T, Inoue K, Abeliovich A (2006) The familial Parkinsonism gene LRRK2 regulates neurite process morphology. *Neuron*, 52:587–593.
- MacLeod DA, Rhinn H, Kuwahara T, Zolin A, Di Paolo G, McCabe BD, Marder KS, Honig LS, Clark LN, Small SA, Abeliovich A (2013) RAB7L1 interacts with LRRK2 to modify intraneuronal protein sorting and Parkinson's disease risk. *Neuron*, 77:425–439.
- Mailloux RJ, Xuan JY, Beauchamp B, Jui L, Lou M, Harper ME (2013) Glutaredoxin-2 is required to control proton leak through uncoupling protein-3. *J Biol Chem*, 288:8365–8379.
- Mani M, Lee SY, Lucast L, Cremona O, Di Paolo G, De Camilli P, Ryan TA (2007) The dual phosphatase activity of synaptojanin1 is required for both efficient synaptic vesicle endocytosis and reavailability at nerve terminals. *Neuron*, 56:1004–1018.
- Martinez-Vicente M, Tallozy Z, Kaushik S, Massey AC, Mazzulli J, Mosharov EV, Hodara R, Fredenburg R, Wu DC, Follenzi A, Dauer W, Przedborski S, Ischiropoulos H, Lansbury PT, Sulzer D, Cuervo AM (2008) Dopamine-modified alpha-synuclein blocks chaperone-mediated autophagy. *J Clin Invest*, 118:777–788.

- Masliah E, Rockenstein E, Veinbergs I, Mallory M, Hashimoto M, Takeda A, Sagara Y, Sisk A, Mucke L (2000) Dopaminergic loss and inclusion body formation in alpha-synuclein mice: implications for neurodegenerative disorders. *Science*, 287:1265–1269.
- Mata IF, Kachergus JM, Taylor JP, Lincoln S, Aasly J, Lynch T, Hulihan MM, Cobb SA, Wu RM, Lu CS, Lahoz C, Wszolek ZK, Farrer MJ (2005) Lrrk2 pathogenic substitutions in Parkinson's disease. *Neurogenetics*, 6:171–177.
- Mata IF, Samii A, Schneer SH, Roberts JW, Griffith A, Leis BC, Schellenberg GD, Sidransky E, Bird TD, Leverenz JB, Tsuang D, Zabetian CP (2008) Glucocerebrosidase gene mutations: a risk factor for Lewy body disorders. *Arch Neurol*, 65:379–382.
- Matsuda N, Sato S, Shiba K, Okatsu K, Saisho K, Gautier CA, Sou YS, Saiki S, Kawajiri S, Sato F, Kimura M, Komatsu M, Hattori N, Tanaka K (2010) PINK1 stabilized by mitochondrial depolarization recruits Parkin to damaged mitochondria and activates latent Parkin for mitophagy. *J Cell Biol*, 189:211–221.
- Mazzulli JR, Xu YH, Sun Y, Knight AL, McLean PJ, Caldwell GA, Sidransky E, Grabowski GA, Krainc D (2011) Gaucher disease glucocerebrosidase and alpha-synuclein form a bidirectional pathogenic loop in synucleinopathies. *Cell*, 146:37–52.
- McIntire LB, Berman DE, Myaeng J, Staniszewski A, Arancio O, Di Paolo G, Kim TW (2012) Reduction of synaptojanin 1 ameliorates synaptic and behavioral impairments in a mouse model of Alzheimer's disease. *J Neurosci*, 32:15271–15276.
- McKinney BC, Murphy GG (2006) The L-Type voltage-gated calcium channel Cav1.3 mediates consolidation, but not extinction, of contextually conditioned fear in mice. *Learn Mem*, 13:584–589.
- McMahon HT, Boucrot E (2011) Molecular mechanism and physiological functions of clathrin-mediated endocytosis. *Nat Rev Mol Cell Biol*, 12:517–533.
- Miller DW, Hague SM, Clarimon J, Baptista M, Gwinn-Hardy K, Cookson MR, Singleton AB (2004) Alpha-synuclein in blood and brain from familial Parkinson disease with SNCA locus triplication. *Neurology*, 62:1835–1838.
- Morgan NV et al. (2006) PLA2G6, encoding a phospholipase A2, is mutated in neurodegenerative disorders with high brain iron. *Nat Genet*, 38:752–754.
- Muenter MD, Forno LS, Hornykiewicz O, Kish SJ, Maraganore DM, Caselli RJ, Okazaki H, Howard FMJ, Snow BJ, Calne DB (1998) Hereditary form of parkinsonism--dementia. *Ann Neurol*, 43:768–781.
- Muppidi JR, Lobito AA, Ramaswamy M, Yang JK, Wang L, Wu H, Siegel RM (2006) Homotypic FADD interactions through a conserved RXDLL motif are required for death receptor-induced apoptosis. *Cell Death Differ*, 13:1641–1650.
- Najim al-Din AS, Wriekat A, Mubaidin A, Dasouki M, Hiari M (1994) Pallido-pyramidal degeneration, supranuclear upgaze paresis and dementia: Kufor-Rakeb syndrome. *Acta Neurol Scand*, 89:347–352.
- Nakamura K, Nemani VM, Azarbal F, Skibinski G, Levy JM, Egami K, Munishkina L, Zhang J, Gardner B, Wakabayashi J, Sesaki H, Cheng Y, Finkbeiner S, Nussbaum RL, Masliah E, Edwards RH (2011) Direct membrane association drives mitochondrial fission by the Parkinson disease-associated protein alpha-synuclein. *J Biol Chem*, 286:20710–20726.
- Narendra DP, Jin SM, Tanaka A, Suen DF, Gautier CA, Shen J, Cookson MR, Youle RJ (2010) PINK1 is selectively stabilized on impaired mitochondria to activate Parkin. *PLoS Biol*, 8:e1000298.

- Nemani VM, Lu W, Berge V, Nakamura K, Onoa B, Lee MK, Chaudhry FA, Nicoll RA, Edwards RH (2010) Increased expression of alpha-synuclein reduces neurotransmitter release by inhibiting synaptic vesicle reclustering after endocytosis. *Neuron*, 65:66–79.
- Neumann J, Bras J, Deas E, O’Sullivan SS, Parkkinen L, Lachmann RH, Li A, Holton J, Guerreiro R, Paudel R, Segarane B, Singleton A, Lees A, Hardy J, Houlden H, Revesz T, Wood NW (2009) Glucocerebrosidase mutations in clinical and pathologically proven Parkinson’s disease. *Brain*, 132:1783–1794.
- Ng EL, Tang BL (2008) Rab GTPases and their roles in brain neurons and glia. *Brain Res Rev*, 58:236–246.
- Nichols WC, Pankratz N, Marek DK, Pauciulo MW, Elsaesser VE, Halter CA, Rudolph A, Wojcieszek J, Pfeiffer RF, Foroud T (2009) Mutations in GBA are associated with familial Parkinson disease susceptibility and age at onset. *Neurology*, 72:310–316.
- Ning YP, Kanai K, Tomiyama H, Li Y, Funayama M, Yoshino H, Sato S, Asahina M, Kuwabara S, Takeda A, Hattori T, Mizuno Y, Hattori N (2008) PARK9-linked parkinsonism in eastern Asia: mutation detection in ATP13A2 and clinical phenotype. *Neurology*, 70:1491–1493.
- Nishioka K, Hayashi S, Farrer MJ, Singleton AB, Yoshino H, Imai H, Kitami T, Sato K, Kuroda R, Tomiyama H, Mizoguchi K, Murata M, Toda T, Imoto I, Inazawa J, Mizuno Y, Hattori N (2006) Clinical heterogeneity of alpha-synuclein gene duplication in Parkinson’s disease. *Ann Neurol*, 59:298–309.
- Nonaka T, Watanabe ST, Iwatsubo T, Hasegawa M (2010) Seeded aggregation and toxicity of {alpha}-synuclein and tau: cellular models of neurodegenerative diseases. *J Biol Chem*, 285:34885–34898.
- Orenstein SJ, Kuo SH, Tasset I, Arias E, Koga H, Fernandez-Carasa I, Cortes E, Honig LS, Dauer W, Consiglio A, Raya A, Sulzer D, Cuervo AM (2013) Interplay of LRRK2 with chaperone-mediated autophagy. *Nat Neurosci*, 16:394–406.
- Osellame LD, Rahim AA, Hargreaves IP, Gegg ME, Richard-Londt A, Brandner S, Waddington SN, Schapira AH, Duchon MR (2013) Mitochondria and quality control defects in a mouse model of Gaucher disease--links to Parkinson’s disease. *Cell Metab*, 17:941–953.
- Ozelius LJ, Senthil G, Saunders-Pullman R, Ohmann E, Deligtisch A, Tagliati M, Hunt AL, Klein C, Henick B, Hailpern SM, Lipton RB, Soto-Valencia J, Risch N, Bressman SB (2006) LRRK2 G2019S as a cause of Parkinson’s disease in Ashkenazi Jews. *N Engl J Med*, 354(4):424–425.
- Paisan-Ruiz C, Bhatia KP, Li A, Hernandez D, Davis M, Wood NW, Hardy J, Houlden H, Singleton A, Schneider SA (2009) Characterization of PLA2G6 as a locus for dystonia-parkinsonism. *Ann Neurol*, 65:19–23.
- Paisan-Ruiz C, Guevara R, Federoff M, Hanagasi H, Sina F, Elahi E, Schneider SA, Schwingenschuh P, Bajaj N, Emre M, Singleton AB, Hardy J, Bhatia KP, Brandner S, Lees AJ, Houlden H (2010) Early-onset L-dopa-responsive parkinsonism with pyramidal signs due to ATP13A2, PLA2G6, FBXO7 and spatacsin mutations. *Mov Disord*, 25:1791–1800.
- Paisan-Ruiz C et al. (2004) Cloning of the gene containing mutations that cause PARK8-linked Parkinson’s disease. *Neuron*, 44:595–600.
- Paisan-Ruiz C, Li A, Schneider SA, Holton JL, Johnson R, Kidd D, Chataway J, Bhatia KP, Lees AJ, Hardy J, Revesz T, Houlden H (2012) Widespread Lewy body and tau accumulation

- in childhood and adult onset dystonia-parkinsonism cases with PLA2G6 mutations. *Neurobiol Aging*, 33:814–823.
- Palmer DN, Barry LA, Tyynela J, Cooper JD (2013) NCL disease mechanisms. *Biochim Biophys Acta*, 1832:1882–1893.
- Papapetropoulos S, Paschalis C, Athanassiadou A, Papadimitriou A, Ellul J, Polymeropoulos MH, Papapetropoulos T (2001) Clinical phenotype in patients with alpha-synuclein Parkinson's disease living in Greece in comparison with patients with sporadic Parkinson's disease. *J Neurol Neurosurg Psychiatry*, 70:662–665.
- Parisiadou L, Xie C, Cho HJ, Lin X, Gu XL, Long CX, Lobbstaël E, Baekelandt V, Taymans JM, Sun L, Cai H (2009) Phosphorylation of ezrin/radixin/moesin proteins by LRRK2 promotes the rearrangement of actin cytoskeleton in neuronal morphogenesis. *J Neurosci*, 29:13971–13980.
- Park J, Chen Y, Tishkoff DX, Peng C, Tan M, Dai L, Xie Z, Zhang Y, Zwaans BM, Skinner ME, Lombard DB, Zhao Y (2013) SIRT5-mediated lysine desuccinylation impacts diverse metabolic pathways. *Mol Cell*, 50:919–930.
- Park J, Lee SB, Lee S, Kim Y, Song S, Kim S, Bae E, Kim J, Shong M, Kim JM, Chung J (2006) Mitochondrial dysfunction in Drosophila PINK1 mutants is complemented by parkin. *Nature*, 441(7097):1157–1161.
- Park JS, Koentjoro B, Veivers D, Mackay-Sim A, Sue CM (2014) Parkinson's disease-associated human ATP13A2 (PARK9) deficiency causes zinc dyshomeostasis and mitochondrial dysfunction. *Hum Mol Genet*,
- Park JS, Mehta P, Cooper AA, Veivers D, Heimbach A, Stiller B, Kubisch C, Fung VS, Krainc D, Mackay-Sim A, Sue CM (2011) Pathogenic effects of novel mutations in the P-type ATPase ATP13A2 (PARK9) causing Kufor-Rakeb syndrome, a form of early-onset parkinsonism. *Hum Mutat*, 32:956–964.
- Petrucelli L, O'Farrell C, Lockhart PJ, Baptista M, Kehoe K, Vink L, Choi P, Wolozin B, Farrer M, Hardy J, Cookson MR (2002) Parkin protects against the toxicity associated with mutant alpha-synuclein: proteasome dysfunction selectively affects catecholaminergic neurons. *Neuron*, 36:1007–1019.
- Plowey ED, Cherra SJ, Liu YJ, Chu CT (2008) Role of autophagy in G2019S-LRRK2-associated neurite shortening in differentiated SH-SY5Y cells. *J Neurochem*, 105:1048–1056.
- Podhajski A, Musso A, Trancikova A, Stafa K, Moser R, Sonnay S, Glauser L, Moore DJ (2012) Common pathogenic effects of missense mutations in the P-type ATPase ATP13A2 (PARK9) associated with early-onset parkinsonism. *PLoS One*, 7:e39942.
- Polymeropoulos MH, Lavedan C, Leroy E, Ide SE, Dehejia A, Dutra A, Pike B, Root H, Rubenstein J, Boyer R, Stenroos ES, Chandrasekharappa S, Athanassiadou A, Papapetropoulos T, Johnson WG, Lazzarini AM, Duvoisin RC, Di Iorio G, Golbe LI, Nussbaum RL (1997) Mutation in the alpha-synuclein gene identified in families with Parkinson's disease. *Science*, 276:2045–2047.
- Poulopoulos M, Levy OA, Alcalay RN (2012) The neuropathology of genetic Parkinson's disease. *Mov Disord*, 27:831–842.
- Pramstaller PP, Schlossmacher MG, Jacques TS, Scaravilli F, Eskelson C, Pepivani I, Hedrich K, Adel S, Gonzales-McNeal M, Hilker R, Kramer PL, Klein C (2005) Lewy body Parkinson's disease in a large pedigree with 77 Parkin mutation carriers. *Ann Neurol*, 58:411–422.

- Puschmann A, Englund E, Ross OA, Vilarino-Guell C, Lincoln SJ, Kachergus JM, Cobb SA, Tornqvist AL, Rehncrona S, Widner H, Wszolek ZK, Farrer MJ, Nilsson C (2012) First neuropathological description of a patient with Parkinson's disease and LRRK2 p.N1437H mutation. *Parkinsonism Relat Disord*, 18:332–338.
- Qiao L et al. (2008) Lysosomal enzyme cathepsin D protects against alpha-synuclein aggregation and toxicity. *Mol Brain*, 1:17.
- Quadri M, Fang M, Picillo M, Olgiati S, Breedveld GJ, Graafland J, Wu B, Xu F, Erro R, Amboni M, Pappata S, Quarantelli M, Annesi G, Quattrone A, Chien HF, Barbosa ER, Oostra BA, Barone P, Wang J, Bonifati V (2013) Mutation in the SYNJ1 gene associated with autosomal recessive, early-onset Parkinsonism. *Hum Mutat*, 34:1208–1215.
- Rademakers R et al. (2007) Phenotypic variability associated with progranulin haploinsufficiency in patients with the common 1477C-->T (Arg493X) mutation: an international initiative. *Lancet Neurol*, 6:857–868.
- Ragothaman M, Sarangmath N, Chaudhary S, Khare V, Mittal U, Sharma S, Komatireddy S, Chakrabarti S, Mukerji M, Juyal RC, Thelma BK, Muthane UB (2004) Complex phenotypes in an Indian family with homozygous SCA2 mutations. *Ann Neurol*, 55:130–133.
- Ramirez A, Heimbach A, Grundemann J, Stiller B, Hampshire D, Cid LP, Goebel I, Mubaidin AF, Wriekat AL, Roeper J, Al-Din A, Hillmer AM, Karsak M, Liss B, Woods CG, Behrens MI, Kubisch C (2006) Hereditary parkinsonism with dementia is caused by mutations in ATP13A2, encoding a lysosomal type 5 P-type ATPase. *Nat Genet*, 38:1184–1191.
- Rappley I, Myers DS, Milne SB, Ivanova PT, Lavoie MJ, Brown HA, Selkoe DJ (2009) Lipidomic profiling in mouse brain reveals differences between ages and genders, with smaller changes associated with alpha-synuclein genotype. *J Neurochem*, 111:15–25.
- Renoux AJ, Todd PK (2012) Neurodegeneration the RNA way. *Prog Neurobiol*, 97:173–189.
- Riis RC, Cummings JF, Loew ER, de Lahunta A (1992) Tibetan terrier model of canine ceroid lipofuscinosis. *Am J Med Genet*, 42:615–621.
- Saiki M, Baker A, Williams-Gray CH, Foltynie T, Goodman RS, Taylor CJ, Compston DA, Barker RA, Sawcer SJ, Goris A (2010) Association of the human leucocyte antigen region with susceptibility to Parkinson's disease. *J Neurol Neurosurg Psychiatry*, 81:890–891.
- Samaranch L, Lorenzo-Betancor O, Arbelo JM, Ferrer I, Lorenzo E, Irigoyen J, Pastor MA, Marrero C, Isla C, Herrera-Henriquez J, Pastor P (2010) PINK1-linked parkinsonism is associated with Lewy body pathology. *Brain*, 133:1128–1142.
- Santoro L, Breedveld GJ, Manganeli F, Iodice R, Pisciotta C, Nolano M, Punzo F, Quarantelli M, Pappata S, Di Fonzo A, Oostra BA, Bonifati V (2011) Novel ATP13A2 (PARK9) homozygous mutation in a family with marked phenotype variability. *Neurogenetics*, 12:33–39.
- Satake W et al. (2009) Genome-wide association study identifies common variants at four loci as genetic risk factors for Parkinson's disease. *Nat Genet*, 41:1303–1307.
- Schneider SA, Paisan-Ruiz C, Quinn NP, Lees AJ, Houlden H, Hardy J, Bhatia KP (2010) ATP13A2 mutations (PARK9) cause neurodegeneration with brain iron accumulation. *Mov Disord*, 25:979–984.

- Schultheis PJ et al. (2013) Atp13a2-deficient mice exhibit neuronal ceroid lipofuscinosis, limited alpha-synuclein accumulation and age-dependent sensorimotor deficits. *Hum Mol Genet*, 22:2067–2082.
- Schultheis PJ, Hagen TT, O'Toole KK, Tachibana A, Burke CR, McGill DL, Okunade GW, Shull GE (2004) Characterization of the P5 subfamily of P-type transport ATPases in mice. *Biochem Biophys Res Commun*, 323:731–738.
- Scott D, Roy S (2012) alpha-Synuclein inhibits intersynaptic vesicle mobility and maintains recycling-pool homeostasis. *J Neurosci*, 32:10129–10135.
- Sekine T, Kagaya H, Funayama M, Li Y, Yoshino H, Tomiyama H, Hattori N (2010) Clinical course of the first Asian family with Parkinsonism related to SNCA triplication. *Mov Disord*, 25:2871–2875.
- Sevlever D, Jiang P, Yen SH (2008) Cathepsin D is the main lysosomal enzyme involved in the degradation of alpha-synuclein and generation of its carboxy-terminally truncated species. *Biochemistry*, 47:9678–9687.
- Shan DE, Soong BW, Sun CM, Lee SJ, Liao KK, Liu RS (2001) Spinocerebellar ataxia type 2 presenting as familial levodopa-responsive parkinsonism. *Ann Neurol*, 50:812–815.
- Sharma M et al. (2012) A multi-centre clinico-genetic analysis of the VPS35 gene in Parkinson disease indicates reduced penetrance for disease-associated variants. *J Med Genet*, 49:721–726.
- Sharon R, Bar-Joseph I, Mirick GE, Serhan CN, Selkoe DJ (2003) Altered fatty acid composition of dopaminergic neurons expressing alpha-synuclein and human brains with alpha-synucleinopathies. *J Biol Chem*, 278:49874–49881.
- Sharon R, Goldberg MS, Bar-Josef I, Betensky RA, Shen J, Selkoe DJ (2001) alpha-Synuclein occurs in lipid-rich high molecular weight complexes, binds fatty acids, and shows homology to the fatty acid-binding proteins. *Proc Natl Acad Sci U S A*, 98:9110–9115.
- Shin N, Jeong H, Kwon J, Heo HY, Kwon JJ, Yun HJ, Kim CH, Han BS, Tong Y, Shen J, Hatano T, Hattori N, Kim KS, Chang S, Seol W (2008) LRRK2 regulates synaptic vesicle endocytosis. *Exp Cell Res*, 314:2055–2065.
- Shojaee S, Sina F, Banihosseini SS, Kazemi MH, Kalhor R, Shahidi GA, Fakhrai-Rad H, Ronaghi M, Elahi E (2008) Genome-wide linkage analysis of a Parkinsonian-pyramidal syndrome pedigree by 500 K SNP arrays. *Am J Hum Genet*, 82:1375–1384.
- Sidransky E, Lopez G (2012) The link between the GBA gene and parkinsonism. *Lancet Neurol*, 11:986–998.
- Sidransky E et al. (2009) Multicenter analysis of glucocerebrosidase mutations in Parkinson's disease. *N Engl J Med*, 361:1651–1661.
- Siegel RM, Martin DA, Zheng L, Ng SY, Bertin J, Cohen J, Lenardo MJ (1998) Death-effector filaments: novel cytoplasmic structures that recruit caspases and trigger apoptosis. *J Cell Biol*, 141:1243–1253.
- Simon-Sanchez J et al. (2009) Genome-wide association study reveals genetic risk underlying Parkinson's disease. *Nat Genet*, 41:1308–1312.
- Singh R, Kaushik S, Wang Y, Xiang Y, Novak I, Komatsu M, Tanaka K, Cuervo AM, Czaja MJ (2009) Autophagy regulates lipid metabolism. *Nature*, 458:1131–1135.
- Singleton AB et al. (2003) alpha-Synuclein locus triplication causes Parkinson's disease. *Science*, 302:841.

- Skibinski G, Nakamura K, Cookson MR, Finkbeiner S (2014) Mutant LRRK2 Toxicity in Neurons Depends on LRRK2 Levels and Synuclein But Not Kinase Activity or Inclusion Bodies. *J Neurosci*, 34:418–433.
- Sleat DE, Wiseman JA, El-Banna M, Kim KH, Mao Q, Price S, Macauley SL, Sidman RL, Shen MM, Zhao Q, Passini MA, Davidson BL, Stewart GR, Lobel P (2004) A mouse model of classical late-infantile neuronal ceroid lipofuscinosis based on targeted disruption of the CLN2 gene results in a loss of tripeptidyl-peptidase I activity and progressive neurodegeneration. *J Neurosci*, 24:9117–9126.
- Small SA, Gandy S (2006) Sorting through the cell biology of Alzheimer’s disease: intracellular pathways to pathogenesis. *Neuron*, 52:15–31.
- Small SA, Kent K, Pierce A, Leung C, Kang MS, Okada H, Honig L, Vonsattel JP, Kim TW (2005) Model-guided microarray implicates the retromer complex in Alzheimer’s disease. *Ann Neurol*, 58:909–919.
- Smith WW, Pei Z, Jiang H, Dawson VL, Dawson TM, Ross CA (2006) Kinase activity of mutant LRRK2 mediates neuronal toxicity. *Nat Neurosci*, 9:1231–1233.
- Smith WW, Pei Z, Jiang H, Moore DJ, Liang Y, West AB, Dawson VL, Dawson TM, Ross CA (2005) Leucine-rich repeat kinase 2 (LRRK2) interacts with parkin, and mutant LRRK2 induces neuronal degeneration. *Proc Natl Acad Sci U S A*, 102:18676–18681.
- Song DD, Shults CW, Sisk A, Rockenstein E, Masliah E (2004) Enhanced substantia nigra mitochondrial pathology in human alpha-synuclein transgenic mice after treatment with MPTP. *Exp Neurol*, 186:158–172.
- Soper JH, Kehm V, Burd CG, Bankaitis VA, Lee VM (2011) Aggregation of alpha-synuclein in *S. cerevisiae* is associated with defects in endosomal trafficking and phospholipid biosynthesis. *J Mol Neurosci*, 43:391–405.
- Spillantini MG, Crowther RA, Jakes R, Hasegawa M, Goedert M (1998) alpha-Synuclein in filamentous inclusions of Lewy bodies from Parkinson’s disease and dementia with lewy bodies. *Proc Natl Acad Sci U S A*, 95:6469–6473.
- Spillantini MG, Schmidt ML, Lee VM, Trojanowski JQ, Jakes R, Goedert M (1997) Alpha-synuclein in Lewy bodies. *Nature*, 388(6645):839–840.
- Stenmark H (2009) Rab GTPases as coordinators of vesicle traffic. *Nat Rev Mol Cell Biol*, 10:513–525.
- Subramony SH, Hernandez D, Adam A, Smith-Jefferson S, Hussey J, Gwinn-Hardy K, Lynch T, McDaniel O, Hardy J, Farrer M, Singleton A (2002) Ethnic differences in the expression of neurodegenerative disease: Machado-Joseph disease in Africans and Caucasians. *Mov Disord*, 17:1068–1071.
- Sung JY, Kim J, Paik SR, Park JH, Ahn YS, Chung KC (2001) Induction of neuronal cell death by Rab5A-dependent endocytosis of alpha-synuclein. *J Biol Chem*, 276:27441–27448.
- Surmeier DJ, Guzman JN, Sanchez J, Schumacker PT (2012) Physiological phenotype and vulnerability in Parkinson’s disease. *Cold Spring Harb Perspect Med*, 2:a009290.
- Tan J, Zhang T, Jiang L, Chi J, Hu D, Pan Q, Wang D, Zhang Z (2011) Regulation of intracellular manganese homeostasis by Kufor-Rakeb syndrome-associated ATP13A2 protein. *J Biol Chem*, 286:29654–29662.
- Tanik SA, Schultheiss CE, Volpicelli-Daley LA, Brunden KR, Lee VM (2013) Lewy body-like alpha-synuclein aggregates resist degradation and impair macroautophagy. *J Biol Chem*, 288:15194–15210.

- Thomas KJ, McCoy MK, Blackinton J, Beilina A, van der Brug M, Sandebring A, Miller D, Maric D, Cedazo-Minguez A, Cookson MR (2011) DJ-1 acts in parallel to the PINK1/parkin pathway to control mitochondrial function and autophagy. *Hum Mol Genet*, 20:40–50.
- Tieu K, Perier C, Caspersen C, Teismann P, Wu DC, Yan SD, Naini A, Vila M, Jackson-Lewis V, Ramasamy R, Przedborski S (2003) D-beta-hydroxybutyrate rescues mitochondrial respiration and mitigates features of Parkinson disease. *J Clin Invest*, 112:892–901.
- Tong Y, Giaime E, Yamaguchi H, Ichimura T, Liu Y, Si H, Cai H, Bonventre JV, Shen J (2012) Loss of leucine-rich repeat kinase 2 causes age-dependent bi-phasic alterations of the autophagy pathway. *Mol Neurodegener*, 7:2.
- Tong Y, Yamaguchi H, Giaime E, Boyle S, Kopan R, Kelleher RJ, Shen J (2010) Loss of leucine-rich repeat kinase 2 causes impairment of protein degradation pathways, accumulation of alpha-synuclein, and apoptotic cell death in aged mice. *Proc Natl Acad Sci U S A*, 107:9879–9884.
- Tsunemi T, Krainc D (2013) Zn²⁺ dyshomeostasis caused by loss of ATP13A2/PARK9 leads to lysosomal dysfunction and alpha-synuclein accumulation. *Hum Mol Genet*,
- Ungewickell E, Ungewickell H, Holstein SE, Lindner R, Prasad K, Barouch W, Martin B, Greene LE, Eisenberg E (1995) Role of auxilin in uncoating clathrin-coated vesicles. *Nature*, 378:632–635.
- Usenovic M, Tresse E, Mazzulli JR, Taylor JP, Krainc D (2012) Deficiency of ATP13A2 leads to lysosomal dysfunction, alpha-synuclein accumulation, and neurotoxicity. *J Neurosci*, 32:4240–4246.
- Uttenweiler A, Mayer A (2008) Microautophagy in the yeast *Saccharomyces cerevisiae*. *Methods Mol Biol*, 445:245–259.
- Valente EM et al. (2004) Hereditary early-onset Parkinson's disease caused by mutations in PINK1. *Science*, 304:1158–1160.
- van Swieten J, Spillantini MG (2007) Hereditary frontotemporal dementia caused by Tau gene mutations. *Brain Pathol*, 17:63–73.
- Vilarino-Guell C et al. (2013) DNAJC13 mutations in Parkinson disease. *Hum Mol Genet*,
- Vilarino-Guell C et al. (2011) VPS35 mutations in Parkinson disease. *Am J Hum Genet*, 89:162–167.
- Vitte J, Traver S, Maues De Paula A, Lesage S, Rovelli G, Corti O, Duyckaerts C, Brice A (2010) Leucine-rich repeat kinase 2 is associated with the endoplasmic reticulum in dopaminergic neurons and accumulates in the core of Lewy bodies in Parkinson disease. *J Neuropathol Exp Neurol*, 69:959–972.
- Vives-Bauza C, Zhou C, Huang Y, Cui M, de Vries RL, Kim J, May J, Tocilescu MA, Liu W, Ko HS, Magrane J, Moore DJ, Dawson VL, Grailhe R, Dawson TM, Li C, Tieu K, Przedborski S (2010) PINK1-dependent recruitment of Parkin to mitochondria in mitophagy. *Proc Natl Acad Sci U S A*, 107:378–383.
- Volpicelli-Daley LA, Luk KC, Patel TP, Tanik SA, Riddle DM, Stieber A, Meaney DF, Trojanowski JQ, Lee VM (2011) Exogenous alpha-synuclein fibrils induce Lewy body pathology leading to synaptic dysfunction and neuron death. *Neuron*, 72:57–71.
- Walkley SU, Suzuki K (2004) Consequences of NPC1 and NPC2 loss of function in mammalian neurons. *Biochim Biophys Acta*, 1685:48–62.

- Waxman EA, Giasson BI (2010) A novel, high-efficiency cellular model of fibrillar alpha-synuclein inclusions and the examination of mutations that inhibit amyloid formation. *J Neurochem*, 113:374–388.
- Webb JL, Ravikumar B, Atkins J, Skepper JN, Rubinsztein DC (2003) Alpha-Synuclein is degraded by both autophagy and the proteasome. *J Biol Chem*, 278:25009–25013.
- Weimer JM, Benedict JW, Getty AL, Pontikis CC, Lim MJ, Cooper JD, Pearce DA (2009) Cerebellar defects in a mouse model of juvenile neuronal ceroid lipofuscinosis. *Brain Res*, 1266:93–107.
- West AB, Moore DJ, Biskup S, Bugayenko A, Smith WW, Ross CA, Dawson VL, Dawson TM (2005) Parkinson's disease-associated mutations in leucine-rich repeat kinase 2 augment kinase activity. *Proc Natl Acad Sci U S A*, 102:16842–16847.
- West AB, Moore DJ, Choi C, Andrabi SA, Li X, Dikeman D, Biskup S, Zhang Z, Lim KL, Dawson VL, Dawson TM (2007) Parkinson's disease-associated mutations in LRRK2 link enhanced GTP-binding and kinase activities to neuronal toxicity. *Hum Mol Genet*, 16:223–232.
- Wider C, Dickson DW, Wszolek ZK (2010) Leucine-rich repeat kinase 2 gene-associated disease: redefining genotype-phenotype correlation. *Neurodegener Dis*, 7:175–179.
- Wilhelmsen KC, Lynch T, Pavlou E, Higgins M, Nygaard TG (1994) Localization of disinhibition-dementia-parkinsonism-amyotrophy complex to 17q21-22. *Am J Hum Genet*, 55:1159–1165.
- Williams DR, Hadeed A, al-Din AS, Wreikat AL, Lees AJ (2005) Kufor Rakeb disease: autosomal recessive, levodopa-responsive parkinsonism with pyramidal degeneration, supranuclear gaze palsy, and dementia. *Mov Disord*, 20:1264–1271.
- Willingham S, Outeiro TF, DeVit MJ, Lindquist SL, Muchowski PJ (2003) Yeast genes that enhance the toxicity of a mutant huntingtin fragment or alpha-synuclein. *Science*, 302:1769–1772.
- Winner B, Jappelli R, Maji SK, Desplats PA, Boyer L, Aigner S, Hetzer C, Loher T, Vilar M, Campioni S, Tzitzilonis C, Soragni A, Jessberger S, Mira H, Consiglio A, Pham E, Masliah E, Gage FH, Riek R (2011) In vivo demonstration that alpha-synuclein oligomers are toxic. *Proc Natl Acad Sci U S A*, 108:4194–4199.
- Winslow AR, Chen CW, Corrochano S, Acevedo-Arozena A, Gordon DE, Peden AA, Lichtenberg M, Menzies FM, Ravikumar B, Imarisio S, Brown S, O'Kane CJ, Rubinsztein DC (2010) alpha-Synuclein impairs macroautophagy: implications for Parkinson's disease. *J Cell Biol*, 190:1023–1037.
- Wohlke A, Philipp U, Bock P, Beineke A, Lichtner P, Meitinger T, Distl O (2011) A one base pair deletion in the canine ATP13A2 gene causes exon skipping and late-onset neuronal ceroid lipofuscinosis in the Tibetan terrier. *PLoS Genet*, 7:e1002304.
- Wszolek ZK, Pfeiffer RF, Bhatt MH, Schelper RL, Cordes M, Snow BJ, Rodnitzky RL, Wolters EC, Arwert F, Calne DB (1992) Rapidly progressive autosomal dominant parkinsonism and dementia with pallido-ponto-nigral degeneration. *Ann Neurol*, 32:312–320.
- Wszolek ZK, Vieregge P, Uitti RJ, Gasser T, Yasuhara O, McGeer P, Berry K, Calne DB, Vingerhoets FJ, Klein C, Pfeiffer RF (1997) German-Canadian family (family A) with parkinsonism, amyotrophy, and dementia - Longitudinal observations. *Parkinsonism Relat Disord*, 3:125–139.

- Xilouri M, Brekk OR, Landeck N, Pitychoutis PM, Papisilekas T, Papadopoulou-Daifoti Z, Kirik D, Stefanis L (2013) Boosting chaperone-mediated autophagy in vivo mitigates alpha-synuclein-induced neurodegeneration. *Brain*, 136:2130–2146.
- Xu J, Kao SY, Lee FJ, Song W, Jin LW, Yankner BA (2002) Dopamine-dependent neurotoxicity of alpha-synuclein: a mechanism for selective neurodegeneration in Parkinson disease. *Nat Med*, 8:600–606.
- Yang Z, Klionsky DJ (2010) Eaten alive: a history of macroautophagy. *Nat Cell Biol*, 12:814–822.
- Zabetian CP, Samii A, Mosley AD, Roberts JW, Leis BC, Yearout D, Raskind WH, Griffith A (2005) A clinic-based study of the LRRK2 gene in Parkinson disease yields new mutations. *Neurology*, 65:741–744.
- Zaidi N, Maurer A, Nieke S, Kalbacher H (2008) Cathepsin D: a cellular roadmap. *Biochem Biophys Res Commun*, 376:5–9.
- Zarranz JJ, Alegre J, Gomez-Esteban JC, Lezcano E, Ros R, Ampuero I, Vidal L, Hoenicka J, Rodriguez O, Adures B, Llorens V, Gomez Tortosa E, del Ser T, Munoz DG, de Yebenes JG (2004) The new mutation, E46K, of alpha-synuclein causes Parkinson and Lewy body dementia. *Ann Neurol*, 55:164–173.
- Zatloukal K, Stumptner C, Fuchsichler A, Heid H, Schnoelzer M, Kenner L, Kleinert R, Prinz M, Aguzzi A, Denk H (2002) p62 Is a common component of cytoplasmic inclusions in protein aggregation diseases. *Am J Pathol*, 160:255–263.
- Zhang J, Deng X, Choi HG, Alessi DR, Gray NS (2012) Characterization of TAE684 as a potent LRRK2 kinase inhibitor. *Bioorg Med Chem Lett*, 22:1864–1869.
- Zhao W, Dumanis SB, Tamboli IY, Rodriguez GA, Jo Ladu M, Moussa CE, William Rebeck G (2014) Human APOE genotype affects intraneuronal Abeta1-42 accumulation in a lentiviral gene transfer model. *Hum Mol Genet*, 23:1365–1375.
- Zhou B, Westaway SK, Levinson B, Johnson MA, Gitschier J, Hayflick SJ (2001) A novel pantothenate kinase gene (PANK2) is defective in Hallervorden-Spatz syndrome. *Nat Genet*, 28:345–349.
- Zhou W, Hurlbert MS, Schaack J, Prasad KN, Freed CR (2000) Overexpression of human alpha-synuclein causes dopamine neuron death in rat primary culture and immortalized mesencephalon-derived cells. *Brain Res*, 866:33–43.
- Zhu L, Zhong M, Zhao J, Rhee H, Caesar I, Knight EM, Volpicelli-Daley L, Bustos V, Netzer W, Liu L, Lucast L, Ehrlich ME, Robakis NK, Gandy SE, Cai D (2013) Reduction of synaptojanin 1 accelerates Abeta clearance and attenuates cognitive deterioration in an Alzheimer mouse model. *J Biol Chem*, 288:32050–32063.
- Zimprich A et al. (2011) A mutation in VPS35, encoding a subunit of the retromer complex, causes late-onset Parkinson disease. *Am J Hum Genet*, 89:168–175.
- Zimprich A et al. (2004) Mutations in LRRK2 cause autosomal-dominant parkinsonism with pleomorphic pathology. *Neuron*, 44:601–607.
- Ziviani E, Tao RN, Whitworth AJ (2010) *Drosophila parkin* requires PINK1 for mitochondrial translocation and ubiquitinates mitofusin. *Proc Natl Acad Sci U S A*, 107:5018–5023.